Roma Tre

Corso di Dottorato di Ricerca in Risorse, Territorio e Ambiente

XXXVIII° Ciclo

Exploring geothermal fluid circulation through the study of CO_2 diffuse degassing: an application to the Acque Albule Basin.

Dottorando: Sara Emili

Tutor: Prof. Claudio Faccenna

Coordinatore: Prof. Valerio Acocella

Success consists of going from failure to failure without loss of enthusiasm.

Winston Churchill.

Abstract

Understanding geothermal fluid circulation in tectonically active settings is essential for reconstructing the structural framework and for assessing deep geothermal resources. One of the principal challenges in geothermal energy production is the permeability of the reservoir, which controls both extraction and reinjection efficiency. Identifying highly permeable zones where deep fluids ascend is therefore crucial. Faults, fractures, and ongoing tectonic activity strongly influence fluid pathways and fluid-rock interactions. Assessing their geometry and behavior is fundamental as the tectonic structures may act either as barriers to fluid flow or as preferential conduits. The Acque Albule Basin (AAB) represents a key case study and one of the most prominent hydrothermal systems in central Italy. This tectonically controlled basin hosts an extensive hydrothermal discharge system, as evidenced by thick travertine deposits and numerous mineralized springs (maximum surface temperature ~23 °C). This diffuse hydrothermal activity is sustained by warm fluids circulating through a Meso-Cenozoic carbonate succession, affected by extensive dissolution and brittle deformation. The travertine deposition in the area is largely governed by fault activity. A detailed soil CO_2 survey was conducted to evaluate the role of faults in controlling hydrothermal circulation. Interpolated CO_2 flux maps reveal distinct high and low-flux anomalies aligned along N-S and NE-SW trends, indicating a clear structural control on fluid migration. $\delta^{13}C$ data further show a progressive decrease in the deep hydrothermal signal from west to east, consistent with a lateral reduction of deep fluid input. These observations highlight active degassing along the principal N-S strike-slip fault, whose southwestern segment functions as the main conduit for hydrothermal fluids. Additional minor transtensive faults in the western sector (parallel to the Collefiorito Ridge) also sustain the fluid circulation. Several transect surveys performed with an accumulation chamber around the AAB, including in the Cretone, Sant'Angelo Romano, Bagni di Tivoli, and Corcolle areas. Hydrothermal springs and soil degassing detected in the Cretone area indicate fluid migration along the northern sector of the main strike-slip system. However, no significant anomalies were identified in Sant'Angelo Romano or Corcolle, suggesting that active fluid circulation is largely confined to the AAB and to Cretone area. Other segments of the fault system (Corcolle and Sant'Angelo) appear inactive with respect to fluid flow. Furthermore, numerical modeling of the AAB shown that shallow meteoric recharge dominates the thermal structure of the system by reducing the temperature in the reservoir, while CO_2 continues to ascend along the fault zone. Gas-lift process seems to control CO_2 exsolution and upward

migration, reproducing the observed coexistence of low temperatures and vigorous degassing at Regina and Colonnelle. Persistent CO_2-rich flow promotes carbonate precipitation and progressive fault sealing, suggesting a repetitive chemical sealing and fluid circulation.

Table of contents

1- Thesis Outline

1.1 Key scientific issues

Geothermal energy represents a strategic resource for the energy transition, as it is a renewable source that can be exploited for multiple applications, such as district heating and electricity production (Lund et al., 2011; Rubio-Maya et al., 2015; Lund & Toth, 2020). Despite this potential, geothermal exploitation in Italy remains restricted. Central Italy is characterized by a remarkable geothermal potential. High geothermal potential relies on the coexistence of a significant heat source, a permeable reservoir hosting a regional aquifer, and an overlying cap rock that provides effective sealing of the geothermal system. Central Italy has a heat flux values exceeding 200 mW/m² (Della Vedova et al., 2001; Giordano, 2013). The highest fluxes are concentrated in correspondence with the major Quaternary volcanic complexes (Della Vedova et al., 2001; Jolivet et al., 1998; Gambardella et al., 2004; Acocella & Funiciello, 2006; Giordano, 2013; Chiodini et al., 2021). Moreover, the coexistence of high heat flow and extensive fractured carbonate reservoir provides highly favorable geological conditions for the development of geothermal resources in central Italy (Giordano et al., 2014). One of the main challenges in geothermal energy exploitation is the estimation of reservoir permeability, which exerts a primary control on fluid flow and resource sustainability (Liotta et al., 2010; Rossetti et al., 2011; Maffucci et al., 2012; Giordano et al., 2014; Invernizzi et al., 2014; Liotta & Brogi, 2020). Identifying and managing the most permeable zones is essential for the optimal siting of boreholes, which requires a clear understanding of subsurface fluid circulation and up flow pathways (Brown et al., 1999; Giordano et al., 2014). For this reason, detailed mapping of fault networks and evaluation of their role in controlling permeability are fundamental steps in assessing the geothermal potential of central Italy. Central Italy, and particularly the Latium region, represents one of the principal geothermal provinces of the country, as evidenced by the widespread occurrence of mineralized springs along the central Apennines (T = 15–50 °C; Minissale et al., 2019; Tamburello et al., 2022). Among these, the Acque Albule Basin (Rome, Italy) horst several hydrothermal spring, releasing large volumes of thermal water with temperatures up to 23 °C; an average discharge of approximately 3 m³/s and a conductivity of 3000 µS/cm (La Vigna & Gnoni, 2013). At present, these springs are mainly exploited for thermal spa use, but their discharge volumes and hydrothermal setting indicate a considerable potential for geothermal energy exploitation.

The Acque Albule Basin (AAB) is a transtensional basin where hydrothermal fluid circulation is strongly controlled by the activity of strike-slip and extensional faults (Faccenna et al., 2008). Understanding how these structures influence permeability and fluid pathways has been the central focus of this work, which integrates non-invasive CO_2 flux surveys, isotopic analyses, structural interpretation, and numerical modeling.

Soil CO_2 flux measurements in the AAB were obtained through the accumulation chamber method. Surveys have proven fundamental for identifying zones of enhanced permeability and detecting active and buried fault systems. The spatial distribution of CO_2 fluxes and $\delta^{13}C$ values highlights the key role of major N-S and NE-SW trending faults in channeling deep hydrothermal fluids toward the surface. The highest degassing areas are distributed near the Regina and Colonnelle thermal lakes and coincide with major fault segments, confirming these as the main up flow zones. $\delta^{13}C$ analyses suggest some points characterized by hydrothermal and mixing biogenic-hydrothermal contribution and an east-to-west increase in deep hydrothermal degassing, consistent with travertine chronology. Data indicate that the westernmost portion of the basin represents the youngest hydrothermal manifestation in the basin. Conversely, low-flux sectors correspond to paleo-conduits progressively sealed by travertine precipitation, and areas where travertine is compact (e.g. quarries). This reflect an evolutionary trend in which older pathways are gradually closed while fluid ascent migrates toward more permeable structures. We then integrated collected spatial CO_2 flux data with existing structural information and transects carried out at Cretone, Sant'Angelo Romano, Bagni di Tivoli, and Corcolle; where the N-S fault is present. The results show that hydrothermal activity is concentrated primarily within the basin along the main N–S shear zone and NW–SE lineaments. Survey results from Cretone, Sant'Angelo Romano, and Corcolle also show minimal anomalies, supporting the idea that active fluid circulation is largely confined within the basin itself. Furthermore, cold water seems to be crucial in masking the real geothermal potential of the AAB. The results the thesis applied to the Acque Albule Basin provide a scientific basis for its redevelopment within broader strategies of territorial regeneration and energy transition. In parallel, the accumulation chamber method was applied across multiple geological settings, including the Acque Albule Basin, the Green Roman Area, Marano Equo, Vulcano Island, and Poás Volcano. These applications confirm its broad usefulness for detecting buried faults, quantifying natural degassing, and assessing volcanic or tectonic activity.

1.2 Aim of the work

This project is framed within the Piano Nazionale di Ripresa e Resilienza (PNRR), and more specifically financed by Rome Technopole Foundation. The Rome Technopole initiative represents a decisive step toward promoting sustainable innovation in the Lazio region, with a strong focus on ecological transition, smart specialization, and the regeneration of the industrial sector. Within this framework, this project aims to advance the understanding of tectonic controls on geothermal reservoirs in Central Italy, combining field-based investigations with laboratory approaches to promote a more sustainable exploitation of subsurface resources.

1.3 Chapters overview

Following the outline part (**Chapter 1**), this thesis is divided into other 6 chapters.

Chapter 2: This chapter examines the interaction between hydrothermal fluids and fault systems, with specific reference to the Central Apennines and the Acque Albule Basin. It provides a comprehensive synthesis of the geological framework of the Acque Albule area, incorporating both direct and indirect investigations carried out over the past three years of research.

Chapter 3: focuses on the geochemical surveys conducted, with a particular focus on the summarizes and elaboration of soil CO_2 surveys in the northern part of the basin. This includes isotopic analysis, and the conceptual model derived from the processing of this direct data.

Chapter 4: focuses on CO_2 flux surveys to detect the regional role of the strike-slip zone, as described in previous studies of the Tivoli-Guidonia area. The article aims to combine structural studies with CO_2 flux profile results from the northern part of the basin (the Cretone area) to the south (the Corcolle area).

Chapter 5: presents a simple numerical simulation about the fluid circulation in the AAB with the TOUGH2 software.

Chapter 6: Conclusion and final remarks. This chapters also provides a comprehensive discussion of the study area and a critical evaluation of the potential use of mineralized waters. Another focus of this chapter would be the efficiency of the accumulation chamber, in particular respect to the volcanic/tectonic degassing and environment gas monitoring.

1.4 References

Acocella, V., & Funiciello, R. (2006). Transverse systems along the extensional Tyrrhenian margin of central Italy and their influence on volcanism. *Tectonics*, *25*(2).

Brown, D., DuTeaux, R., Kruger, P., Swenson, D., & Yamaguchi, T. (1999). Fluid circulation and heat extraction from engineered geothermal reservoirs. *Geothermics*, *28*(4-5), 553-572.

Chiodini, G., Cardellini, C., Bini, G., Frondini, F., Caliro, S., Ricci, L., & Lucidi, B. (2021). The carbon dioxide emission as indicator of the geothermal heat flow: Review of local and regional applications with a special focus on Italy. *Energies*, *14*(20), 6590.

Della Vedova, B., Bellani, S., Pellis, G., Squarci, P., Vai, G. B., & Martini, I. P. (2001). Deep temperatures and surface heat flow distribution. *Anatomy of an orogen: The Apennines and adjacent Mediterranean basins*, 65-76.

Faccenna, C., Soligo, M., Billi, A., De Filippis, L., Funiciello, R., Rossetti, C., & Tuccimei, P. (2008). Late Pleistocene depositional cycles of the Lapis Tiburtinus travertine (Tivoli, Central Italy): possible influence of climate and fault activity. *Global and Planetary Change*, *63*(4), 299-308.

Gambardella, B., Cardellini, C., Chiodini, G., Frondini, F., Marini, L., Ottonello, G., & Zuccolini, M. V. (2004). Fluxes of deep CO2 in the volcanic areas of central-southern Italy. *Journal of volcanology and geothermal research*, *136*(1-2), 31-52.

Giordano, G. (2013). La geotermia e gli acquiferi dell'Italia centrale. *Acque Sotterranee-Italian Journal of Groundwater*, *2*(4).

Giordano, G., De Benedetti, A. A., Bonamico, A., Ramazzotti, P., & Mattei, M. (2014). Incorporating surface indicators of reservoir permeability into reservoir volume calculations: Application to the Colli Albani caldera and the Central Italy Geothermal Province. *Earth-Science Reviews*, *128*, 75-92.

Jolivet, L., Faccenna, C., Goffé, B., Mattei, M., Rossetti, F., Brunet, C., ... & Parra, T. (1998). Midcrustal shear zones in postorogenic extension: example from the northern Tyrrhenian Sea. *Journal of Geophysical Research: Solid Earth*, *103*(B6), 12123-12160.

Invernizzi, C., Pierantoni, P. P., Chiodi, A., Maffucci, R., Corrado, S., Baez, W., ... & Viramonte, J. (2014). Preliminary assessment of the geothermal potential of Rosario de la Frontera area (Salta, NW Argentina): Insight from hydro-geological, hydro-geochemical and structural investigations. *Journal of South American Earth Sciences*, *54*, 20-36.

La Vigna, F., & Gnoni, A. (2013). Groundwater-Geothermal preliminary model of the Acque Albule Basin (Rome): future perspectives of geothermal resources exploitation. *Acque Sotterranee-Italian Journal of Groundwater*, *2*(4).

Liotta, D., Ruggieri, G., Brogi, A., Fulignati, P., Dini, A., & Nardini, I. (2010). Migration of geothermal fluids in extensional terrains: the ore deposits of the Boccheggiano-Montieri area (southern Tuscany, Italy). *International Journal of Earth Sciences*, *99*(3), 623-644.

Liotta, D., & Brogi, A. (2020). Pliocene-Quaternary fault kinematics in the Larderello geothermal area (Italy): Insights for the interpretation of the present stress field. *Geothermics*, *83*, 101714.

Lund, J. W., Freeston, D. H., & Boyd, T. L. (2011). Direct utilization of geothermal energy 2010 worldwide review. *Geothermics*, 40(3), 159-180.

Lund, J. W., & Toth, A. N. (2021). Direct utilization of geothermal energy 2020 worldwide review. *Geothermics*, *90*, 101915.

Maffucci, R., Corrado, S., Aldega, L., Bigi, S., Chiodi, A., Di Paolo, L., ... & Invernizzi, C. (2016). Cap rock efficiency of geothermal systems in fold-and-thrust belts: Evidence from paleo-thermal and structural analyses in Rosario de La Frontera geothermal area (NW Argentina). *Journal of Volcanology and Geothermal Research*, *328*, 84-95.

Rossetti, F., Aldega, L., Tecce, F., Balsamo, F., Billi, A., & Brilli, M. (2011). Fluid flow within the damage zone of the Boccheggiano extensional fault (Larderello–Travale geothermal field, central Italy): structures, alteration and implications for hydrothermal mineralization in extensional settings. *Geological Magazine*, *148*(4), 558-579.

Rubio-Maya, C., Díaz, V. A., Martínez, E. P., & Belman-Flores, J. M. (2015). Cascade utilization of low and medium enthalpy geothermal resources− A review. *Renewable and Sustainable Energy Reviews*, *52*, 689-716.

2- Introduction

Abstract

Earth degassing is a relevant process for understanding the thermal and chemical evolution of the planet. This mechanism is fundamental to investigate fluid reservoirs sequestered within the mantle and crust, as well as their interactions with the atmosphere (Chiodini et al., 2004; Frezzotti et al., 2009; Batista Cruz et al., 2019; Erlanger et al., 2024). While the scientific community has traditionally attributed primary carbon dioxide (CO_2) discharge to active volcanism, geochemical evidence in recent decades has challenged this paradigm (Tamburello et al., 2018; Chiodini et al., 2020; Randazzo et al., 2022). It is widely known that fault zones function as preferential permeability pathways capable of sustaining continuous gas and fluids discharge (Irwin and Barnes., 1980; Stibson, 1996; Giammanco et al., 1997; Jolie et al., 2015; Di Maio et al., 2021). This phenomenon is called tectonic degassing, and it constitutes an amount component of the global carbon budget (Chiodini et al., 2000). Within this framework, structural discontinuities (faults and fractures) play a key role in determining the permeability of the crust (Stibson, 1996; Gregorio et al., 2002). These features influence the migration of hydrothermal fluids and gases (e.g. CO_2, SO_2, He) and short-lived radioisotopes (e.g. Rn) towards the surface (Chiodini et al., 2004; Jolie et al., 2015; Sun et al., 2021; Zhang et al., 2024). The fluid circulation represents a dynamic evolution of the system, driven by fluctuations in crustal stress and complex fluid-rock interactions. Such processes may result in self-sealing processes through mineral precipitation or the creation of permeable conduits during various stages of the seismic cycle (Stibson, 2000; Frery et al., 2015; Uysal et al., 2019). The Acque Albule Basin (AAB, Tivoli, Central Italy) provides to be an exceptional natural laboratory for investigating this hydrothermal fluid circulation. The basin is located within an extensional and strike-slip tectonic setting along the Tyrrhenian margin (Faccenna et al., 2008; De Filippis et al., 2013). The AAB is characterized by the vigorous upwelling of carbon dioxide-rich thermal fluids and the extensive deposition of the Lapis Tiburtinus travertine sequence (Faccenna et al., 2008; Petitta et al., 2010; Carucci et al., 2012; De Filippis et al., 2013; La Vigna et al., 2013). Beyond their historical economic significance, these deposits constitute an important geochemical and sedimentary archive. Travertines originate from the circulation of deep-seated, bicarbonate-supersaturated waters, which ascend along north-south-trending faults

and degas at the surface, triggering the calcium carbonate ($CaCO_3$) precipitation (Carucci et al., 2012). This context reflects an intense fluid circulation that generates cold hydrothermalism at the surface and sustains a significant amount of mineralized groundwater resource. For these reasons, the system requires investigation from the fault-fluid interaction perspective.

2.1- The Global role of the tectonic degassing

Earth degassing is a geological process in which gas species and volatiles are transferred from the solid Earth (the mantle and crust) into the atmosphere and oceans (Condie, 2005). The continuous release of fluids derived from the Earth's depths is a critical component of the global carbon cycle. Earth degassing has played a fundamental role in regulating the planet's surface temperatures over geological timescales by way of the greenhouse effect (Frezzotti et al., 2009). The gases released during this process typically consist of more than 95% water vapor, carbon dioxide (CO_2), sulfur species (SO_2 and H_2S), and nitrogen (N_2). Other important components include methane (CH_4) and noble gases (Christenson and Tassi, 2015). While water vapor is usually the most abundant species in magmatic settings, CO_2 is often the dominant gas in tectonic areas because of a combination of its physical properties, chemical behavior, and the diversity of its geological sources. The primary reason for the high concentration of CO_2 in degassed fluids is its low solubility in silicate melts compared to other major volatiles, such as water. As CO_2 is relatively insoluble at moderate to low pressures, it is released from rising magmas earlier and in larger quantities than more soluble species. Because of the low solubility, CO_2 is already saturated and present as a separate vapor phase at deep crustal or even mantle depths. Another reason is that CO_2 is a relatively inert and non-reactive gas compared to other magmatic volatiles, such as SO_2, HCl and HF (Carapezza et al., 2009). While hydrothermal systems often absorb or neutralize these other acidic gases through water-rock interactions, CO_2 has a lower reactivity. This allows it to migrate more easily through the crust and reach the surface in higher proportions, especially in quiescent or tectonic areas where more soluble gases have been removed (Carapezza et al., 2009; Li Vigni et al., 2025).

Natural CO_2 degassing occurs across various geological contexts. It is primarily associated with volcanic activity, which encompasses both active eruptions and passive (quiescent) emissions from the craters and plumes of subaerial and submarine volcanoes. Furthermore, CO_2 is released through non-volcanic degassing processes (Chiodini et al., 2004). This refers to the migration of gases in the absence of active volcanism, typically occurring via faults and fractures or through biogenic processes such as plant respiration (Chiodini et al., 2004; Chiodini et al., 2019). Another significant source is represented by geothermal systems. These emissions originate from hydrothermal environments, which may or may not be volcanic in nature, and are predominantly released through tectonic discontinuities.

In the following section, we provide a more detailed analysis of the several geological environments responsible for the release of CO_2 at the Earth's surface.

2.1.1- Volcanic Degassing

Volcanic degassing represents a primary flux in the global carbon cycle, accounting for approximately up 10% of the total carbon released from the Earth's interior (Chiodini et al., 2004). The most evident form of release is active eruptive degassing, which is characterized by concentrated emissions through volcanic plumes and explosive activity. This is typical of open-conduit systems such as Stromboli, where continuous magmatic activity ensures a constant flow of carbon dioxide. However, a significant proportion of volcanic gases are released through quiescent (non-eruptive) pathways, including open vents, volcanic lakes and fumarolic fields. These processes are often influenced by underlying hydrothermal systems, such as those found on Vulcano Island and at Campi Flegrei, where magmatic gases interact with hydrothermal fluids prior to reaching the surface. Beyond these visible features, diffuse soil degassing represents a critical component of the total gas output (Carapezza et al., 2009). This process involves CO_2 migrating through the interstitial spaces of soil and fractured rock. Although diffuse degassing is not usually visible, its cumulative contribution can equal or even exceed that from focused fumarolic vents (Chiodini et al., 2008). In many volcanic systems, structural discontinuities such as faults and caldera rims act as preferential "high permeability" pathways, focusing diffuse emissions into specific tectonic sectors (Chiodini et al., 2010; Jolie et al., 2015). To understand these processes, it is important to consider the scale of observed CO_2 fluxes. Campi Flegrei, for instance, is one of the most active degassing areas in the world. Recent studies have estimated its total CO_2 output at 1.500–2000 tons per day (t/d), just from the Solfatara area and its surroundings (Chiodini et al., 2016; 2021, Figure 2.1a). Likewise, it has been documented that Mount Etna releases large quantities of CO_2, with total emissions (both eruptive and quiescent) reaching 10,000–20,000 tons per day (Aiuppa et al., 2017, Figure 2.1 b). Similarly, crater lakes are important for releasing CO_2 at the surface. In these environments, CO_2 can be released steadily through the lake surface, or it can accumulate in the depths and cause phreatic events. Examples such as Lake Voui in Vanuatu, where fluxes reached 2.000 tons per day (Mazot et al., 2011). Volcanic degassing can be a serious hazard. Because of CO_2 is denser than air, it can accumulate in unventilated spaces, leading to lethal concentrations. This 'invisible' hazard can cause asphyxiation and respiratory distress (Chiodini et al., 1999). Tragic historical examples include the phreatic eruptions at Lake Nyos in Cameroon and the lethal degassing episodes in Cava de' Selci in Italy, where high concentrations of CO_2 in the soil and atmosphere have resulted in fatalities among humans and animals (Giggenbach et al., 1990; Carapezza et al., 2009).

Figure 2.1- a) Phlegrean Field Solfatara (Naples, Italy) where fumaroles and diffuse degassing are present; b) Mount Etna eruption releasing gases and ash into the atmosphere.

2.1.2- Non-volcanic degassing

While volcanic activity is a primary driver of carbon release, a significant portion of the Earth's total CO_2 budget is discharged in non-volcanic settings. This type of degassing, often occurring in tectonically active regions and it takes a multi-source process involving deep-seated crustal and mantle reservoirs, as well as shallower biogenic and chemical interactions. Non volcanic degassing can include:

- **Upper Mantle Escape:** Volatiles such as CO_2 and helium migrate through the lithosphere from the upper mantle, often aided by deep-reaching permeable pathways like faults. One prominent example of upper mantle escape of CO_2 found in the sources is the westernmost part of the Pannonian Basin, specifically in the border region between southeast Austria and northeast Slovenia. In this region, geochemical investigations of fourteen different degassing sites, such as mofettes and wells, provided evidence for active lithospheric mantle degassing (Brauer et al 2016; Wycherley et al 1999; Demeny et al 2010).
- **Crustal Carbonate-Bearing Rocks:** Degassing occurs when carbonate minerals (like calcite, dolomite, or magnesite) undergo metamorphic decarbonation or hydrolysis releasing CO_2. For example, most hydrothermal area related to the Central Apennines shows this type of degassing (Tamburello et al., 2018).

- **Hydrocarbon Reservoirs:** Significant amounts of carbon gas (primarily methane and CO_2) escape from maturation levels in sedimentary beds or from leaking oil and gas fields. In geothermal fields like Istibanja, Katlanovo, and Kumanovo, CO_2 is associated with metamorphic decarbonation reactions within reservoirs hosted in carbonate-rich aquifers. Tamang et al., 2024 characterized the metamorphism of Proterozoic dolomitic and magnesite rocks within the Lesser Himalayan Sequence. The study concluded that metasediments containing 15-40% carbonate are highly productive, releasing 5.5 to 10.5 wt% CO_2 at depth, which contributes to the diffuse degassing observed along the Himalayan belt.
- **Organic Decomposition:** Degassing also occurs through the maturation of hydrocarbons and the oxidation of ancient organic carbon in sedimentary rocks. Sedimentary basin can be affected by this type of degassing. A significant component of non-volcanic degassing is associated with the thermal maturation of hydrocarbons and the oxidation of ancient organic carbon (kerogen) within sedimentary basins. These processes represent a major long-term flux of "fossil" CO_2 to the atmosphere, independent of modern biological cycles.
- **Surface Deposits and Processes:** Degassing can originate from biogenic activity in soil, permafrost, or shallow sediments, as well as from the oxidation of ancient organic carbon (Chiodini et al., 2000).

Di Salvo et alii.,2013 propose a schematic representation of Tiber Valley (Italy), where tectonic degassing and biogenic degassing occur.

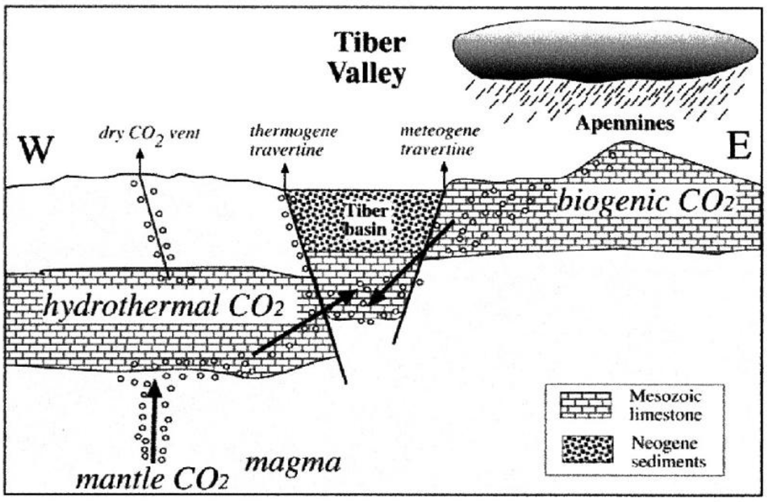

Figure 2.2- Representation of the Tiber Valley CO2 degassing. In particular, the figure shows the active tectonic (hydrothermal) degassing, and the biogenic degassing related to the plant respiration. Di Salvo et alii., 2013 (modified after Minissale et al., 2002).

2.1.3- Geothermal degassing

Geothermal systems discharge significant volumes of CO_2 trough tectonic discontinuities. These reservoirs host circulating hydrothermal and supercritical fluids whose vertical migration is controlled by advective and convective transport mechanisms (Agostinetti et al., 2017; Taussi et al., 2023). While the primary fluid circulation is sequestered by a low-permeability cap rock, crustal discontinuities facilitate the ascent of these fluids toward the surface. Such processes are geologically evidenced by surface expressions, including geysers, hydrothermal manifestations, and extensive mineral precipitation (e.g., travertine Li Vigni et al., 2025). The Larderello geothermal system (Northern Apennines, Italy Fig. 2.3a) represents a pilot case study of global relevance for understanding the interplay between extensional tectonics and deep-seated fluid circulation. Larderello is located in a region of significant lithospheric thinning and anomalous heat flow. Today, Larderello is recognized as the world's oldest industrial geothermal field. However, its scientific importance extends beyond energy production, providing as a primary laboratory for the study of deep regional fluid pathways in "non-volcanic" settings. According to recent geochemical and structural characterizations (Taussi et al., 2023), the Larderello system is characterized by a complex network of high-permeability discontinuities that facilitate the ascent of deeply sourced CO_2. A pivotal aspect of this system is the role of regional transfer zones penetrate into the shallow brittle-ductile transition of the crust (Liotta et al., 1991; Taussi et al., 2023 Fig.2.3b). These zones act as the primary engines for fluid bypass, connecting the deep reservoir to the surface and modulating the distribution of both hydrothermal hot-degassing areas (associated with thermal manifestations) and cold-degassing areas. The global significance of Larderello lies in its ability to demonstrate how structural framework and active extension govern fluid circulation. The CO_2 degassing, characterized by a distinct carbon isotopic signature, provides evidence of a hydrothermal system where fluids are actively channeled toward the surface through these transfer zones (Taussi et al., 2023). This mechanism makes Larderello as a fundamental proxy for studying crustal permeability dynamics and global geogenic greenhouse gas emissions.

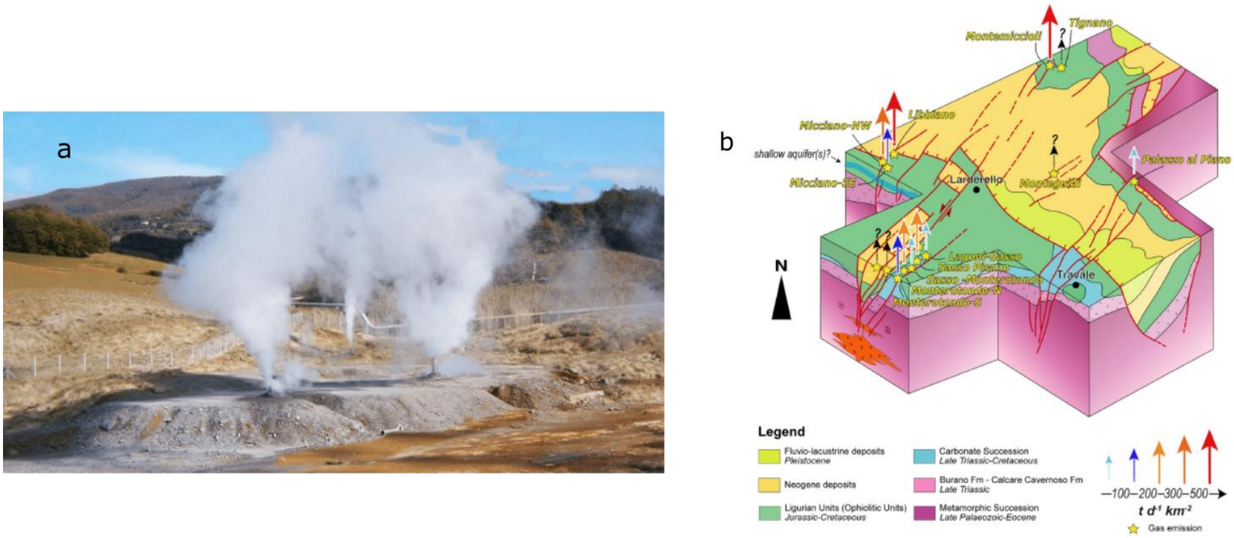

Figure 2.3- a) Larderello Geothermal field (Sasso Pisano Fumaroles); b) Schematic representation about the tectonic settings and the CO_2 degassing in the Larderello Geothermal field (Taussi et al., 2023).

2.1.4- Tectonic degassing

Understanding crustal fluid circulation requires a rigorous analysis of fault zones, which function as complex 3D systems acting as either conduits or barriers to hydrothermal flow. Fluid-fault interaction is governed by the effective stress principle, which controls shear strength and seismic reactivation mechanics. The internal architecture of a fault zone typically comprises a fault core which is the locus of primary displacement, and a surrounding damage zone characterized by secondary fracturing. The fault core consists of highly deformed rocks, such as phyllosilicate-rich gouge, often organized into interlaced lenses or striated slip surfaces that constrain kinematic markers. Between the gouge and the undeformed host rock, the damage zone exhibits a high density of secondary fractures, minor faults, and veins. The host rock itself represents the protolith, affected only by regional background fracturing and unaffected by fault-related deformation. Fault architecture evolves with pressure and temperature regimes along the crustal profile. Shallow crustal levels are dominated by brittle deformation, producing breccias and gouges. In the seismogenic zone (~5-10 km depth), deformation yields cohesive cataclasites, whereas at the Brittle-Ductile Transition (BDT) (~10–15 km), increasing P-T conditions shift deformation mechanisms from brittle to plastic (Fig.2.4).

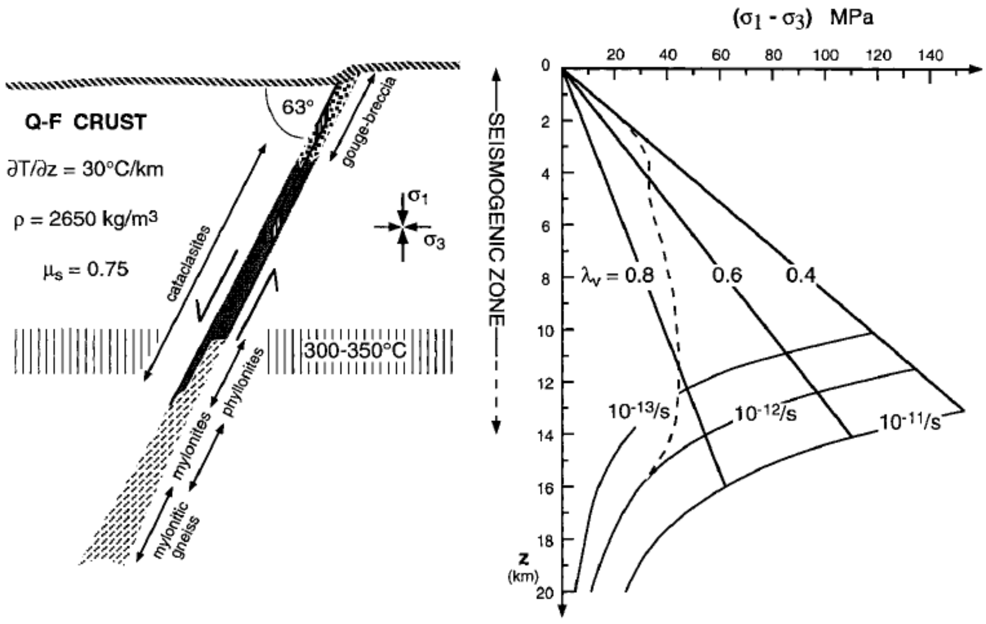

Figure 2.4- Fault rock distribution and rheological strength profile for an optimally oriented crustal-scale normal fault (Sibson et al., 2000).

This transition facilitates the development of phyllonites and mylonites (Sibson et al., 1996). Within this framework, fluid circulation drives diverse flow patterns, resulting in mineral precipitation and host rock dissolution (Uysal et al., 2019). In fact, fault zones control crustal fluid migration as dynamic regulators (Di Maio et al., 2021). Their hydraulic behavior is determined by their internal architecture and the directional variations in permeability. The fault core, representing the structural volume where strain and displacement are most intensely localized, typically functions as a primary hydraulic barrier to cross-fault flow. The matrix permeability, generally ranging between 10^{-20}, 10^{-21} m^2 (Bense and Person, 2006). Seismic slip or fluid overpressure breaches the seal, triggering the sudden upward discharge of deep-seated volatiles and hydrothermal fluids. The damage zone surrounds the fault core. Its dense fracture network serves as the primary fluid conduit. With permeability between 10^{-13} and $10^{-16} m^2$, this zone far exceeds the conductivity of the core or the host rock (Figure 2.5). This contrast creates a strong hydraulic anisotropy, channeling flow parallel to the fault; specifically, along the σ2 axis (the intermediate principal stress). Such directional transport, usually, it allows fluids to bypass regional seals and connect isolated aquifers. By alternating between barrier and conduit during the seismic cycle, the fault regulates the crustal distribution of heat, solutes, and pore pressure (Sibson et al., 2000).

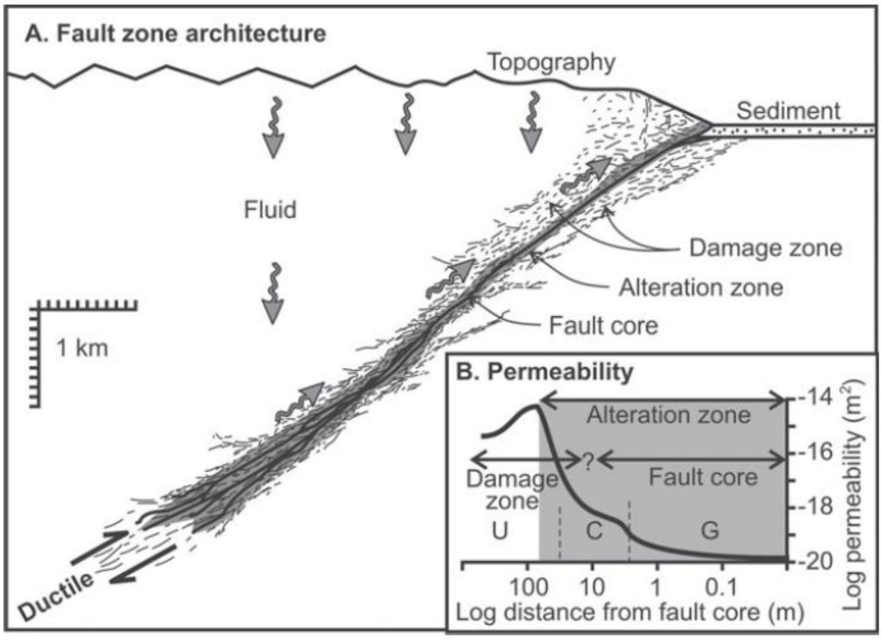

Figure 2.5- A: Schematic of an oblique reverse fault showing damage zone, alteration zone (shaded), and fault core. B: Permeability, showing low permeability in the alteration zone. U—hanging-wall ultra mylonite; C—cataclasite; G—gouge and ultracataclasite (from Sutherland et al., 2012).

2.2- Fault architecture and hydraulic regimes

2.2.1- Fluids circulation and seismic cycle

The interaction between crustal fluids and seismic dynamics allow to understand the mechanical processes governing the seismic cycle and crustal permeability. Fluid circulation can trigger weakening processes across various timescales, facilitating both aseismic slip and earthquake nucleation in a fault zone. Specifically, the increase in pore water pressure generated by high-pressure fluids reduces the effective stress the frictional resistance on the fault, promoting seismic slip (Collettini et al., 2008). Fault zone permeability is a dynamic enviroment directly influenced by seismotectonic activity (Sibson et al., 2000). Faults act as preferential conduits for the migration of crustal and mantle gases toward the surface, particularly in extensional tectonic regimes where fracturing facilitates the opening of migration pathways. Active deformation and dilatancy-related micro-fracturing enhance the release of volatiles, from rock pores into circulating fluids. Furthermore, fault activity increases overall permeability, allowing meteoric water to infiltrate deeply into the crust and interact with rising deep-seated fluids. This interaction influence the chemistry of hydrothermal springs. In high-seismicity regions like the Apennines, CO_2 overpressures reaching up to 85% of the lithostatic load have been documented in deep wells (4–5 km), highlighting the potential of these gases to generate mechanical instability (Miller et al., 2004; Collettini et al., 2008). A strong spatial correlation often exists between CO_2 degassing anomalies and active fault zones, indicating that structural permeability is maintained by active crustal stress, which prevents the sealing of conduits (Taussi et al., 2023; Tamburello et al., 2018). The analysis of permeability regimes within fault systems requires a detailed understanding of the hydro-mechanical interactions governing the seismic cycle; specifically, regarding fault-valve mechanisms, seismic pumping, and suction pump effects (Sibson et al., 2000). According to Sibson et al., 2000, fluids and faults can interact through several mechanism (Fig.2.6):

- **The Fault-Valve Mechanism**: the fault-valve behavior describes a fault's ability to regulate crustal fluid flow through cycles of pressure accumulation and discharge. In this model, the fault core (often composed of fine-grained cataclasites or clay minerals) acts as an impermeable seal allowing for the accumulation of overpressured fluids in the lower compartment. Following seismic rupture, the permeability of the sealed zone increases due to the fracturing process. Thi leads to a rapid release of fluids. This seismogenically induced outflow is often traced by anomalies in CO_2 and fluids discharging.
- **Seismic Pumping**: This process refers to large-scale fluid migration induced by changes in the stress field and crustal deformation during and after a seismic event. Active faults create vertical permeability pathways that connect the lower crust and mantle to the surface.
- **Suction Pump**: During rapid seismic rupture propagation, the sudden opening of volumes (such as extensional jogs or damage zones) generates instantaneous drops in fluid pressure. This negative differential pressure acts as a "suction pump," drawing fluids from the surrounding wall rocks toward the fault plane.

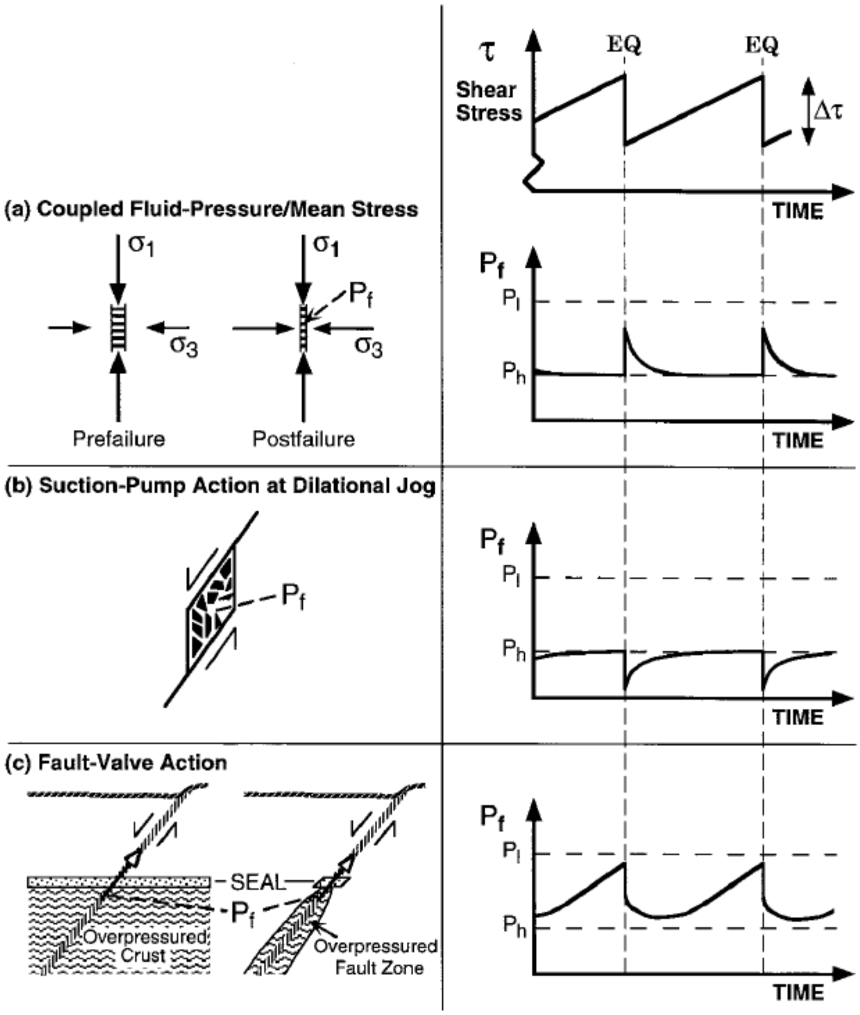

Figure 2.6- Dynamic fluid interactions coupled to the seismic shear stress cycle on normal faults (EQ: seismic slip increment, Ph hydrostatic fluid pressure, Pl lithostatic fluid pressure): (a) fluid pressure rise from fracture closure linked to increased horizontal and mean stress at failure; (b) localized coseismic reduction of fluid pressure within a dilatational fault jog; (c) fault-valve action from both distributed and localized overpressuring beneath sealing horizons (Sibson et al., 2000).

These mechanisms (pressure drop and CO_2 degassing) lead to the precipitation of secondary minerals, such as calcite veins and cemented breccias, which seal the fault during the post-seismic period. The texture of these veins is often featuring like euhedral crystals grown in open cavities, provides a geochronological record of hydrofracturing and suction episodes (Hickman et al., 1995; Sibson et al., 1996; Bons et al., 2012). Finally, seismicity and fluids are linked by a positive feedback mechanism. Tectonic activity creates a conduit-barrier system that drives macro-scale pressure-solution, sealing the fault and maintaining high internal pressure of the fluids. The sealing and healing of faults are critical phases in the hydro-mechanical evolution of the crust, governing the transition of a fault zone from a conduit to a barrier (Hickman et al., 1995). These phenomena regulate pore pressure accumulation and, consequently, the periodicity of the seismic cycle.

Sealing can be physical and mineralogical. In physical sealing fine-grained cataclasites or the formation of phyllosilicates (clays) create impermeable barriers. These "weak" mineral aggregates promote sealing and frictional-viscous creep at low friction coefficients (mu < 0.3). In chemical sealing process, the circulation of CO_2-rich hydrothermal fluids induces the dissolution of host rocks and the subsequent precipitation of secondary minerals, such as calcite veins and cemented breccias. This is accelerated by pressure drops; seismic rupture triggers sudden fluid pressure decreases, leading to CO_2 degassing and carbonate precipitation. Finally, sealing can be influenced by the climate period. In southwestern Turkey, damage zone sealing occurs preferentially during dry glacial periods (Uysal et al., 2019). Reduced meteoric recharge limits acidic flow were the chemical conditions for mineral precipitation in the reservoirs. It allows gas overpressure accumulation prior to the next rupture (Uyusal et al., 2019). The Healing process refers to the restoration of the fault's cohesive and frictional strength through recrystallization and cementation. The Evidence of healing is given by the laminated texture of calcite veins, where each lamina represents a micro-fracturing episode followed by immediate "healing" by mineral precipitation. Through healing, the fault returns to a sealed configuration until the next rupture.

2.2.2- Kinematics and Fluid Dynamics

The geological characterization of fault systems implies an integrated analysis of kinematic properties. These is governed by regional stress fields, and results in some structural architectures. According to Andersonian theory (1905), fault classification is determined by the spatial relationship between the principal stress axes σ_1, σ_2 and σ_3 producing a specific deformation on the earth surface (Figure 2.7). Fault kinematics includes normal, reverse, or strike-slip movements. They govern the spatial distribution of hydraulic conduits and barriers, driving fluid pressure evolution during the seismic cycle.

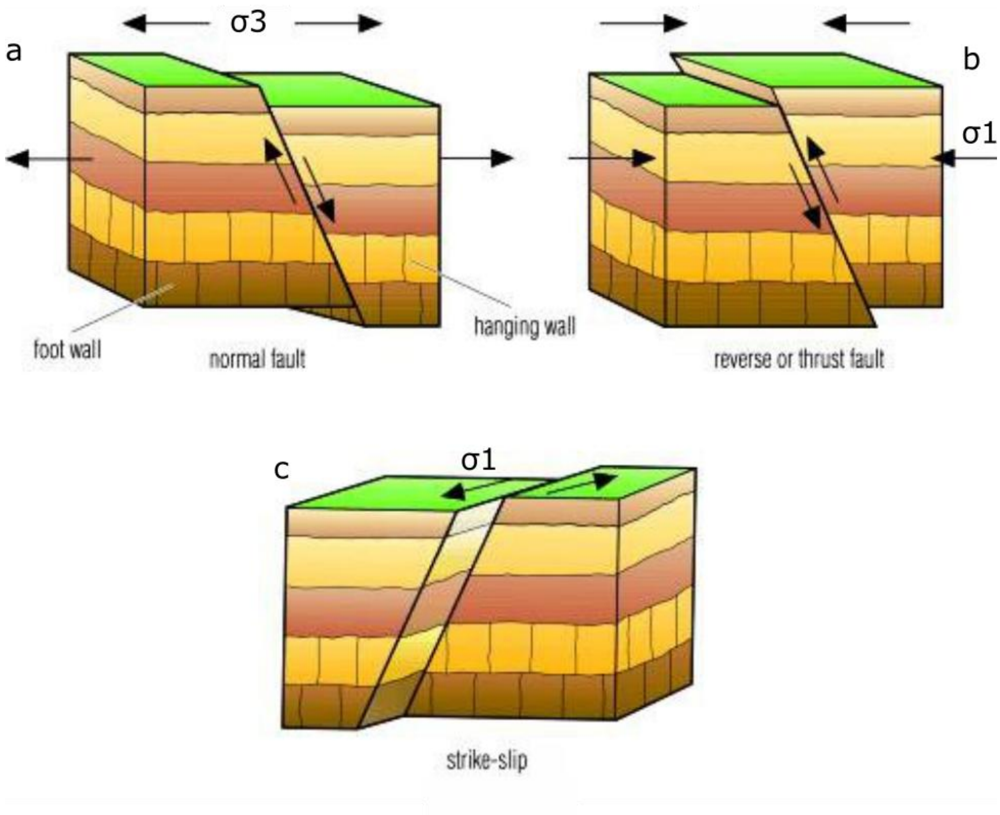

Figure 2.7- a) normal fault; b) reverse fault; c) strike-slip fault. Andersonian theory (1905).

The characterization of brittle failure in the upper crust relies on an integration of Anderson's theory of faulting and the Mohr-Coulomb failure criterion. The Mohr-Griffith-Coulomb failure criterion (1960) is a fundamental tool used in structural geology to explain the different rock failures and the resulting orientations of fractures and veins. This theory is based on principal stresses (σ_1, σ_2, σ_3) and on the mechanical properties of the rock. While Andersonian theory establishes the spatial orientation of the stress field based on boundary conditions at the Earth's surface, the Mohr-Coulomb criterion take into account the mechanical principles under which failure occurs. The criterion is typically established using a Mohr diagram, which plots normal stress (σ_n) on the horizontal axis and shear stress (τ) on the vertical axis. The diagram is shown in Figure 2.8.

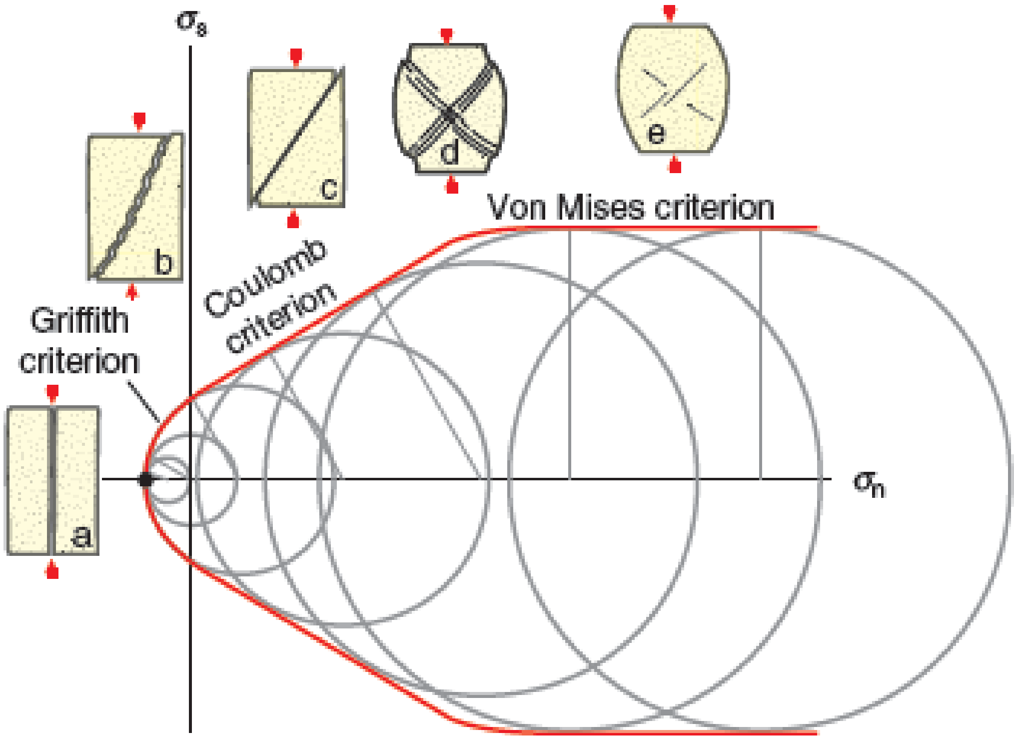

Figure 2.8- Three different fracture criteria combined in Mohr space. Different styles of fracturing are related to confining pressure: a) Tensile fracture; b) hybrid or mixed fracture; c) shear fracture; d) semi-ductile shear bands; e) plastic deformation (Van Der Pluijm & Marshak, 2004)

The Mohr Circle defines the stress conditions acting on all potential failure planes for a specified principal stress (σ_1 and σ_3). The failure envelope (Fig. 2.8) defines the limit beyond which the applied stress induces rock failure. A rock fails as soon as its Mohr circle touches this envelope. The failure envelope itself is defined by three key parameters:

1. **Tensile Strength (*T*)**: The maximum tensional stress a material can withstand.
2. **Cohesion (*C*)**: The shear stress required for failure when the normal stress is zero; it is roughly equal to twice the tensile strength (***C*≈2*T***).
3. **Internal friction angle (*β*)**: The slope of the linear portion of the failure envelope (Coulomb criterion), representing the increase in shear resistance with increasing confining pressure.

2.2.2.1- The Role of Fluid Pressure (Pf)

Fluid pressure is critical for the formation of veins at depth, where lithostatic load is high. By reducing the effective normal stress, fluid pressure translates the Mohr circle to the left of the diagram. This effective stress allows the rock to reach the tensile part of the failure envelope even in high-pressure environments, leading to hydro-fractures and the ubiquitous extensional veins found throughout the crust (Bons et al., 2012).

Furthermore, rocks often have pre-existing weaknesses direction (visible with some cleavage or bedding). In layered sequences, different beds (e.g., sandstone vs. shale) have different mechanical properties, usually re-activated by the pore pressure. During deformation, the "competent" layers often reach failure first, explaining why veins are frequently confined to specific and oriented layers (Bons et al., 2012).

2.2.3- Normal Faults (Extensional Regimes)

In extensional tectonic regimes, the crustal architecture is governed by a vertical principal stress σ_1 (the main stress axis), which drives hanging-wall subsidence and the development of normal fault systems (Figure 2.7a). While Andersonian geometries typically manifest as high-angle planes with dips of approximately 55°, these structures often undergo significant rotation to lower angles during progressive "domino-style" extension or within listric systems that root into basal detachments (Figure 2.9). These fault systems, often organized into 10-30 km segments linked by relay ramps, exhibit a distinct internal anatomy consisting of a discrete core and a characteristically asymmetric damage zone (Fossen et al., 2000). The nature of the fault rocks within these zones evolves significantly with depth. Shallow-level are characterized by incoherent breccias and clay-rich gouges. The Deeper level change into cohesive cataclasites, phyllonite or mylonite facies (Figure 2.5).

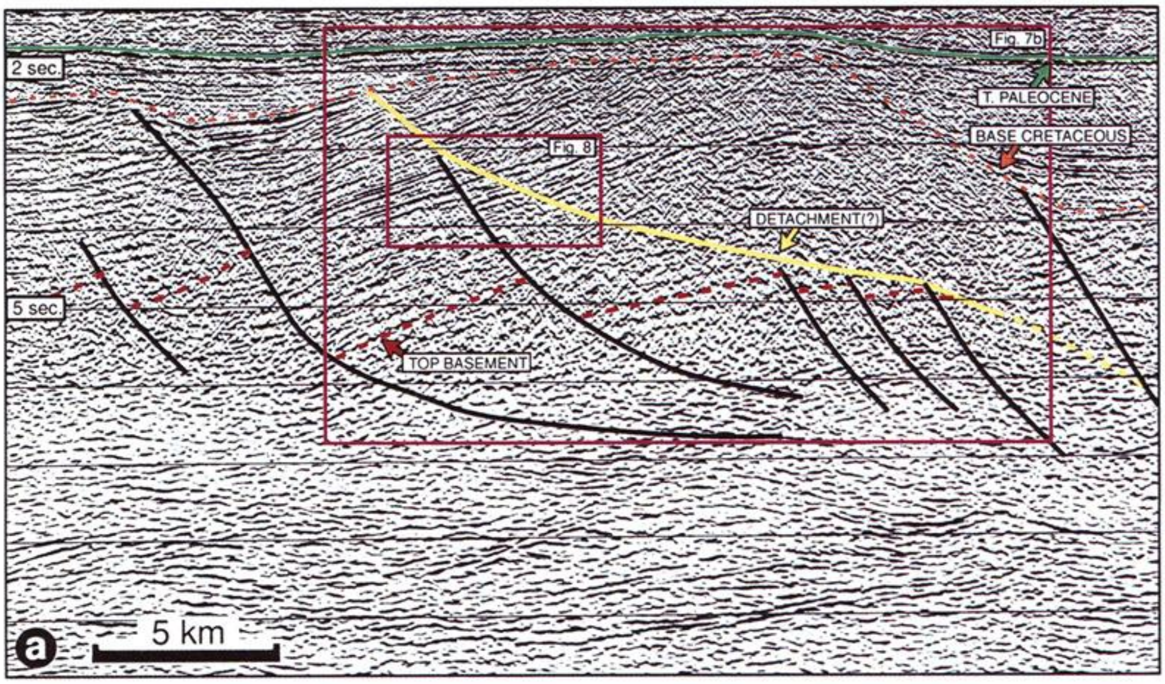

Figure 2.9- Seismic line shows basal detachment accommodate the domino style deformation (North sea; Fossen et al., 2000).

From a hydraulic perspective, the vertical orientation of σ_1 promotes the formation of sub-vertical extension fractures, creating an anisotropic permeability field. In these settings, permeability is maximized along the sub-horizontal intermediate stress axis σ_3 (parallel to the fault strike) which supports longitudinal fluid communication and reservoir connectivity over large distances (Sibson et al., 1996, 2000). This structure usually drives hydrothermal convection. In geothermal settings, high dilation tendency controls hydrothermal resources (De Filippis et al., 2013). The seismic cycle modulates these dynamics via 'fault-valve' action: fluids recharge during stress accumulation and discharge rapidly during slip (Sibson et al., 2000). In extensional environments formed by different rocks type creates dilational sites known as boudin necks, where vein minerals (fluids) precipitate due to the localized low pressure or advective fluid flow into the new pathways. The extensional fractures form perpendicular to the minimum principal stress ($\sigma 3$). The "ubiquitous" presence of these veins at depth indicates that fluid pressures often approach lithostatic levels, allowing rocks to fail in tension even under high confining pressure (Bons et al., 2012).

2.2.4- Reverse and Thrust Faults

In contractional tectonic regimes, crustal shortening is governed by a horizontal principal stress σ_1 and a vertical least principal stress σ_3. Reverse faults are characterized by a low-angle dipping (30°). These systems are frequently characterized by the structural reactivation of inherited discontinuities. The reactivation process is driven by elevated fluid pressures that reduce the effective normal stress acting upon the fault plane (Van Der Pluijm & Marshak., 2004). The geometry of these faults often drives the development of fault-propagation or fault-bend folding, where the low-angle thrust planes act as regional seals. This type of faults promotes the entrapment of fluids, allowing pore pressures to approach or even exceed lithostatic levels beneath the basal detachment (Figure 2.7). From a hydraulic perspective, contractional regimes are defined by extreme fluid over-pressuring and the most intense manifestations of fault-valve action (Sibson et al., 2000). Because the vertical stress is the minimum principal stress (σ_3), hydraulic fracturing and the resulting damage zones host complex arrays of sub-horizontal vein networks that extend into the host rock. Coseismic seal failure triggers the upward discharge of deep fluids. This fault-valve mechanism redistributes volatiles and solutes, driving the hydrothermal mineralization and fluid migration through the crust (Bons et.,2012).

2.2.5- Strike-Slip Faults

In strike-slip tectonic regimes, the stress state is defined by horizontal principal stresses σ_1 and σ_3 and a vertical intermediate stress σ_2, resulting in sub-vertical fault planes with a predominant strike-parallel displacement. These fault zones typically develop a complex internal structure, where low-permeability fault rocks surrounded the fractured host rock. This geometry creates a strong hydraulic anisotropy, driven by sealed and healed zones. The tectonic regime can have a strong control on these flow patterns. Extensional settings generate pull-apart basins where fluid flow is facilitated. In contrast, compressive regimes produce structural ridges allow to trap fluids at the depth (Sibson et al., 1992; Caine et al., 1996; Mitchell & Faulkner et al., 2009). The vertical orientation of σ_2 promotes vertical fluid flow. Tthe fault zone behaves as a high-conductivity vertical bypass, channeling deep fluids toward the surface while maintaining a strong pressure contrast with the surrounding host rock. (Fig.2.7, Mitchell & Faulkner et al., 2009). In strike-slip or shear zones, veins typically form as part of complex arrays reflecting the rotational nature of the deformation. Veins can form on the sliding plane itself; they often develop a striped or fibrous appearance known as slickenfibres. These form as minerals fill small, incrementally opening "jogs" or gaps on the fracture surface. They are excellent indicators of the shear direction and sense of movement (Bons et al., 2012). An example of slickenfibres veins is visible in Cephalonia-Lefkada fault zone, where calcium carbonate precipitate following the tectonic stress in multiple growth generations (Crosetto et al., 2025).

2.3- Geochemical and geothermal evidence of a fractured zone

Geochemical tracer characterization is essential for reconstructing crustal fluid architecture and mapping fault-zone permeability. Noble gases, carbon isotopes, and minor volatiles provide critical constraints on fault penetration depth, effectively discriminating between shallow systems and lithospheric-scale discontinuities rooting into the mantle (Batista Cruz et al., 2019). Helium is one of the most effective natural tracers for evaluating the origin of volatiles and the vertical connectivity of active faults. The isotopic ratio $^3He/^4He$ (often normalized to air ratio at R/R_a) discriminates between crustal and mantle sources (Ciotoli et al., 2004):

- **Crustal Contribution**: it is characterized by a prevalence of radiogenic ^4He produced by the decay of U and Th, with R/R_a values between 0.01 and 0.05. Faults such as the Karakoram in Tibet exhibit a dominance of crustal helium, suggesting either deformation confined within the crust or heavy dilution of mantle fluids (Zhang et al., 2024).
- **Mantle Contribution**: Mantle or magmatic sources are identified by high R/R_a ratios (up to 8 for Mid-Ocean Ridge Basalts). The presence of mantle helium along strike-slip faults, indicates that these structures penetrate through the ductile lower crust into the lithospheric mantle.

The carbon dioxide (CO_2) is another tracer for fault zones (Chiodini et al., 2000). It represents the primary component of hydrothermal gases and acts as the principal gas for tracer species. The isotopic signature of soil gas samples ($\delta^{13}C$) is essential for determining their provenance. A deep mantle-derived CO_2 component typically shows $\delta^{13}C$ values between -1‰ and -5‰; especially in correspondence of high CO_2 flux measured (Chiodini et al., 2000; Cerlig et al., 1991). In contrast, a biogenic origin is characterized by more negative values (approximately -15‰ to -30‰), reflecting the decomposition of organic matter (Cerling et al., 1991). Intermediate $\delta^{13}C$ values, generally ranging from -6‰ to -15‰, often indicate a mixture of biogenic and hydrothermal/magmatic contributions (Chiodini et al., 2000; Chiodini et al., 2004). When the CO_2 contribution is purely biogenic or represents a biogenic–hydrothermal mixture, the measured soil CO_2 fluxes are significantly lower than those associated with a purely hydrothermal or magmatic source. This behavior is well documented in volcanic and geothermal systems (e.g., Chiodini et al., 1998; Cardellini et al., 2003; Chiodini et al., 2004; Lewicki et al., 2000).

Other tracers Radon (Rn), Mercury (Hg), and Hydrogen (H_2) are good to evaluate the presence of fault fluid circulation as certain tracers are hypersensitive to crustal stress variations and micro-fracturing. Radon (^{222}Rn) is an inert gas with a short half-life, its emission increases near fault intersections and high-density damage zones. It is an excellent tracer for relative structural permeability (Ciotoli et al., 1998; Jolie et al., 2015). At the same time, mercury (Hg) and hydrogen (H_2) are released during seismic fracturing episodes. Studies on the Xianshuihe–Xiaojiang fault system in China show that Hg and H_2 anomalies coincide with maximum strain rate areas, confirming their role as indicators of fault activity (Sun et al., 2021). Another possible tracer is methane. Methan can have biogenic, thermogenic, or abiogenic origins. In the Maltese Islands, active CH_4 and CO_2 degassing through submarine faults has revealed neotectonics deformation within the last 20 ka in systems, previously considered inactive (Micallef et al., 2019).

2.4- Central Apennines

2.4.1- Focus on the Central Apennines: Faults and Seismic Crises

The Central Apennines (Umbria-Marche-Abruzzo) provide the most documented evidence of the link between fluids and faults through recent seismic sequences (Fig.2.10).

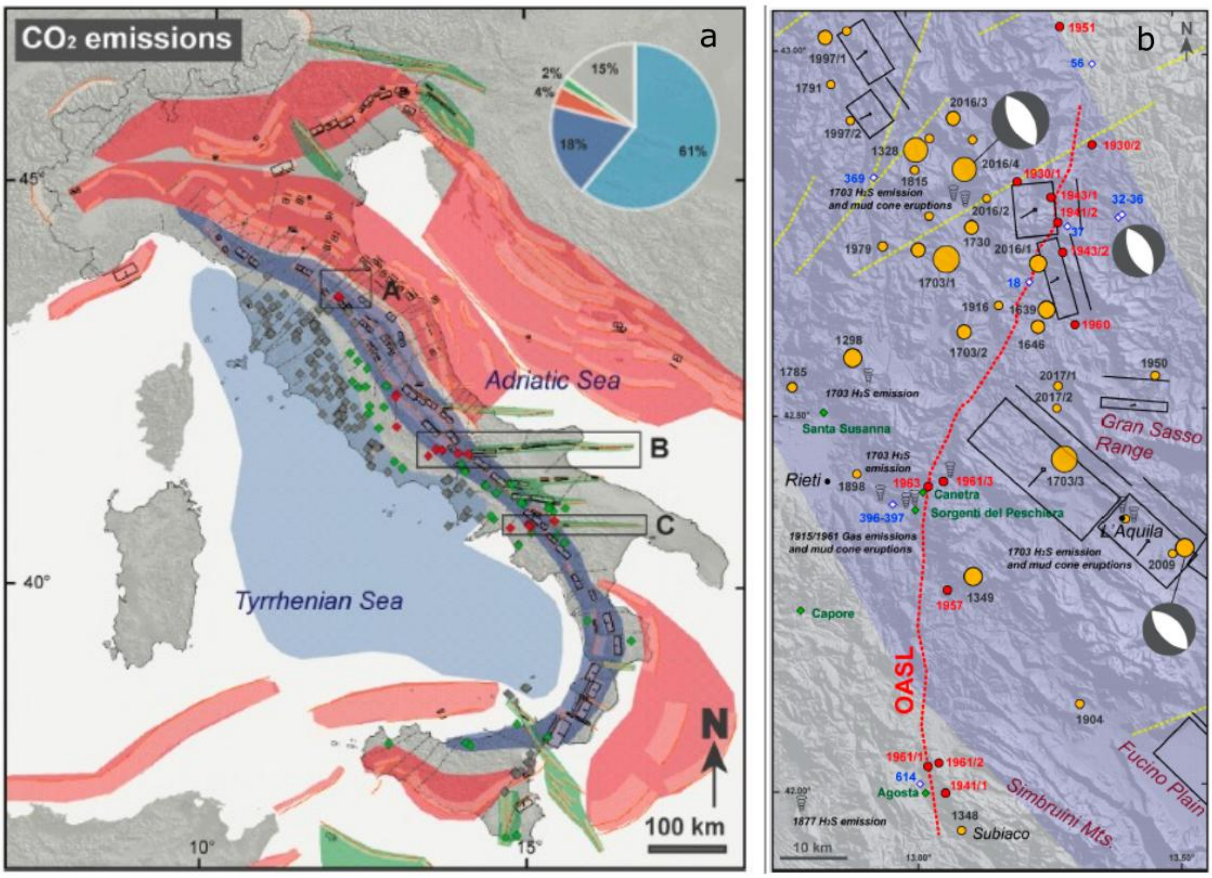

Figure 2.10- (a) Map showing the the distribution of the tectonic settings and the CO2degassing. (b)Map showing the location of the hydrothermalism in central Italy (Vannoli et al., 2021).

Chiodini et al., 2020 provides a groundbreaking 10-year record (2009–2018) that demonstrates a clear statistical correlation between tectonic CO_2 degassing and seismicity in the Italian Apennines. The authors analyzed what they termed the Central Apennine Seismic Sequence (CASS), a decade-long period of intense activity that included the major earthquakes in L'Aquila (2009), Amatrice (2016), and Norcia (2016). The data reveal that peaks in deep CO_2 flux occur concurrently with main shocks (Magnitude > 6) and that the degassing rate subsequently decays as the frequency and energy of aftershocks decrease. Over the 10-year CASS period, the total amount of CO_2 released was estimated at roughly 1,800 kilotons (kt), a volume comparable to the gas emitted during significant volcanic eruptions.

The article proposes a geodynamic model where CO_2 is produced by the melting of carbonates in the subducting Adriatic plate. This gas then upwells and accumulates in crustal reservoirs at 10–15 km depth. The high fluid pressure within these reservoirs reduces fault strength, essentially modulating the timing and evolution of the earthquake sequences.

Chiodini et al., 2011 focuses on the geochemical impact of the 2009 L'Aquila earthquake (Abruzzo region) to understand how deep-seated fluids influence seismic crises. The study involved a detailed hydrogeochemical campaign monitoring 36 large springs within the Gran Sasso and Velino regional aquifers. The source of this gas was localized directly beneath the seismic epicentral area, where seismological data previously suggested the existence of high-pressure fluid pockets at 7–10 km depth. The study estimated that approximately 530 tons per day of deep CO_2 were dissolved and transported by these groundwaters. The authors concluded that these pressurized gas reservoirs act as a primary mechanism for weakening Apennine faults, thereby triggering seismic events.

Another example in the Apennines chain the link between fluid circulation and some faults, as the The Alto Tiberina Fault (ATF). ATF is a low-angle normal fault (LANF) situated within the inner sector of the northern Apennines, at the boundary between the Tuscany, Umbria, and Marche regions. The fault bounds the western flank of the Upper Tiber Quaternary basin. The lineaments is an NNW-trending structure approximately 60 km long. It is classified as a low-angle normal fault (LANF), dipping toward the east-northeast at a shallow angle of only 15°–25°. It plays a crucial role in the circulation and trapping of deep-seated fluids. High-pressure CO_2 reservoirs (reaching 85% of the lithostatic load) have been documented in its footwall, specifically in the San Donato and Pieve Santo Stefano deep borehole (Chiaraluce et al., 2014). The ATF may act as a structural seal, creating over pressurized pockets leads to trigger seismicity in the region. The background seismicity and aftershock sequences are interpreted as the result of pore-pressure fluid pulse from the ductile shear zone toward the brittle crust. This is also evidenced by some springs, aquifers and degassing spots (Chiaraluce et a., 2014).

Also, in the southern Apennines (Matese and Irpinia), the southern sector, degassing is even more vigorous and closely tied to crustal faults. The Matese Fault System (The Ailano-Pratella-Ciorlano area) exhibits some of the highest non-volcanic CO_2 fluxes globally. Active Faults and Sinkholes shows that degassing occurs along fault segments such as the Aquae Iuliae and the South Matese fault. These acidic fluids accelerate the formation of sinkholes. Another example of southern appennine is Mefite d'Ansanto. Melfite d'ansanto is located above the hypocenter of the 1980 earthquake. Improta et al., 2014 demonstrate the presence of a mantle fault zone where gases ascend along deep lithospheric faults under the southern Apennines. Also, the seismic tomography showed that Low-velocity zones (Vp/Vs anomalies) identified beneath Irpinia are interpreted as rock volumes saturated with high-pressure gas, influencing the rupture process of large earthquakes.

2.4.2- Transverse Lineaments and Segmentation

Structural lineaments (e.g., the Olevano-Antrodoco-Sibillini Line (OASL) and the Val Marecchia Line) play a crucial role (Vannoli et al.,2021). These crustal structures segment the primary normal faults and facilitate the ascent of deep fluids and CO_2, even in areas with low heat flow. The OASL is an NNE-SSW trending structure, historically known as the Ancona–Anzio Line. It represents a fundamental geological boundary, marking the contact between the Latium–Abruzzi carbonate platform units and the Umbro–Marchean units. The authors describe it as the surface expression of a deep lithospheric discontinuity. While it is most visible in the uplifting and extending axial portion of the chain, evidence from fluid emissions and travertine deposits (e.g. Triponzo travertine) suggests it extends deeply beneath both Tyrrhenian volcanic cover and Adriatic sediments. A primary finding of the study is that the OASL acts as a deep pathway for fluids, even in areas characterized by low heat flow. The lineament hosts a high concentration of geofluid manifestations, including:

- **Thermal Springs**: At least 11 thermal springs are aligned along the structure, such as those at Acquasanta Terme (26–38°C), Amandola (38°C), Accumoli, and Marano Equo.
- **CO_2 Emissions**: At least three major CO2 degassing sites are located here: Canetra, Agosta, and the Sorgenti del Peschiera.
- **Earthquake-Induced emissions**: Following the major earthquake sequences of 1703 and 1915, the OASL was the site of transient gas and H_2S emissions, as well as mud volcano activity near Cittaducale.

The OASL plays a critical role in controlling how seismic energy is released in Central Italy. It acts as a major structural barrier that segments large seismogenic normal faults. For example, during the 1703 seismic sequence, the OASL bounded two large ruptures (Mw 6.7–6.9) that occurred to its northwest and southeast. It acts as "seismic barriers" or transfer zones control the length of the seismic rupture. Vannoli et al.,2021 conclude that the OASL is not a shallow feature of the latest tectonic phase but a permanent lithospheric weakness.

Its ability to channel mantle-derived CO_2 and thermal waters in a "cold" (low heat flow) region provides critical information on lower crustal processes and helps define the actual physical extent of the major faults responsible for Italy's largest earthquakes.

The synthesis of current evidence demonstrates that the Apennines are a complex hydrodynamic system where faults are the primary conduits for CO_2 transport from the mantle to the atmosphere. CO_2 is originating from the melting of carbonates in the subducting plate at depths of approximately 130 km, rises and accumulates in deep crustal reservoirs between 10 and 15 km (Chiodini et al., 2004). When the fluid pressure within these reservoirs exceeds the resistance of the surrounding rock, it reduces the effective stress on faults, facilitating their rupture (Frezzotti et al., 2009; Miller et al., 2004).

Chiodini et al demonstrates a statistically significant correlation between the release of tectonic CO_2 and the evolution of seismicity in the Central Apennines (Chiodini et al., 2021). Data from a 10-year record (2009–2018) shows that peaks in deep CO_2 flux occur concurrently with major shocks (Mw>6.0). The degassing rate decays following the decrease in the frequency and energy of the aftershock sequence (Chiodini et al., 2021). The architecture of faults strictly controls the migration of deep fluids. Fault damage zones and fracture networks provide high-permeability pathways for rapid gas ascent, as observed in the Matese system (Vitale et al., La Rocca et al 2023). Also, certain geological formations, particularly the Triassic Evaporites (Burano Fm), act as hydraulic seals that trap CO_2, allowing it to accumulate at pressures reaching 85% of the lithostatic load. Structures like the Alto Tiberina Fault (ATF) play a crucial role in trapping these pressurized fluids within their footwall (Minissale et al., 2004).

The flux of tectonic CO_2 emitted from Italy is massive, estimated at over 21 billion moles per year, a quantity comparable to the emissions of all subaerial volcanoes worldwide (Chiodini et al., 2021). Consequently, the large regional carbonate aquifers (such as Gran Sasso and Velino) act as giant "natural strain-meters" that monitor crustal stress by absorbing and transporting deep CO2 and hydrothermal fluids (Bonfanti et al., 2012).

2.5- Acque Albule Basin: geological framework, previous studies and new insight

2.5.1 Introduction

In this context, The Acque Albule Basin (AAB) represents a “natural laboratory” for investigating the role of active faulting in controlling deep-seated fluid pathways, as it hosts one of the most prominent hydrothermal manifestations in Central Italy. The mineralised springs in this area and the world's most productive travertine deposit seem to be related to a normal to strike-slip fault system. Understanding how faults affect fluid circulation, and the practical applications of this knowledge can be crucial for modelling geothermal areas and future geothermal energy exploration worldwide.

2.5.2 Geological and structural context

The Acque Albule Basin (AAB) is a morphological depression of about 30 km^2 located between the two towns of Bagni di Tivoli and Guidonia-Montecelio (Latium region, Rome). The AAB is bounded by Cornicolani and Lucretili Mounts on the north-east, by Aniene River on the south and by Alban Hills Volcano on the south- western sector (Fig.2.11).

Figure 2.11- Study area.

The AAB is located along the western boundary of the Neogene central Apennines fold–thrust belt (De Filippis et al.,2013; Cipollari & Cosentino, 1995; Cosentino et al., 2010; Cosentino et al., 2017). Reduced thickness of the lithosphere, volcanism, extensional basins, and high heat flow (Mongelli and Zito, 1991; De Filippis et al., 2013) are the results of the Neogene–Quaternary back-arc and post-orogenic extensional processes (Chiodini et al., 2004; Acocella and Funiciello, 2006). In this context, several pull apart basin in Central Italy developed to accommodate the deformation in the late Pleistocene; in particular, Acque Albule is mainly characterized by N-NE striking transtensional-to-normal faults (Faccenna et al., 1994; De Filippis et al., 2013) (Fig.2.12).

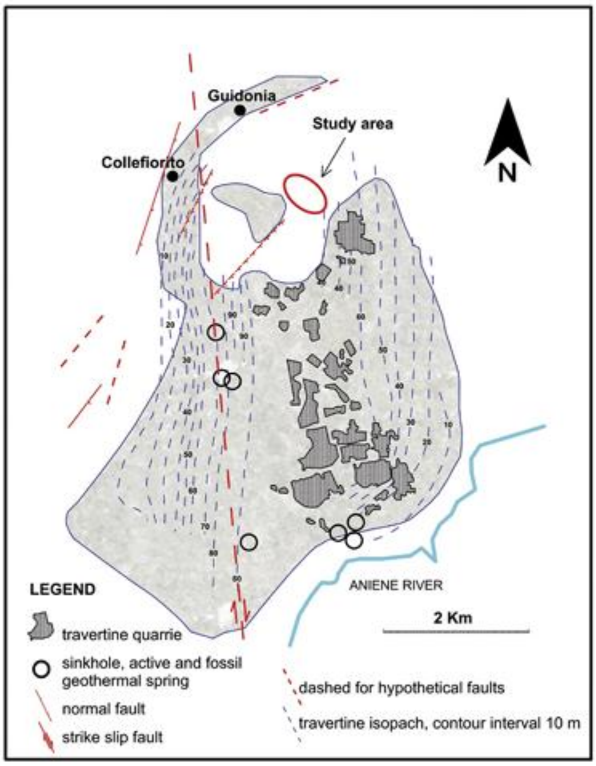

Figure 2.12- Schematic representation about the AAB (Modified after Faccenna et al., 2008).

These structures generated the transtensive depression of the Acque Albule basin. The travertine deposition is controlled by the faults activity resulting in the largest and thickest travertine plateaus in the world (Faccenna et al., 2008; De Filippis et al., 2013). The N-S strike-slip zone is well visible from Google Earth on the south side of the Cornicolani mounts (Fig.2.13).

Figure 2.13- Outcropping of the N-NE striking transtensional-to-normal faults zone in Sant'Angelo Romano.

The fault zone passes under the AAB, where numerous sinkholes and the major thickness of the travertine deposit are located (Billi et al., 2007; Faccenna et al., 2008; De Filippis et al. 2013). Presence of the N-S right striking, and NE-SW extensional faults are testified by some evidences are present, as the epicentres of the seismic swarms (2001 seismic events; Gasparini et al., 2002), the thickness and the location of the travertine deposit (Faccenna et al., 2008) and several old morphological ramp in which, faults evidence outcrops (e.g. Colle Fiorito ridge; Gasparini et al 2002.; De Filippis et al. 2013). In particular, the kinematics of the main strike-slip fault system has a right-lateral component. At Colle Fiorito di Guidonia, faults segments branch off from the main system in a N20°-40° direction with predominantly oblique kinematics (extensional and right-lateral component) (Faccenna et al., 1994, 2008). Figure 2.14 shows structures appear as faults between N-S or N20° right-lateral faults associated with extensional fractures and normal faults with an average direction around N40° 70°. The basin also hosts one of the world's most productive travertine plateaus. Travertine deposits can reach up to 90 m in thickness, particularly along the N-S fault zone.

This means that the faults activity is largely contemporary with the deposition of the travertine, suggesting a link between tectonic deformation and hydrothermal circulation. It is testified by a series of extensional fractures in the quarry area, which are the result of the fragile response of travertine lithologies to tectonic stresses, often affected by the rise of deep fluids (De Filippis et al., 2013; Faccenna et al., 2008; Billi et al., 2007).

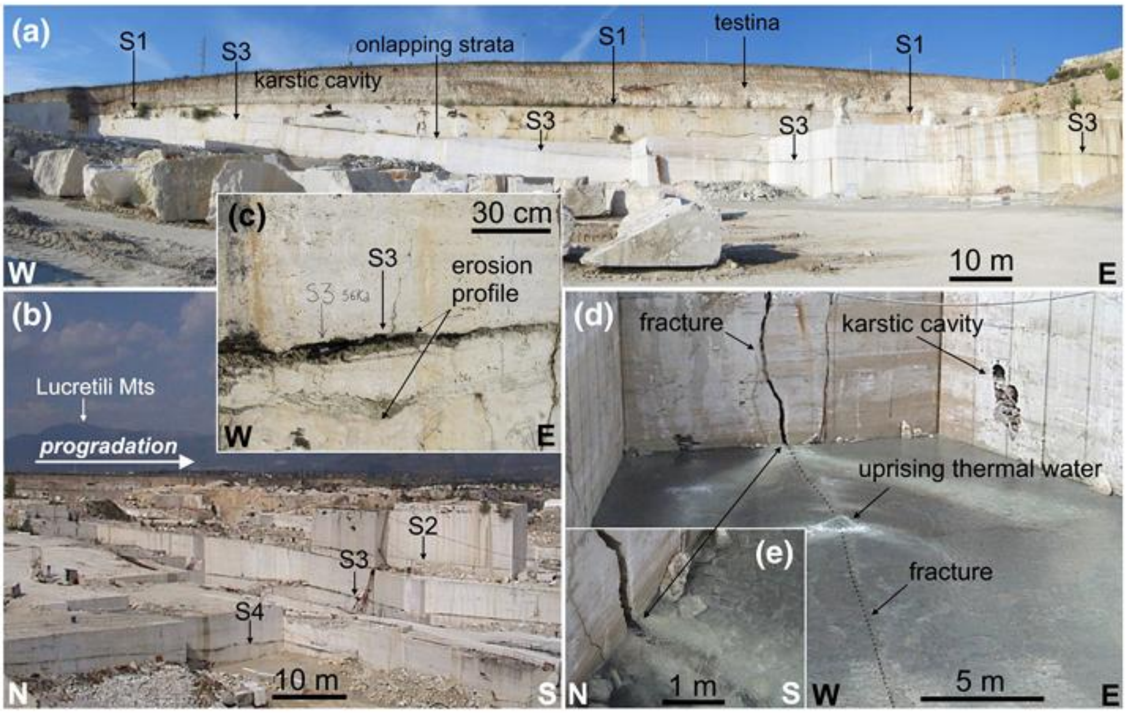

Figure 2.14- Evidence of travertine structures. Travertine is characterized by the presence of several karstic cavities, depositional structures and fractures where thermal water rise (from De Filippis et al., 2013).

2.5.3 Stratigraphic Framework

The AAB is located between the Colli Albani volcanic complex (SE); the Aniene river and and the Apennines chain on east. Lucretili and Cornicolani mounts are characterized by a thick carbonate stratigraphic succession related to the Sabine succession. Sabine deposition was characterized by a transition domain between the Laziale- Abruzzese carbonate platform and the Umbria-Marche pelagic basin. Lucretili mounts are characterized by several thrust overlapping on the recent terms of Sabine succession. The Lucretili range consists mainly of Sabina sedimentary sequences, including debris deposits derived from the adjacent carbonate platform. In contrast, the Cornicolani Mountains represent a basin-platform transition domain, largely isolated and influenced by local tectonic deformation (Cosentino et al., 2017).

On the Cornicolani mounts, the main shear zone of the Acque Albule basin is outcropping. The shear zone is characterized by the presence of several high angle faults at NNE-SSW segments.

The tectonic framework and stratigraphic setting observed at the base of the Acque Albule Basin (AAB) are comparable to those identified in the surrounding structural domains. Data from several boreholes drilled by *Società del Travertino Romano (STR)* indicate the presence of a thick carbonate succession underlying the AAB (Faccenna and Capelli, 2006, unpublished report). Moreover, the occurrence of a shear zone is supported by the alignment of sinkholes, thermal springs, and fracture networks within the travertine deposits of the basin (Billi et al., 2007; Faccenna et al., 2008; De Filippis et al., 2013; Argentieri et al., 2015).

The Acque Albule Basin is also bounded by the Colli Albani volcanic complex. Volcanism evidence in the stratigraphy is outcropping in the southern part of the AAB and to the north of the AAB (Cava Buzzi Unicem), prevalently characterized by distal volcanic deposits (fall deposits, Tufo Lionato, Pozzolane Rosse, Pozzolane Nere,Villa Senni syntem). (Fig.2.15)

Figure 2.15- Pozzolane Rosse (pyroclastic deposits) from Colli Albani Volcanic Complex (from Cava Buzzi Unicem).

On the southern part of the basin, also the Aniene and Paleo-Aniene deposits are present in the stratigraphic sequence of the AAB. These deposits are predominantly composed of clay-sandy and conglomeratic facies (Fig. 2.16).

Figure 2.16- Sandy facies from the alluvial deposits coming from lacustrine paleo-enviroment. Guidonia, Italy.

The volcanic, fluvial, and Lapidus Travertine deposits were formed contemporaneously, indicating overlapping depositional processes within the same geological timeframe. Travertine represents the most significant lithological unit in the area, not only due to its wide spatial distribution but also because of its long history of anthropogenic quarrying, which started in the Roman period. The Acque Albule Basin hosts one of the most productive travertine deposits worldwide, with thicknesses ranging from 30 to 90 meters, particularly along the N–S strike-slip fault zone (Faccenna et al., 2008). Travertine precipitation is primarily associated with extensive cold hydrothermal circulation along fault systems and was further influenced by paleoclimatic conditions that favored carbonate deposition. The deposit is characterized by strata gently dipping toward the southeast (De Filippis et al., 2013), with a progressive reduction in thickness observed toward the western sector of the fault zone. In the northern sector of the basin, Plio-Pleistocene clays outcrop above the underlying carbonate succession. According to the previous studies, the thickness of this unit ranges between approximately 200 and 300 meters.

2.5.4- Direct surveys and Geophysical Evidence

A borehole was drilled to a depth of around 100 metres in March 2023. The drilling stratigraphy is shown in Figure 2.17.

Figure 2.17- Borehole stratigraphy and location.

Drilling operations were conducted in the southern sector of Villalba, within the southernmost portion of the quarry area. The stratigraphic sequence reveals a thick travertine plateau extending to a depth of approximately 24 meters, underlain by alluvial deposits that are likely associated with the paleo-Aniene River. Specifically, borehole data indicate 24 meters of gravel, overlain by 26 meters of black clay, and a deeper sand aquifer. This investigation provided a detailed stratigraphic framework for the southern portion of the basin and offered valuable insights into the potential exploitation of the alluvial aquifer for geothermal energy purpose.

Additional geophysical investigations were conducted in the Acque Albule Basin (AAB) to identify tectono-stratigraphic discontinuities and better characterize the subsurface structure (Fig.2.18). Geophysical investigations was part of the master thesis “Vincoli sulla struttura geologica dell’area delle Acque Albule (Tivoli) dall’analisi del rumore sismico”, by MS Federica Davani.

Figure 2.18- MASW location (yellow points) and geophones location (red points) for the geophysical investigation of the Basin.

The study combined passive and active surface-wave methods, specifically Frequency Cross-Correlation (FCC) and Multichannel Analysis of Surface Waves (MASW). Passive seismic measurements were obtained from 12 stations continuously recording ambient noise for one month, enabling the extraction of Rayleigh wave dispersion curves over low frequencies (0.4–4 Hz) and exploration of greater depths, up to -300 m. Active MASW surveys employed conventional 8 kg hammer sources and, more effectively, a 20-ton travertine block, allowing acquisition of higher-frequency data (3–11 Hz) and improved resolution of shallow subsurface layers. The FCC technique determined surface-wave phase velocities by analyzing the zeros of the Bessel function in the cross-correlation spectrum, while MASW evaluated Rayleigh-wave dispersion through a frequency–wavenumber transform.

Integration of these methods provided one-dimensional profiles and a three-dimensional shear-wave velocity (Vs) model, supporting a three-layer geological framework. High-frequency MASW data revealed a thin, low-velocity intermediate layer (~25 m thick) beneath the travertine deposits, interpreted as Pliocene marine clays and sands. The Vs model showed a general NW–SE trend at the surface, with velocities increasing with depth.

Limitations related to anthropogenic noise, topography, and frequency coverage highlight the need for longer acquisition periods to enhance resolution. Overall, combining MASW and passive seismic methods provided complementary insights: MASW effectively resolves shallow, high-frequency features, while passive seismic analysis probes deeper structures. The inferred subsurface model consists of surface travertine, a thin low-velocity intermediate zone, and deeper consolidated rocks interpreted as carbonate rocks.

2.5.5- Hydrogeological framework

The Acque Albule Basin (AAB) is characterized by the interaction of multiple aquifers with distinct recharge areas (La Vigna et al., 2010). The Aniene River constitutes the main river, flowing through the southern sector of the basin before joining the Tiber River in the Roman plain. The complex tectono-stratigraphic configuration of the area results in a complex groundwater circulation system. The basin is also characterized by widespread hydrothermal activity and a significant abundance of groundwater resources.

According to the hydrogeological model proposed by La Vigna et al., 2012, three main hydrogeological complexes can be distinguished within the AAB (Figure 2.19):

- the deep Meso–Cenozoic carbonate aquifer.
- the Plio–Pleistocene sandy–clayey aquitard/aquiclude.
- the unconfined, fractured travertine aquifer forming the surface plateau.

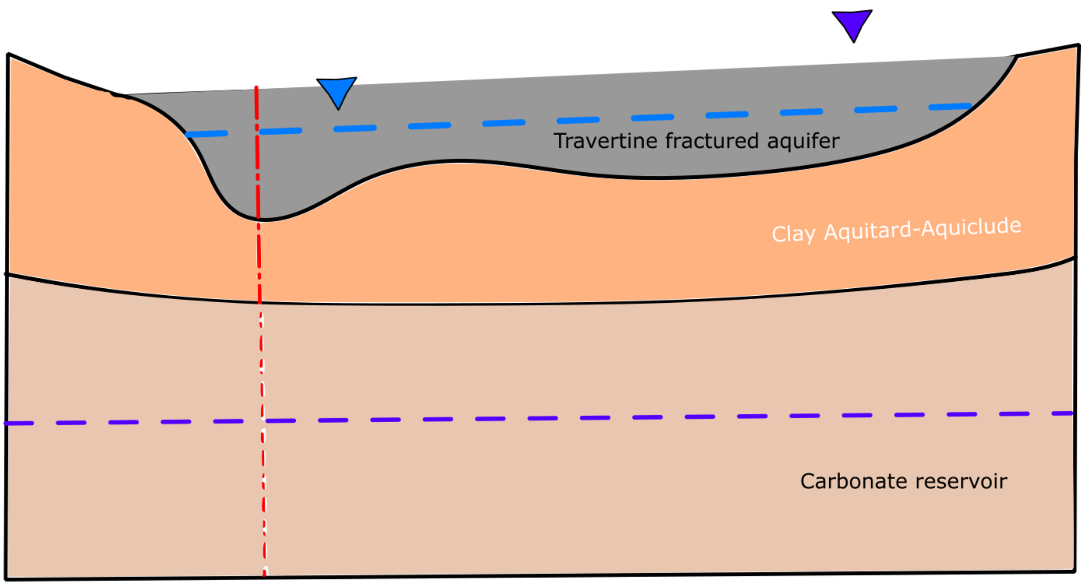

Figure 2.19- Conceptual hydrogeological scheme showing Meso-Cenozoic carbonate reservoir; Plio-pleistocene deposits aquitard and travertine aquifer.

Secondary hydrogeological units include the volcanoclastic deposits of the Alban Hills volcanic complex and the alluvial deposits surrounding the travertine plateau (Nisio, 2008).

The oldest and deepest hydrogeological unit consists of the Meso-Cenozoic carbonate bedrock, which hosts a deep, karstified aquifer laterally recharged from the carbonate ridges of the Lucretili and Cornicolani Mountains to the east and north of the basin. This unit exhibits high permeability related to their strata, fracturing and karst networks (Carucci et al., 2012; Bozzano et al., 2015; Brunetti et al., 2013). Over carbonates, Plio-Pleistocene marine and continental deposits composed predominantly of sandy-clayey sediments, which act as a discontinuous aquitard beneath the travertine body. The uppermost unit, the travertine aquifer, is characterized by a fractured and locally karstified structure, with high secondary permeability and direct recharge from meteoric infiltration (Carucci et al., 2012; Bozzano et al., 2015; Nisio, 2008; De Filippis et al., 2013).

Groundwater circulation within the AAB is strongly influenced by the structural setting and by the interaction between deep carbonate aquifers and the overlying travertine system (La Vigna et al.,2012). On the northern side of the basin, near the Cornicolani Mountains, groundwater from the carbonate substratum ascends through Neogene clayey-epivolcanic and alluvial deposits, entering the travertine aquifer (Carucci et al., 2012). Pumping tests conducted by ACEA confirmed a hydraulic connection between the carbonate aquifer and the travertine deposits, revealing the presence of thermal waters consistent with the geochemical signature of the travertine system (La Vigna et al., 2013). This link is also testified by La Vigna et al., 2012 in which, during L'Aquila earthquake (2009; 5.2 Mw) the uppermost travertine aquifer received a deeper contribution, due to the carbonate mineralized aquifer. Furthermore, the regional karst network plays a key role in sustaining groundwater recharge of the several hydrothermal springs in the basin (2 m^3/s), suggesting the presence of a deep carbonate aquifer, prevalently characterized by great geothermal temperatures and mineralization, mask by the cold karst recharge. Thus, thermal fluids ascending from the deep carbonate aquifer contribute significantly to the overall water budget of the basin. These fluids are of low-to-medium enthalpy, with temperatures reaching up to 90 °C at depth (Castorina et al., 2023; Mancini et al., 2024). At the surface, thermal springs exhibit temperatures around 23 °C, electrical conductivities of approximately 3700 μS/cm, and a total discharge estimated at about 2000 l/s (La Vigna et al., 2012).

The main hydrothermal springs within the AAB include Le Colonnelle, Regina, Barco, Autostrada, Lago dell'Inferno, and Lago Pantani (the latter two springs are now largely obliterated by anthropogenic activities). Additional thermal sources, such as Acqua Marcia and Acquoria, are actively exploited for municipal water supply by ACEA (Electricity production). Overall, the hydrogeological configuration of the Acque Albule Basin reveals a vertically and laterally connected system, where deep thermos-mineralized waters ascend through tectonic discontinuities, feeding the travertine aquifer and sustaining the long-standing hydrothermal activity that has shaped the basin since the Pleistocene. Hydrogeological sketch is represented in Figure 2.20.

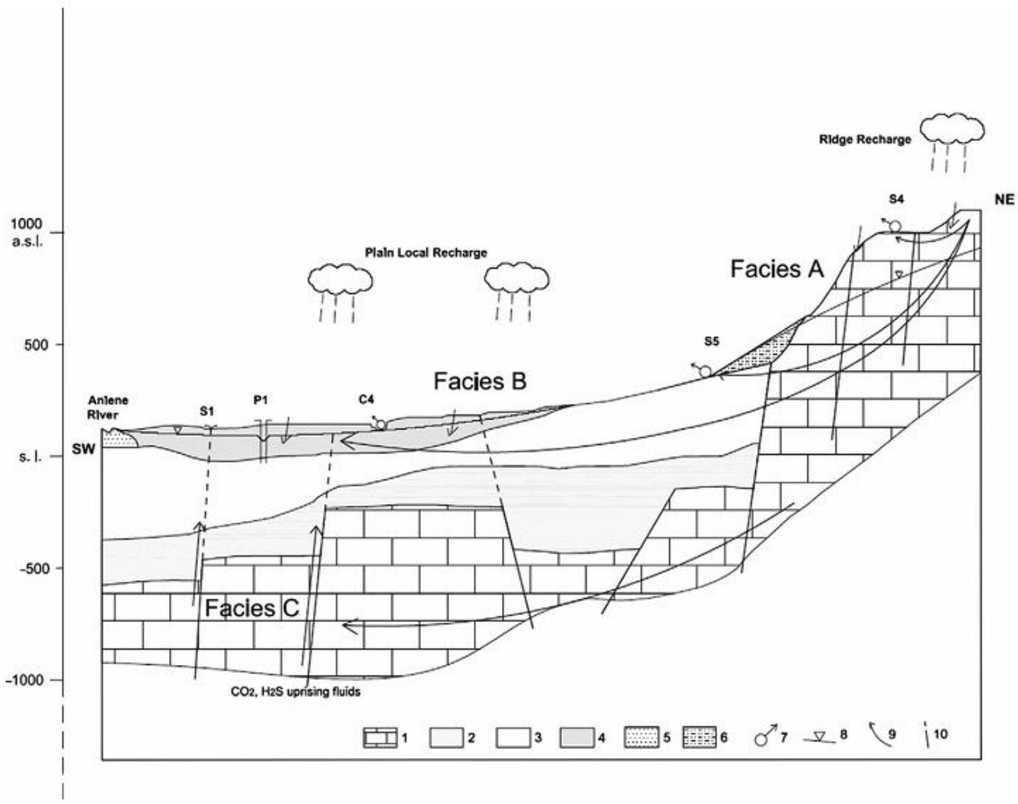

Figure 2.20- Conceptual hydrogeological and hydrogeochemical cross-section from Carucci et al., 2012. 1) Meso-Cenozoic carbonate aquifer; 2) Plio-pleistocene deposits aquitard; 3) Pleistocene alluvial and volcanic layers; 4) travertine aquifer; 5) Alluvial Aniene deposits; 6) debris deposits; 7) springs; 8) water table; 9) groundwater flowpath; 10) main faults. (From Carucci et al., 2012).

2.5.6- Anthropic activity and industrialization

Human activity in the Acque Albule Basin has been deeply influenced by travertine extraction, which has represented the dominant economic driver of the area since Roman times. Quarrying operations have significantly shaped both the landscape and the local economy. While extraction activities have ceased in the southern sector of the basin, they remain active in the northern portion, particularly around Guidonia and Collefiorito. The travertine industry also supports numerous secondary enterprises, including stone-cutting and sculpture companies. Quarry area is reported in Figure 2.21.

Figure 2.21- Photo of the STR (Società del Travertino Romano) quarry area (Guidonia, Italy).

Another major anthropogenic use of the basin's natural resources is associated with thermal water exploitation. Thermal baths are widespread throughout the area, with the principal water captions derived from the Regina and Colonnelle lakes.

The Guidonia area today is highly urbanized and industrialized, requiring substantial environmental and urban redevelopment. Large volumes of groundwater extracted from quarrying activities and other industrial processes are discharged into the Aniene River, representing a potential resource currently underutilized. The recovery and the use of this water resource, particularly for geothermal applications, could provide sustainable energy while supporting environmental rehabilitation. Integrating geothermal systems with landscape restoration and the redevelopment of abandoned quarries could convert the area into a green energy and ecological hub within the metropolitan region of Rome.

2.5.7- Geothermal Framework

From a geothermal perspective, the stratigraphy of the Acque Albule Basin (AAB) can be simplified into a permeable, fractured carbonate bedrock overlain by a complex caprock composed of Plio-Pleistocene clayey, alluvial, and epivolcanic deposits, and by the travertine plateau. While this caprock partially limits fluid migration, it still allows significant volumes of thermal water to ascend, emerging at localized springs or within the travertine deposits themselves (La Vigna et al., 2013). The area is characterized by widespread hydrothermal activity, with surface temperatures around 23 °C. Geochemical analyses of rare earth elements in the travertine indicate that sulfur in the thermal waters likely originates from Triassic evaporites at depths of approximately 90 °C; suggesting a predominantly mantle-driven thermal system rather than a magmatic contribution from the Colli Albani volcanic complex (Castorina et al., 2023; Mancini et al., 2024).

The AAB hosts one of the thickest and most productive travertine deposits worldwide, reflecting the magnitude of the hidden hydrothermal system (Minissale et al., 2002). Hydrothermal manifestations and large water volumes are closely associated with major tectonic structures, which may act as natural fluid pathways or seals. These thermal waters can be harnessed for low-enthalpy geothermal applications, offering both renewable energy and potential benefits for landscape requalification (La Vigna et al., 2013). Furthermore, the AAB provides an ideal natural laboratory to study geothermal reservoir behavior and fluid circulation. The area allows detailed investigation of how faults control permeability, how sealing processes influence fluid pathways, and how water–rock interactions occur under various chemical conditions. Understanding these dynamics is crucial for assessing reservoir potential and designing sustainable exploitation strategies in fault-controlled geothermal systems.

2.6- References

Acocella, V., & Funiciello, R. (2006). Transverse systems along the extensional Tyrrhenian margin of central Italy and their influence on volcanism. *Tectonics*, *25*(2).

Agosta, F., & Kirschner, D. L. (2003). Fluid conduits in carbonate-hosted seismogenic normal faults of central Italy. *Journal of Geophysical Research: Solid Earth*, *108*(B4).

Agosta, F., Prasad, M., & Aydin, A. (2007). Physical properties of carbonate fault rocks, fucino basin (Central Italy): implications for fault seal in platform carbonates. *Geofluids*, *7*(1), 19-32.

Argentieri, A., Carluccio, R., Cecchini, F., Chiappini, M., Ciotoli, G., De Ritis, R., ... & Venuti, A. (2015). Early stage sinkhole formation in the Acque Albule basin of central Italy from geophysical and geochemical observations. *Engineering Geology*, *191*, 36-47.

Ascione, A., Ciotoli, G., Bigi, S., Buscher, J., Mazzoli, S., Ruggiero, L., ... & Valente, E. (2018). Assessing mantle versus crustal sources for non-volcanic degassing along fault zones in the actively extending southern Apennines mountain belt (Italy). *Bulletin*, *130*(9-10), 1697-1722.

Barberio, M. D., Gori, F., Barbieri, M., Billi, A., Caracausi, A., De Luca, G., ... & Doglioni, C. (2020). New observations in Central Italy of groundwater responses to the worldwide seismicity. *Scientific Reports*, *10*(1), 17850.

Barberio, M. D., Gori, F., Barbieri, M., Boschetti, T., Caracausi, A., Cardello, G. L., & Petitta, M. (2021). Understanding the origin and mixing of deep fluids in shallow aquifers and possible implications for crustal deformation studies: San Vittorino plain, central Apennines. *Applied Sciences*, *11*(4), 1353.

Batista Cruz, R. Y., Rizzo, A. L., Grassa, F., Bernard Romero, R., González Fernández, A., Kretzschmar, T. G., & Gómez-Arias, E. (2019). Mantle degassing through continental crust triggered by active faults: The case of the Baja California Peninsula, Mexico. *Geochemistry, Geophysics, Geosystems*, *20*(4), 1912-1936.

Bellot, J. P. (2008). Hydrothermal fluids assisted crustal-scale strike-slip on the Argentat fault zone. Tectonophysics, 450(1-4), 21-33.

Bense, V. F., & Person, M. A. (2006). Faults as conduit-barrier systems to fluid flow in siliciclastic sedimentary aquifers. *Water Resources Research*, *42*(5).

Billi, A., Valle, A., Brilli, M., Faccenna, C., & Funiciello, R. (2007). Fracture-controlled fluid circulation and dissolutional weathering in sinkhole-prone carbonate rocks from central Italy. *Journal of Structural Geology*, *29*(3), 385-395.

Billi, A., Smeraglia, L., Aldega, L., Balsamo, F., Barberio, M. D., Boschi, C., ... & Tavani, S. (2023). Dolostone pulverization induced by coseismic rapid decompression of CO2-rich gas in nature (Matese, Apennines, Italy). *Earth and Planetary Science Letters*, *604*, 117996.

Bonfanti, P., Genzano, N., Heinicke, J., Italiano, F., Martinelli, G., Pergola, N., ... & Tramutoli, V. (2012). Evidence of CO 2-gas emission variations in the central Apennines (Italy) during the L'Aquila seismic sequence (March-April 2009). *Bollettino di Geofisica Teorica ed Applicata*, *53*(1).

Bonini, M. (2009). Structural controls on a carbon dioxide-driven mud volcano field in the Northern Apennines (Pieve Santo Stefano, Italy): Relations with pre-existing steep discontinuities and seismicity. *Journal of Structural Geology*, *31*(1), 44-54.

Bons, P. D., Elburg, M. A., & Gomez-Rivas, E. (2012). A review of the formation of tectonic veins and their microstructures. *Journal of structural geology*, *43*, 33-62.

Bozzano, F., Esposito, C., Franchi, S., Mazzanti, P., Perissin, D., Rocca, A., & Romano, E. (2015). Understanding the subsidence process of a quaternary plain by combining geological and hydrogeological modelling with satellite InSAR data: The Acque Albule Plain case study. *Remote Sensing of Environment*, *168*, 219-238.

Bräuer, K., Geissler, W. H., Kämpf, H., Niedermannn, S., & Rman, N. (2016). Helium and carbon isotope signatures of gas exhalations in the westernmost part of the Pannonian Basin (SE Austria/NE Slovenia): Evidence for active lithospheric mantle degassing. *Chemical Geology*, *422*, 60-70.

Brogi, A. (2008). Fault zone architecture and permeability features in siliceous sedimentary rocks: Insights from the Rapolano geothermal area (Northern Apennines, Italy). *Journal of Structural Geology*, *30*(2), 237-256.

Bruhn, R. L., Parry, W. T., Yonkee, W. A., & Thompson, T. (1994). Fracturing and hydrothermal alteration in normal fault zones. *Pure and applied geophysics*, *142*(3), 609-644.

Brunetti, E., Jones, J. P., Petitta, M., & Rudolph, D. L. (2013). Assessing the impact of large-scale dewatering on fault-controlled aquifer systems: a case study in the Acque Albule basin (Tivoli, central Italy). *Hydrogeology journal*, *21*(2), 401-423.

Carapezza, M. L., Ricci, T., Ranaldi, M., & Tarchini, L. (2009). Active degassing structures of Stromboli and variations in diffuse CO2 output related to the volcanic activity. *Journal of Volcanology and Geothermal Research*, *182*(3-4), 231-245.

Carucci, V., Petitta, M., & Aravena, R. (2012). Interaction between shallow and deep aquifers in the Tivoli Plain (Central Italy) enhanced by groundwater extraction: a multi-isotope approach and geochemical modeling. *Applied Geochemistry*, *27*(1), 266-280.

Castorina, F., Masi, U., Billi, A., De Filippis, L., & Nisi, S. (2023). Elemental and Sr–Nd isotopic evidence for unravelling the origin of the low-temperature geothermal fluids of Tivoli Terme (Latium, central Italy) between erosional S4 and S3 phases (upper Pleistocene) and neotectonics implications. *Applied Geochemistry*, *158*, 105794.

Cello, G., Invernizzi, C., Mazzoli, S., & Tondi, E. (2001). Fault properties and fluid flow patterns from Quaternary faults in the Apennines, Italy. *Tectonophysics*, *336*(1-4), 63-78.

Cerling, T. E., Solomon, D. K., Quade, J. A. Y., & Bowman, J. R. (1991). On the isotopic composition of carbon in soil carbon dioxide. *Geochimica et Cosmochimica Acta*, *55*(11), 3403-3405.

Chiaraluce, L., Amato, A., Carannante, S., Castelli, V., Cattaneo, M., Cocco, M., ... & Valoroso, L. (2014). The alto Tiberina near fault observatory (northern Apennines, Italy). *Annals of geophysics*, *57*(3).

Chiodini, G., Frondini, F., Kerrick, D. M., Rogie, J., Parello, F., Peruzzi, L., & Zanzari, A. R. (1999). Quantification of deep CO2 fluxes from Central Italy. Examples of carbon balance for regional aquifers and of soil diffuse degassing. *Chemical Geology*, *159*(1-4), 205-222.

Chiodini, G., Frondini, F., Cardellini, C., Parello, F., & Peruzzi, L. (2000). Rate of diffuse carbon dioxide Earth degassing estimated from carbon balance of regional aquifers: The case of central Apennine, Italy. *Journal of Geophysical Research: Solid Earth*, *105*(B4), 8423-8434.

Chiodini, G., Frondini, F., Cardellini, C., Granieri, D., Marini, L., & Ventura, G. (2001). CO2 degassing and energy release at Solfatara volcano, Campi Flegrei, Italy. *Journal of Geophysical Research: Solid Earth*, *106*(B8), 16213-16221.

Chiodini, G., Cardellini, C., Amato, A., Boschi, E., Caliro, S., Frondini, F., & Ventura, G. (2004). Carbon dioxide Earth degassing and seismogenesis in central and southern Italy. *Geophysical Research Letters*, *31*(7).

Chiodini, G., Baldini, A., Barberi, F., Carapezza, M. L., Cardellini, C., Frondini, F., ... & Ranaldi, M. (2007). Carbon dioxide degassing at Latera caldera (Italy): evidence of geothermal reservoir and evaluation of its potential energy. *Journal of Geophysical Research: Solid Earth*, *112*(B12).

Chiodini, G., Caliro, S., Cardellini, C., Granieri, D., Avino, R., Baldini, A., ... & Minopoli, C. (2010). Long-term variations of the Campi Flegrei, Italy, volcanic system as revealed by the monitoring of hydrothermal activity. *Journal of Geophysical Research: Solid Earth*, *115*(B3).

Chiodini, G., Caliro, S., Cardellini, C., Frondini, F., Inguaggiato, S., & Matteucci, F. (2011). Geochemical evidence for and characterization of CO2 rich gas sources in the epicentral area of the Abruzzo 2009 earthquakes. *Earth and Planetary Science Letters*, *304*(3-4), 389-398.

Chiodini, G., Cardellini, C., Di Luccio, F., Selva, J., Frondini, F., Caliro, S., ... & Ventura, G. (2020). Correlation between tectonic CO2 Earth degassing and seismicity is revealed by a 10-year record in the Apennines, Italy. *Science Advances*, *6*(35), eabc2938.

Cipollari, P., & Cosentino, D. (1995). Miocene unconformities in the Central Apennines: geodynamic significance and sedimentary basin evolution. *Tectonophysics*, *252*(1-4), 375-389.

Cosentino, D., Cipollari, P., Marsili, P., & Scrocca, D. (2010). Geology of the central Apennines: a regional review. *Journal of the virtual explorer*, *36*(11), 1-37.

Cosentino, D., Asti, R., Nocentini, M., Gliozzi, E., Kotsakis, T., Mattei, M., ... & Di Fiore, V. (2017). New insights into the onset and evolution of the central Apennine extensional intermontane basins based on the tectonically active L'Aquila Basin (central Italy). *Bulletin*, *129*(9-10), 1314-1336.

Crosetto, S., Faccenna, C., Ballato, P., Mouslopoulou, V., Begg, J., Shen, C. C., & Hu, H. M. (2025). Kinematic evolution of the Cephalonia-Lefkada transform fault zone: Strain partitioning in response to subduction margin dynamics. *Tectonics*, *44*(10), e2025TC008862.

Dallai, L., Magro, G., Petrucci, E., & Ruggieri, G. (2005). Stable isotope and noble gas isotope compositions of inclusion fluids from Larderello geothermal field (Italy): Constraints to fluid origin and mixing processes. *Journal of Volcanology and Geothermal Research*, *148*(1-2), 152-164.

De Gregorio, S., Diliberto, I. S., Giammanco, S., Gurrieri, S., & Valenza, M. (2002). Tectonic control over large-scale diffuse degassing in eastern Sicily (Italy). *Geofluids*, *2*(4), 273-284.

De Filippis, L., Anzalone, E., Billi, A., Faccenna, C., Poncia, P. P., & Sella, P. (2013). The origin and growth of a recently-active fissure ridge travertine over a seismic fault, Tivoli, Italy. *Geomorphology*, *195*, 13-26.

De Filippis, L., Faccenna, C., Billi, A., Anzalone, E., Brilli, M., Soligo, M., & Tuccimei, P. (2013). Plateau versus fissure ridge travertines from Quaternary geothermal springs of Italy and Turkey: Interactions and feedbacks between fluid discharge, paleoclimate, and tectonics. *Earth-Science Reviews*, *123*, 35-52.

Demény, A., Dallai, L., Frezzotti, M. L., Vennemann, T. W., Embey-Isztin, A., Dobosi, G., & Nagy, G. (2010). Origin of CO2 and carbonate veins in mantle-derived xenoliths in the Pannonian Basin. *Lithos*, *117*(1-4), 172-182.

Di Maio, R., Salone, R., De Paola, C., Piegari, E., & Vitale, S. (2021). 3D numerical simulations of non-volcanic CO2 degassing in active fault zones based on geophysical surveys. *Surveys in Geophysics*, *42*(6), 1443-1478.

Doglioni, C., Barba, S., Carminati, E., & Riguzzi, F. (2014). Fault on–off versus coseismic fluids reaction. *Geoscience Frontiers*, *5*(6), 767-780.

Edmonds, M. (2008). New geochemical insights into volcanic degassing. *Philosophical Transactions of the Royal Society A: Mathematical, Physical and Engineering Sciences*, *366*(1885), 4559-4579.

Erlanger, E., Bufe, A., Paris, G., D'Angeli, I., Pisani, L., Kemeny, P. C., ... & Hovius, N. (2024). Deep CO2 release and the carbon budget of the central Apennines modulated by geodynamics. *Nature Geoscience*, *17*(5), 465-471.

Etiope, G., Beneduce, P., Calcara, M., Favali, P., Frugoni, F., Schiattarella, M., & Smriglio, G. (1999). Structural pattern and CO2–CH4 degassing of Ustica Island, Southern Tyrrhenian basin. *Journal of Volcanology and Geothermal Research*, *88*(4), 291-304.

Evans, James P., Craig B. Forster, and James V. Goddard. "Permeability of fault-related rocks, and implications for hydraulic structure of fault zones." *Journal of structural Geology* 19.11 (1997): 1393-1404.

Fabrizio, A., Mulch, A., Chamberlain, P., & Aydin, A. (2008). Geochemical traces of CO2-rich fluid flow along normal faults in central Italy. *Geophysical Journal International*, *174*(2), 758-770.

Faccenna, C., Funiciello, R., Montone, P., Parotto, M., & Voltaggio, M. (1994). Late Pleistocene strike-slip tectonics in the Acque Albule basin (Tivoli, Latium). *Memorie Descrittive della Carta Geologica d'Italia*, *49*, 37-50.

Faccenna, C., Soligo, M., Billi, A., De Filippis, L., Funiciello, R., Rossetti, C., & Tuccimei, P. (2008). Late Pleistocene depositional cycles of the Lapis Tiburtinus travertine (Tivoli, Central Italy): possible influence of climate and fault activity. *Global and Planetary Change*, *63*(4), 299-308.

Fairley, J. P., & Hinds, J. J. (2004). Field observation of fluid circulation patterns in a normal fault system. *Geophysical Research Letters*, *31*(19).

Fyfe, W. S. (1997). Deep fluids and volatile recycling: crust to mantle. *Tectonophysics*, *275*(1-3), 243-251.

Frezzotti, M. L., Peccerillo, A., & Panza, G. (2009). Carbonate metasomatism and CO2 lithosphere–asthenosphere degassing beneath the Western Mediterranean: an integrated model arising from petrological and geophysical data. *Chemical Geology*, *262*(1-2), 108-120.

Frondini, F., Cardellini, C., Caliro, S., Chiodini, G., & Morgantini, N. (2012). Regional groundwater flow and interactions with deep fluids in western Apennine: the case of Narni-Amelia chain (Central Italy). *Geofluids*, *12*(2), 182-196.

Faulkner, D. R., & Rutter, E. H. (2001). Can the maintenance of overpressured fluids in large strike-slip fault zones explain their apparent weakness?. *Geology*, *29*(6), 503-506.

Gasparini, C., Di Maro, R., Pagliuca, N. M., Pirro, M., & Marchetti, A. (2002). Recent seismicity of the «Acque Albule» travertine basin. *Annals of Geophysics*, *45*(3-4).

Ghisetti, F., Kirschner, D. L., Vezzani, L., & Agosta, F. (2001). Stable isotope evidence for contrasting paleofluid circulation in thrust faults and normal faults of the central Apennines, Italy. *Journal of Geophysical Research: Solid Earth*, *106*(B5), 8811-8825.

Giammanco, S., Gurrieri, S., & Valenza, M. (1997). Soil CO2 degassing along tectonic structures of Mount Etna (Sicily): the Pernicana fault. *Applied Geochemistry*, *12*(4), 429-436.

Giammanco, S., Gurrieri, S., & Valenza, M. (2006). Fault-controlled soil CO2 degassing and shallow magma bodies: summit and lower east rift of Kilauea volcano (Hawaii), 1997. *pure and applied geophysics*, *163*(4), 853-867.

Gudmundsson, A. (2001). Fluid overpressure and flow in fault zones: field measurements and models. *Tectonophysics*, *336*(1-4), 183-197.

Healy, D. (2008). Damage patterns, stress rotations and pore fluid pressures in strike-slip fault zones. *Journal of Geophysical Research: Solid Earth*, *113*(B12).

Hickman, S., Sibson, R., & Bruhn, R. (1995). Introduction to special section: Mechanical involvement of fluids in faulting. *Journal of Geophysical Research: Solid Earth*, *100*(B7), 12831-12840.

Iacono-Marziano, G., Gaillard, F., Scaillet, B., Pichavant, M., & Chiodini, G. (2009). Role of non-mantle CO2 in the dynamics of volcano degassing: The Mount Vesuvius example. *Geology*, *37*(4), 319-322.

Improta, L., De Gori, P., & Chiarabba, C. (2014). New insights into crustal structure, Cenozoic magmatism, CO2 degassing, and seismogenesis in the southern Apennines and

Irpinia region from local earthquake tomography. *Journal of Geophysical Research: Solid Earth*, *119*(11), 8283-8311.

Italiano, F., Martinelli, G., & Plescia, P. (2008). CO2 degassing over seismic areas: the role of mechanochemical production at the study case of Central Apennines. *Pure and Applied Geophysics*, *165*(1), 75-94.

Jolie, E., Klinkmueller, M., & Moeck, I. (2015). Diffuse Degassing Measurements in Geothermal Exploration of Fault Controlled Systems. In *World Geothermal Congress 2015*.

Jolie, E., Klinkmueller, M., & Moeck, I. (2015). Diffuse surface emanations as indicator of structural permeability in fault-controlled geothermal systems. *Journal of Volcanology and Geothermal Research*, *290*, 97-113.

Jolie, E., Moeck, I., & Faulds, J. E. (2015). Quantitative structural–geological exploration of fault-controlled geothermal systems—a case study from the Basin-and-Range Province, Nevada (USA). *Geothermics*, *54*, 54-67.

Kerrick, D. M., & Caldeira, K. (1998). Metamorphic CO2 degassing from orogenic belts. *Chemical Geology*, *145*(3-4), 213-232.

Kerrick, D. M. (2001). Present and past nonanthropogenic CO2 degassing from the solid Earth. *Reviews of Geophysics*, *39*(4), 565-585.

Knipe, R. J., Jones, G., & Fisher, Q. J. (1998). Faulting, fault sealing and fluid flow in hydrocarbon reservoirs: an introduction. *Geological Society, London, Special Publications*, *147*(1), vii-xxi.

La Rocca, M., Galluzzo, D., Nardone, L., Gaudiosi, G., & Di Luccio, F. (2023). Hydrothermal seismic tremor in a wide frequency band: the nonvolcanic CO 2 degassing site of mefite d'Ansanto, Italy. *Bulletin of the Seismological Society of America*, *113*(3), 1102-1114.

La Vigna, F., Carucci, V., Mariani, I., Minelli, L., Pascale, F., Mattei, M., ... & Tallini, M. (2012). Intermediate-field hydrogeological response induced by L'Aquila earthquake: the Acque Albule hydrothermal system (Central Italy). *Italian Journal of Geosciences*, *131*(3), 475-485.

La Vigna, F., Mazza, R., & Capelli, G. (2013). Detecting the flow relationships between deep and shallow aquifers in an exploited groundwater system, using long-term monitoring data and quantitative hydrogeology: the Acque Albule basin case (Rome, Italy). *Hydrological Processes*, *27*(22), 3159-3173.

Lacroix, B., Travé, A., Buatier, M., Labaume, P., Vennemann, T., & Dubois, M. (2014). Syntectonic fluid-flow along thrust faults: Example of the South-Pyrenean fold-and-thrust belt. *Marine and Petroleum Geology*, *49*, 84-98.

Lee, H., Kim, H., Kagoshima, T., Park, J. O., Takahata, N., & Sano, Y. (2019). Mantle degassing along strike-slip faults in the Southeastern Korean Peninsula. *Scientific Reports*, *9*(1), 15334.

Leclère, H., Fabbri, O., Daniel, G., & Cappa, F. (2012). Reactivation of a strike-slip fault by fluid overpressuring in the southwestern French-Italian Alps. *Geophysical Journal International*, *189*(1), 29-37.

Lewicki, J. L., & Brantley, S. L. (2000). CO2 degassing along the San Andreas fault, Parkfield, California. *Geophysical Research Letters*, *27*(1), 5-8.

Li Vigni, L., Temovski, M., Cardellini, C., Molnár, K., Ionescu, A., Mirčovski, V., ... & D'Alessandro, W. (2025). Toward solving the mystery of elevated tectonic degassing in South Eastern Europe: Insights from gas discharges along the Vardar suture (North Macedonia). *Geochemistry, Geophysics, Geosystems*, *26*(7), e2025GC012177.

Lombardi, S., Altunina, L. K., & Beaubien, S. E. (Eds.). (2006). *Advances in the geological storage of carbon dioxide: international approaches to reduce anthropogenic greenhouse gas emissions* (Vol. 65). Springer Science & Business Media.

Magro, G., Ruggieri, G., Gianelli, G., Bellani, S., & Scandiffio, G. (2003). Helium isotopes in paleofluids and present-day fluids of the Larderello geothermal field: Constraints on the heat source. *Journal of Geophysical Research: Solid Earth*, *108*(B1), ECV-3.

Mancini, A., Cornacchia, I., Lamal, J., Capezzuoli, E., Swennen, R., & Brandano, M. (2024). Using stable isotopes in deciphering climate changes from travertine deposits: the case of the Lapis Tiburtinus succession (Acque Albule Basin, Tivoli, Central Italy). *Frontiers in Earth Science*, *12*, 1355693.

Martinelli, G., Ciolini, R., Facca, G., Fazio, F., Gherardi, F., Heinicke, J., & Pierotti, L. (2021). Tectonic-related geochemical and hydrological anomalies in Italy during the last fifty years. *Minerals*, *11*(2), 107.

Matthäi, S. K., & Roberts, S. G. (1996). The influence of fault permeability on single-phase fluid flow near fault-sand intersections: Results from steady-state high-resolution models of pressure-driven fluid flow. *AAPG bulletin*, *80*(11), 1763-1779.

McCaig, A. M., Wickham, S. M., & Taylor Jr, H. P. (1990). Deep fluid circulation in alpine shear zones, Pyrenees, France: field and oxygen isotope studies. *Contributions to Mineralogy and Petrology*, *106*(1), 41-60.

Micallef, A., Spatola, D., Caracausi, A., Italiano, F., Barreca, G., D'Amico, S., ... & Taviani, M. (2019). Active degassing across the Maltese Islands (Mediterranean Sea) and implications for its neotectonics. *Marine and Petroleum Geology*, *104*, 361-374.

Minissale, A., Magro, G., Martinelli, G., Vaselli, O., & Tassi, G. F. (2000). Fluid geochemical transect in the Northern Apennines (central-northern Italy): fluid genesis and migration and tectonic implications. *Tectonophysics*, *319*(3), 199-222.

Minissale, A., Kerrick, D. M., Magro, G., Murrell, M. T., Paladini, M., Rihs, S., ... & Vaselli, O. (2002). Geochemistry of Quaternary travertines in the region north of Rome (Italy): structural, hydrologic and paleoclimatic implications. *Earth and Planetary Science Letters*, *203*(2), 709-728.

Minissale, A. (2004). Origin, transport and discharge of CO2 in central Italy. *Earth-Science Reviews*, *66*(1-2), 89-141.

Mitchell, T. M., & Faulkner, D. R. (2009). The nature and origin of off-fault damage surrounding strike-slip fault zones with a wide range of displacements: A field study from the Atacama fault system, northern Chile. *Journal of Structural Geology*, *31*(8), 802-816.

Mongelli, F., Zito, G., Della Vedova, B. R. U. N. O., Pellis, G., Squarci, P., & Taffi, L. (1991). Geothermal regime of Italy and surrounding seas. In *Terrestrial heat flow and the lithosphere structure* (pp. 381-394). Berlin, Heidelberg: Springer Berlin Heidelberg.

Mörner, N. A., & Etiope, G. (2002). Carbon degassing from the lithosphere. *Global and Planetary Change*, *33*(1-2), 185-203.

Nisio, S. (2008). I sinkholes: problemi terminologici, meccanismi genetici, classificazione. *Memorie descrittive della carta geologica d'Italia*, *85*, 17-32.

Peiffer, L., Wanner, C., & Lewicki, J. L. (2018). Unraveling the dynamics of magmatic CO2 degassing at Mammoth Mountain, California. *Earth and planetary science letters*, *484*, 318-328.

Randazzo, P. (2022). Earth Degassing in Tectonically Active Regions: New Evidences from Southern Italy and the Balkans. Ph.D. Thesis.

Randazzo, P., Caracausi, A., Aiuppa, A., Cardellini, C., Chiodini, G., Apollaro, C., ... & Vespasiano, G. (2022). Active degassing of crustal CO2 in areas of tectonic collision: A case study from the Pollino and Calabria sectors (Southern Italy). *Frontiers in Earth Science*, *10*, 946707.

Roberts, S. J., Nunn, J. A., Cathles, L., & Cipriani, F. D. (1996). Expulsion of abnormally pressured fluids along faults. *Journal of Geophysical Research: Solid Earth*, *101*(B12), 28231-28252.

Rodríguez, F., Pérez, N. M., Melián, G. V., Padrón, E., Hernández, P. A., Asensio-Ramos, M., ... & D'Auria, L. (2021). Exploration of deep-seated geothermal reservoirs in the Canary Islands by means of soil CO2 degassing surveys. *Renewable Energy*, *164*, 1017-1028.

Rotevatn, A., & Peacock, D. C. (2018). Strike-slip reactivation of segmented normal faults: Implications for basin structure and fluid flow. *Basin Research*, *30*(6), 1264-1279.

Rufino, F., Cuoco, E., Busico, G., Caliro, S., Maletic, E. L., Avino, R., ... & Tedesco, D. (2021). Deep carbon degassing in the Matese massif chain (Southern Italy) inferred by geochemical and isotopic data. *Environmental Science and Pollution Research*, *28*(34), 46614-46626.

Sbrana, A., Marianelli, P., Belgiorno, M., Sbrana, M., & Ciani, V. (2020). Natural CO2 degassing in the Mount Amiata volcanic–geothermal area. *Journal of Volcanology and Geothermal Research*, *397*, 106852.

Seebeck, H., Nicol, A., Walsh, J. J., Childs, C., Beetham, R. D., & Pettinga, J. (2014). Fluid flow in fault zones from an active rift. *Journal of Structural Geology*, *62*, 52-64.

Sibson, R. H. (1996). Structural permeability of fluid-driven fault-fracture meshes. *Journal of Structural geology*, *18*(8), 1031-1042.

Sibson, R. H. (2000). Fluid involvement in normal faulting. *Journal of geodynamics*, *29*(3-5), 469-499.

Smeraglia, L., Berra, F., Billi, A., Boschi, C., Carminati, E., & Doglioni, C. (2016). Origin and role of fluids involved in the seismic cycle of extensional faults in carbonate rocks. *Earth and Planetary Science Letters*, *450*, 292-305.

Smith, R. Y., Lesueur, M., Kelka, U., Poulet, T., & Koehn, D. (2022). Using fractured outcrops to calculate permeability tensors: implications for geothermal fluid flow and the influence of seismic-scale faults. *Geological Magazine*, *159*(11-12), 2262-2278.

Sun, Y., Zhou, X., Yan, Y., Li, J., Fang, W., Wang, W., & Liu, Y. (2021). Soil degassing from the Xianshuihe–Xiaojiang fault system at the eastern boundary of the Chuan–Dian rhombic block, southwest China. *Frontiers in Earth Science*, *9*, 635178.

Tamang, S., Groppo, C., Girault, F., Perrier, F., & Rolfo, F. (2024). Metamorphism of dolomitic and magnesitic rocks in collisional orogens and implications for orogenic CO2 degassing. *Journal of Petrology*, *65*(4), egae021.

Tamburello, G., Aiuppa, A., Kantzas, E. P., McGonigle, A. J. S., & Ripepe, M. (2012). Passive vs. active degassing modes at an open-vent volcano (Stromboli, Italy). *Earth and Planetary Science Letters*, *359*, 106-116.

Tamburello, G., Pondrelli, S., Chiodini, G., & Rouwet, D. (2018). Global-scale control of extensional tectonics on CO2 earth degassing. *Nature communications*, *9*(1), 4608.

Taussi, M., Nisi, B., Brogi, A., Liotta, D., Zucchi, M., Venturi, S., ... & Vaselli, O. (2023). Deep regional fluid pathways in an extensional setting: The role of transfer zones in the hot and cold degassing areas of the Larderello geothermal system (Northern Apennines, Italy). *Geochemistry, Geophysics, Geosystems*, *24*(6), e2022GC010838.

Travé, A., Labaume, P., Calvet, F., & Soler, A. (1997). Sediment dewatering and pore fluid migration along thrust faults in a foreland basin inferred from isotopic and elemental geochemical analyses (Eocene southern Pyrenees, Spain). *Tectonophysics*, *282*(1-4), 375-398.

Trippetta, F., Collettini, C., Barchi, M. R., Lupattelli, A., & Mirabella, F. (2013). A multidisciplinary study of a natural example of a CO2 geological reservoir in central Italy. *International Journal of Greenhouse Gas Control*, *12*, 72-83.

Uysal, I. T., Ünal-İmer, E., Shulmeister, J., Zhao, J. X., Karabacak, V., Feng, Y. X., & Bolhar, R. (2019). Linking CO2 degassing in active fault zones to long-term changes in water balance and surface water circulation, an example from SW Turkey. *Quaternary Science Reviews*, *214*, 164-177.

Van der Pluijm, B. A., & Marshak, S. (2004). Earth structure: an introduction to structural geology and tectonics. *(No Title)*.

Vannoli, P., Martinelli, G., & Valensise, G. (2021). The seismotectonic significance of geofluids in Italy. *Frontiers in Earth Science*, *9*, 579390.

Vitale, S., Di Giuseppe, M. G., Fabozzi, C., Albanese, S., Ambrosino, M., Cicchella, D., ... & Ciarcia, S. (2025). Geophysical, geochemical, and structural investigations of natural non-volcanic degassing in Oliveto Citra area (southern Apennines): Understandings of structural controls on CO2 leakage. *Marine and Petroleum Geology*, *173*, 107264.

Wibberley, C. A., Yielding, G., & Di Toro, G. (2008). Recent advances in the understanding of fault zone internal structure: a review.

Wycherley, H., Fleet, A., & Shaw, H. (1999). Some observations on the origins of large volumes of carbon dioxide accumulations in sedimentary basins. *Marine and Petroleum Geology*, *16*(6), 489-494.

Wu, Z., & Hu, M. (2024). Definitions, classification schemes for active faults, and their application. *Geosciences*, *14*(3), 68.

Yehya, A., & Rice, J. R. (2020). Influence of fluid-assisted healing on fault permeability structure. *Journal of Geophysical Research: Solid Earth*, *125*(10), e2020JB020553.

Zhang, M., Xie, X. G., Liu, W., Liu, Y., Wang, L., Sano, Y., ... & Xu, S. (2024). Hydrothermal degassing through the Karakoram fault, western Tibet: Insights into active deformation driven by continental strike-slip faulting. *Geophysical Research Letters*, *51*(4), e2023GL106647.

Zhou, X., Chen, Z., & Cui, Y. (2016). Environmental impact of CO2, Rn, Hg degassing from the rupture zones produced by Wenchuan M s 8.0 earthquake in western Sichuan, China. *Environmental geochemistry and health*, *38*(5), 1067-1082.

3- An application of soil CO_2 degassing surveys for studying geothermal fluid circulation in pull apart basin: the case of the Acque Albule Basin.

Abstract

Soil CO_2 flux surveys represent a valuable tool for assessing subsurface permeability. While they are predominantly applied in volcanic monitoring, these measurements can also provide key insights into permeability within geothermal systems. The Acque Albule basin represents an ideal natural laboratory for investigating the role of faults in fluid circulation, as it hosts one of the most prominent cold hydrothermal manifestations worldwide. For this reason, it is of particular interest to evaluate geothermal fluid circulation, as well as the associated sealing and dissolution processes related to both ancient and newly formed fluid conduits. For constraining subsurface permeability and geothermal fluid circulation, we planned several soil CO_2 flux surveys using the accumulation chamber method. After data acquisition, a spatial distribution analysis was carried out. Soil gas samples were collected also to assess the $\delta^{13}C$ hydrothermal contribution. Results show that high-degassing zones are characterized by fluxes between 30 and 45 g/m²·day, with the maximum anomaly (~120 g/m²·day) recorded near the Regina and Colonnelle thermal lakes. The $\delta^{13}C$ define two patterns. A cluster around -1‰ and 5%, mostly spread in the western sector and a cluster of -15% and -19‰ prevalently distributed in the eastern part of the study area. The CO_2 interpolation map reveals high and low anomalies that align with N-S and NE-SW degassing trends, suggesting a structural control on fluid migration. $\delta^{13}C$ values further indicate a progressive reduction of the hydrothermal contribution from west to east, consistent with a lateral decrease in deep fluid input. These patterns show the degassing of the main N-S strike-slip fault. The south-western part of the tectonic lineament acts as the primary conduit for hydrothermal fluids. Other minor transtensive structures in the western sector (parallel to Collefiorito ridge) continue to accommodate active degassing and fluid circulation. The northern sector characterized by low degassing may be interpreted as a former fluid conduit that has progressively evolved into a structural trap, likely due to the continuous deposition of travertine along the fault zone, which reduces permeability over time. This progressive sealing process could limit the efficiency of vertical fluid migration in certain segments of the

fault, redistributing the hydrothermal flow toward more permeable pathways. As a result, fluid CO_2-rich ascent is now concentrated in localized zones and along fault segments that still act as effective conduits, highlighting the dynamic interaction between tectonic structures and mineral travertine deposition in controlling present-day fluid circulation.

3.1 Introduction

Soil CO_2 flux surveys are a valuable tool for evaluating subsurface permeability. Although primarily used in volcanic monitoring, these measurements can also offer important insights into the permeability of geothermal systems. This type of survey has been widely used in some geothermal fields, such as Larderello (Taussi et al., 2022), Torre Alfina (Carapezza et al., 2015), Latera Caldera (Chiodini et al., 2004), Reykjanes, Iceland (Fridriksson, 2006), Los Humeros in Mexico (Jentsch et al., 2006), and the Taupō Volcanic Zone, New Zealand (Rissmann et al., 2012; Hanson et al., 2014).

CO_2 flux measurements are also used to evaluate fault's activity, especially in the central Apennines (es. Chiodini et al., 2020; Amatrice and Norcia, Italy, Ciotoli et al., 2016; Italiano et al., 2008) where a large tectonic degassing is occurring (Chiodini et al., 2008). Degassing plays a crucial role as it can serve as an indicator of permeability across different geological systems, particularly in areas where gas emissions exceed the local background levels (~14 $gm^{-2}day^{-1}$). Identifying zones of enhanced permeability provides insights into the potential presence of geothermal resources at depth and helps to delineate the most suitable locations for drilling. In broader contexts, soil CO_2 flux measurements can serve as a preliminary tool for investigating fluid circulation in areas characterized by active tectonics and potential geothermal activity. Such surveys provide valuable insights into the role of faults in controlling geothermal fluid pathways and into the possible evolution of the geothermal system in real time. The Acque Albule basin represents an ideal natural laboratory for investigating the role of faults in fluid circulation, as it hosts one of the most prominent cold hydrothermal manifestations worldwide and is characterized by one of the largest travertine plateaus globally. AAB shows a distinct degassing anomaly. Despite that, no previous study about the soil CO2 degassing has been carried out before. The area is defined by a thick travertine sequence, gently dipping to the southeast, which formed contemporaneously with fault activity (Faccenna et al., 2008; De Filippis et al., 2013). The area also represents a major degassing site within the central Apennines, showing significantly higher emissions compared to neighboring regions. This is evidenced by several degassing manifestations observed following regional and local seismic events

(Gasparini et al., 2002; La Vigna et al., 2012). Thermal water discharge within the basin is closely linked to the extensive geothermal fluid circulation occurring in the plain. This circulation results from the hydraulic interaction between two different aquifers: a shallow aquifer within the travertine deposits and the deeper carbonate reservoir (La Vigna et al., 2009; La Vigna et al., 2013). The latter is a mineralized aquifer with temperatures reaching ~90 °C, and its hydrothermal activity is likely sustained either by the Colli Albani volcanic complex or by mantle-derived fluids (Castorina et al., 2023; Mancini et al., 2024). The deep aquifer significantly contributes to surface manifestations, as evidenced by numerous thermal and paleo-thermal springs outcropping across the plain (Petitta et al., 2012; La Vigna et al., 2009). Despite that, most of these springs are no longer feed today due to intensive industrial exploitation and anthropogenic development (e.g., Acqua Marcia, Barco, and Oasi). Nevertheless, several springs are still feeded today, including Regina and Colonnelle, as well as Acquoria and additional springs along the Aniene River. Their total discharge amounts to approximately 3 m^3/s, with most being exploited either for thermal bathing purposes (e.g., Regina and Colonnelle) or for electricity production (e.g., Acquoria).

The overall discharge of these thermal springs has declined, largely as a consequence of dewatering induced by quarrying activities. The area is characterized by widespread hydrothermal activity across the plain and by a substantial water supply. For this reason, it is of particular interest to evaluate geothermal fluid circulation, as well as the associated sealing and dissolution processes related to both ancient and newly formed fluid conduits. In this framework, faults can play a crucial role in controlling geothermal fluids circulation. Such an approach is also of broader relevance, as it may be applied to other geothermal systems that share similar geological and geothermal settings.

3.2 Geological background

The Acque Albule Basin (AAB) is located between the towns of Bagni di Tivoli and Guidonia (Latium region, near Rome). It is bounded to the northeast by the Cornicolani and Lucretili Mountains, to the south by the Aniene River, and to the southwest by the Alban Hills volcanic complex. The basin lies along the western margin of the Neogene Central Apennines fold-thrust belt (De Filippis et al., 2013). The AAB is predominantly characterized by N–NE striking transtensional to normal faults (Faccenna et al., 1994; De Filippis et al., 2013). Travertine deposition is strongly controlled by fault activity, leading to the development of one of the thickest and most extensive travertine plateaus worldwide (Faccenna et al., 2008; De Filippis et al., 2013). In addition, a N–S strike-slip fault zone crops out along the southern flank of the Cornicolani Mountains (Sant'Angelo Romano) and continues beneath the AAB, where numerous sinkholes are concentrated (Billi et al., 2007; Faccenna et al., 2008; De Filippis et al., 2013; Fig.3.1).

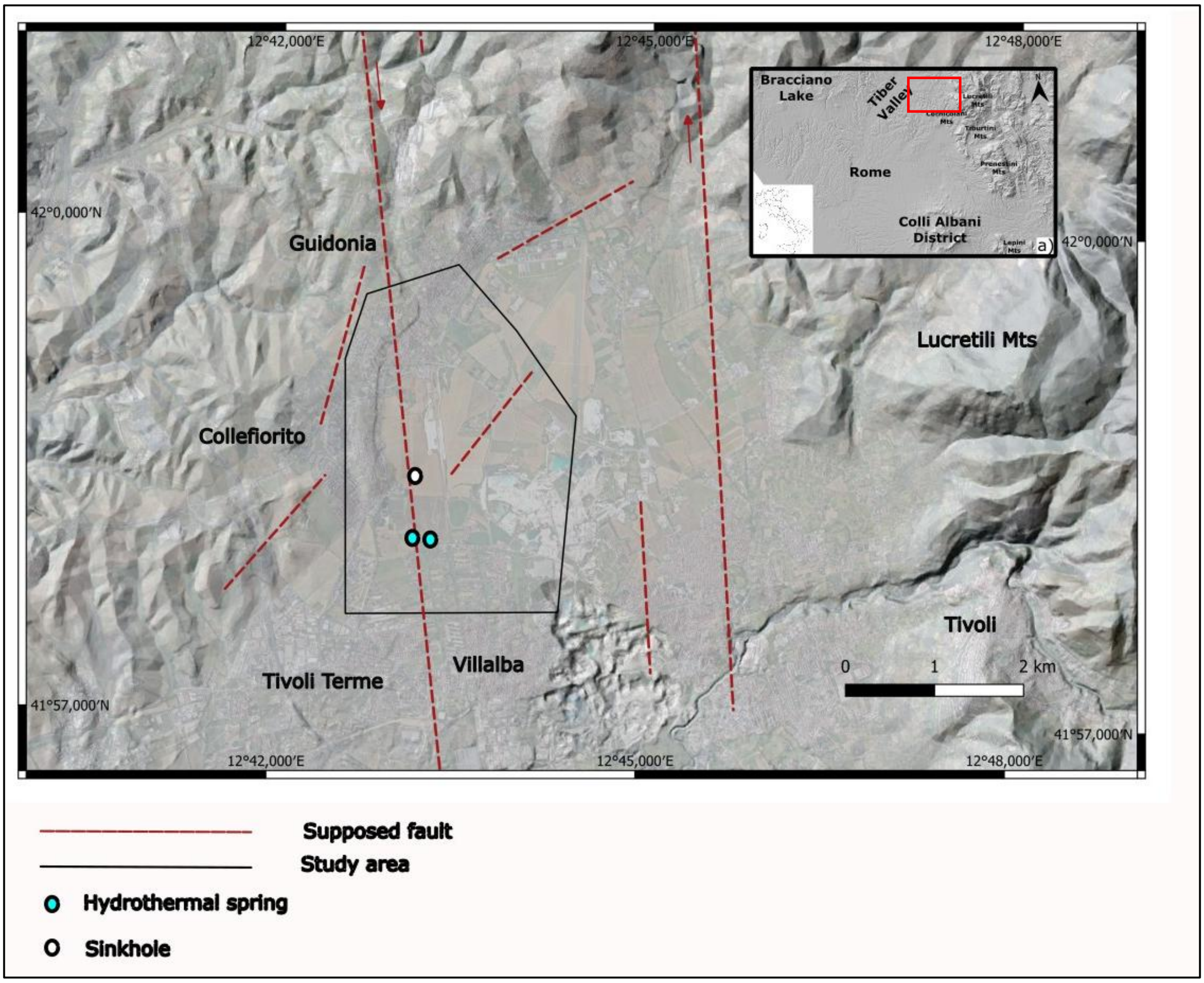

Figure 3.1 - Location of the study area

Along the Apennine chain (Mt. Lucretili and Cornicolani), Mesozoic carbonate bedrock is exposed, and these carbonate units also form the basement of the Acque Albule Basin (Petitta et al., 2011). The basin infill consists of thick Pliocene marine and continental sandy-clayey and gravelly deposits, subsequently overlain by the Lapidus Tiburtinus Travertine (Minissale et al., 2002; Faccenna et al., 2008; De Filippis et al., 2013). Within this geological framework, the fractured carbonate basement hosts a leaky confined thermal aquifer, whereas an unconfined thermal aquifer is developed within the fractured travertine and the associated porous sediments (La Vigna et al., 2013). Pliocene deposits form discontinuous aquicludes (Petitta et al., 2011; La Vigna et al., 2012). The travertine sequences record the upwelling of hot, mineralized fluids from the deep carbonate reservoir (Fig.3.2). The Regina and Colonnelle hydrothermal springs (2,000 L/s; La Vigna et al., 2012), together with several minor sources (300 L/s; La Vigna, 2012), exemplify the extensive hydrothermal circulation occurring across the plain (La Vigna et al., 2009; La Vigna et al., 2013).

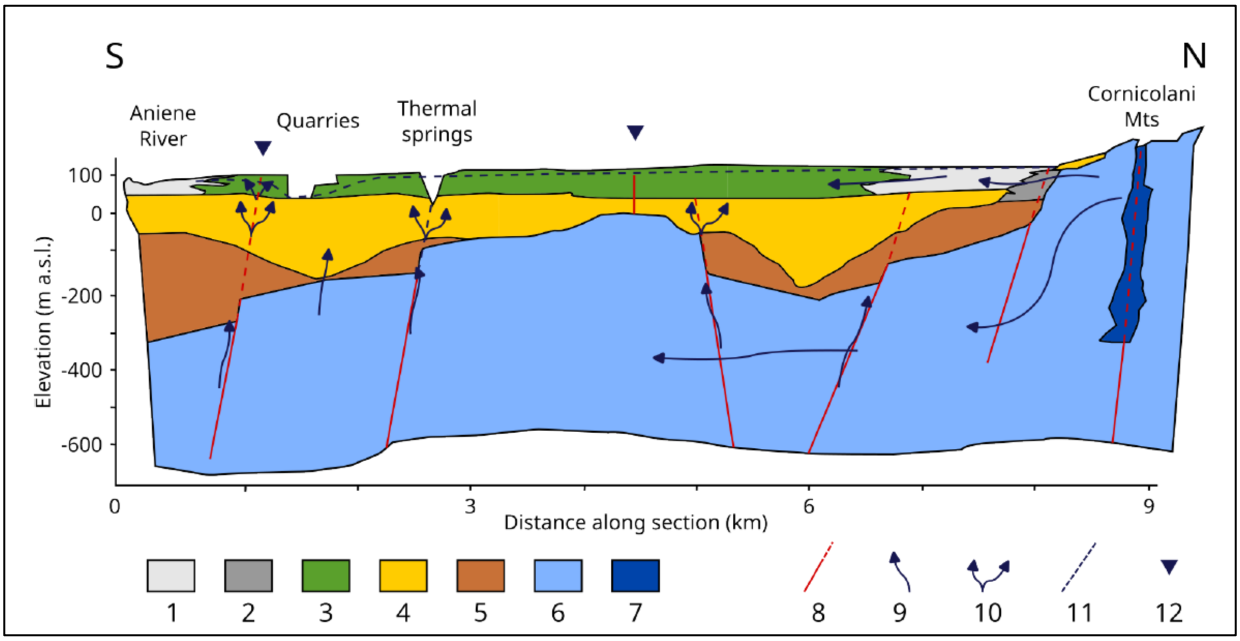

Figure 3.2 - N-S cross section modified after La Vigna et al., 2009. The main lithologies and the hydrogeological model of the AAB is represented. Respectively 1) Alluvial and colluvial deposits; 2) Debris deposits; 3) Travertine and lacustrine deposits; 4) Pleistocene alluvial and lacustrine deposits/ epivolcanic deposits; 5) Pliocene marine deposits; 6) Carbonate bedrocks; 7) Karts structure (Pozzo del Merro); 8) Faults; 9) Direction of the hydrothermal fluids; 10) Groundwater overflow; 11) Groundwater level for unconfined aquifer; 12) Groundwater level for confined aquifer.

The travertine aquifer is recharged by deep hydrothermal fluids ascending from the carbonate units, as well as by karst systems outcropping in the Cornicolani Mountains (e.g., Pozzo del Merro). These karstic structures convey cold recharge waters to depth, where they mix with hot, mineralized fluids rising along fault zones. According to recent studies (Del Bon et al., 2015; Petitta et al., 2010; La Vigna et al., 2013), the travertine aquifer is characterized by temperatures exceeding 20 °C, pH values of 6.5–7, electrical conductivity >3000 µS/cm, CO_2 saturation, and Ca-Mg-HCO_3-SO_4 chemical facies. Natural groundwater flow has been substantially altered by the large dewatering produced by quarry activity in the central part of the plain (La Vigna et al., 2012).

3.3 Methodology

3.3.1 Soil CO_2 diffuse degassing measurements

Soil CO_2 emissions are a common feature of geothermal areas (Chiodini et al., 1998; Carapezza et al., 2003; Carapezza & Granieri, 2004; Chiodini et al., 2007; Werner et al., 2006; Frondini et al., 2009; Carapezza et al., 2009; Chiodini et al., 2008). Soil CO_2 flux surveys have proven to be a robust method for constraining subsurface permeability, as geothermal zones of enhanced permeability are typically expressed as surface degassing anomalies (Chiodini et al., 2007). Permeability is a key property of geothermal fields, as it controls both the occurrence and the exploitation potential of the geothermal resource. Accumulation chamber method (Parkinson, 1981; Baubron et al., 1991) is the methodology chosen for this survey as it does not require corrections or assumptions on the characteristics of the soil. The accumulation chamber method is used to measure the soil CO_2 flux, representing the rate at which carbon dioxide is released from the soil surface to the atmosphere. The chamber is placed airtight on the soil, allowing the emitted CO_2 to accumulate within a known volume over a specific time interval. The increase in CO_2 concentration inside the chamber is continuously monitored using an infrared gas analyzer. The CO_2 flux (F) is then calculated using the 3.1 equation:

$$F = \frac{\Delta C}{\Delta t} \cdot \frac{V}{A}$$

Equation 3.1- CO_2 flux equation.

where ΔC/Δt is the rate of change in CO_2 concentration over time, V is the chamber volume, and A is the soil surface area covered by the chamber.

In this project, the accumulation chamber was developed by West Systems and consists of an infrared spectrometer (LI-COR LI-8100), a smartphone interface displaying the real-time accumulation of CO_2, and the chamber unit itself. Accumulation chamber is shown in Figure 3.3.

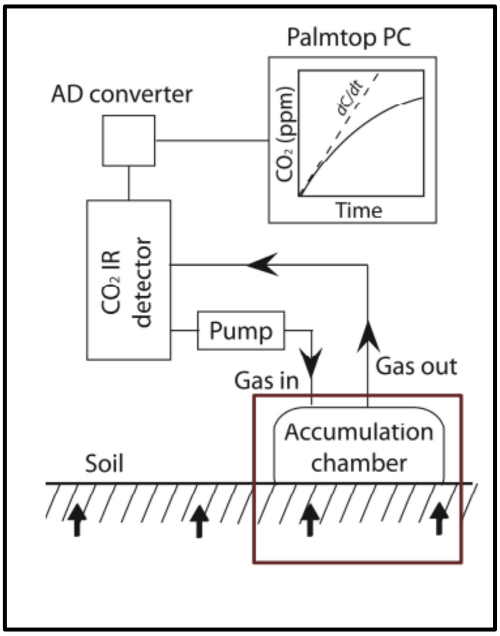

Figure 3.3- Schematic representation of the accumulation chamber for CO_2 measurements.

After data acquisition, a spatial distribution analysis was carried out to identify the pattern of faults and fractures. In addition, isotopic characterization of the CO_2 degassing allows the detection of deep hydrothermal contributions, which can be distinguished from the biogenic CO_2 background associated with plant respiration. A 100-m spaced measurement grid was implemented to investigate the main N–S fault zone (Faccenna et al., 2008) and its influence on the mineralization of the travertine aquifer. Surveys were carried out in the northern sector of the Acque Albule Basin, including the fault zone, and within an additional grid covering the Guidonia area. Unfortunately, it was not possible to investigate the military airport area in the northern part, which remain elusive. We acquired the data between January 2024 and May 2025, performing measurements only during clear and stable high-pressure conditions. The choice was made for minimizing interruptions periods and to complete the survey in the shortest time possible. Investigation points cover an area of 7 km^2 in the neighbor of Guidonia (Fig.3.4).

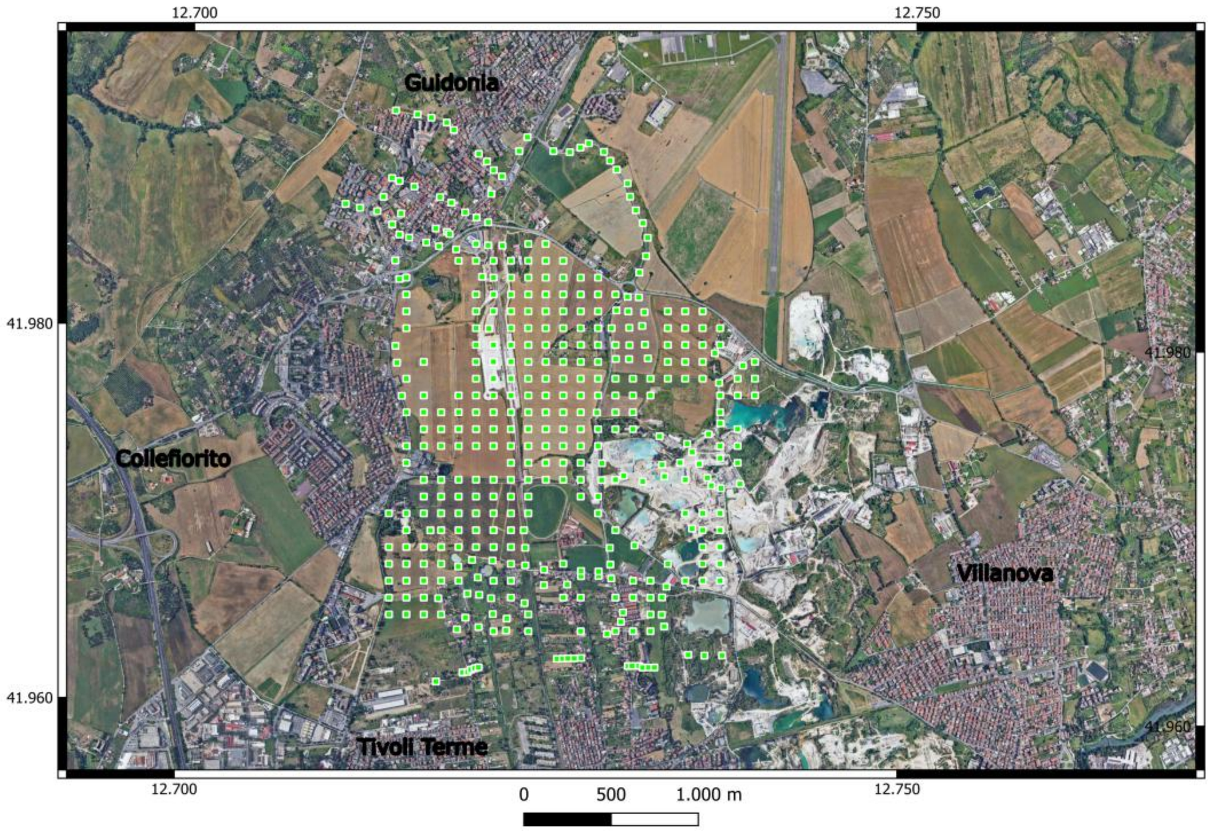

Figure 3.4 - Space grid of CO_2 measurements.

We used geostatistical methods to interpolate the spatial data. We inferred that Kriging method (David, 2012) could best fit our data. The fundamental principle behind kriging interpolation is the assumption that the spatial correlation between data points can be modelled using a variogram. By analyzing the spatial structure of the data, kriging can provide not only predictions of unknown values but also a measure of the uncertainty associated with these predictions, which is a significant advantage over other interpolation methods (eg. IDW interpolation, Voronoi polygons etc.). Kriging interpolation was performed in QGIS using the Smart Map plugin, applying an exponential model to represent the variograms (Figure 3.5a). The exponential model provided a good fit to the data distribution (distance vs. semi-variance), as confirmed by cross-validation diagrams where R^2=0.28 and RMSE= 9.047 on 405 punctual data (3.5b).

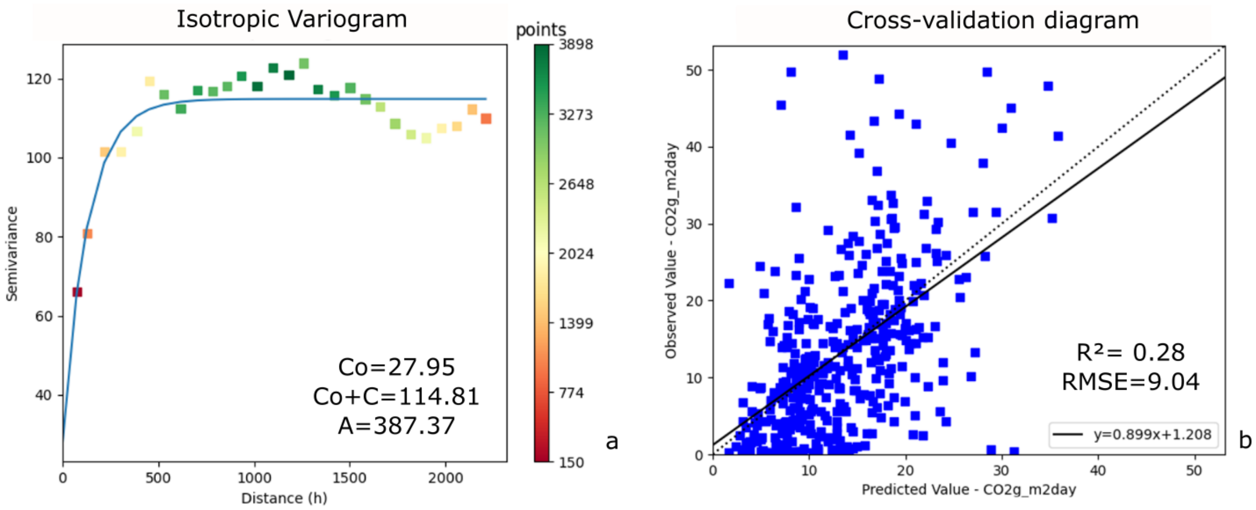

Figure 3.5- a) Isotropic variogram; b) cross validation diagram.

3.3.2 $\delta^{13}C$ analyses on gas samples

To assess the hydrothermal contribution to $\delta^{13}C$, soil gas samples were collected throughout the study area. Nineteen points were selected based on the intensity and persistence of degassing anomalies. Sampling was carried out at a depth of 30 cm using a resistant plastic probe connected via a silicone tube to a syringe, which was used to transfer the gas into pre-evacuated glass vials (Figure 3.6a). Samples were collected between January and June 2025 and subsequently analyzed at GFZ Potsdam using a Delta V Plus mass spectrometer, with an analytical precision better than ±0.1‰ relative to the VPDB (Vienna Pee Dee Belemnite) standard (3.6b).

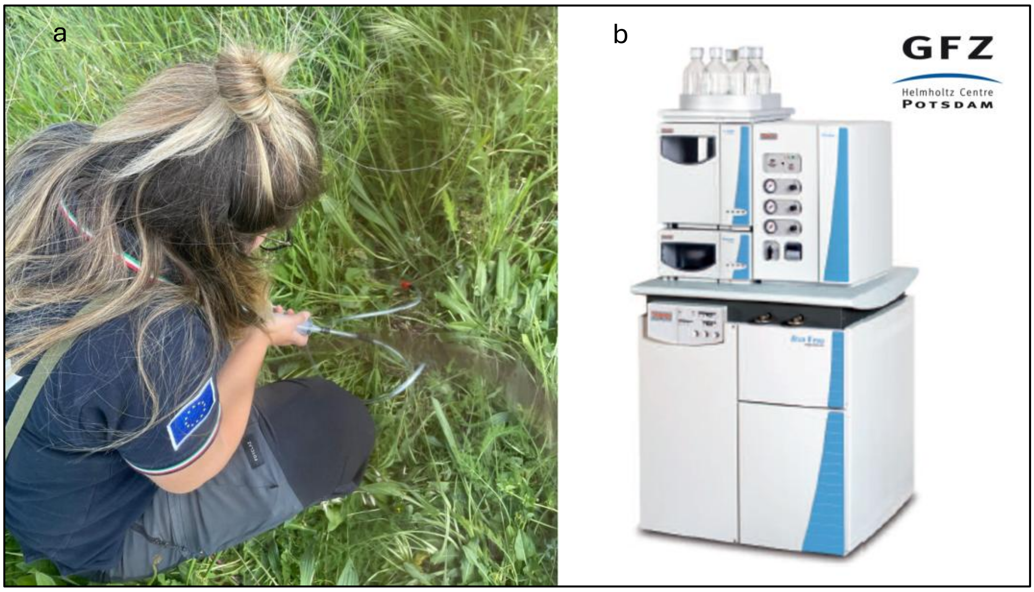

Figure 3.6- (a) Soil Gas sampling for the $\delta^{13}C$ analyses. (b) Delta V Plus mass spectrometer

3.4 Results

The interpolation results are presented in Fig. 3.7.

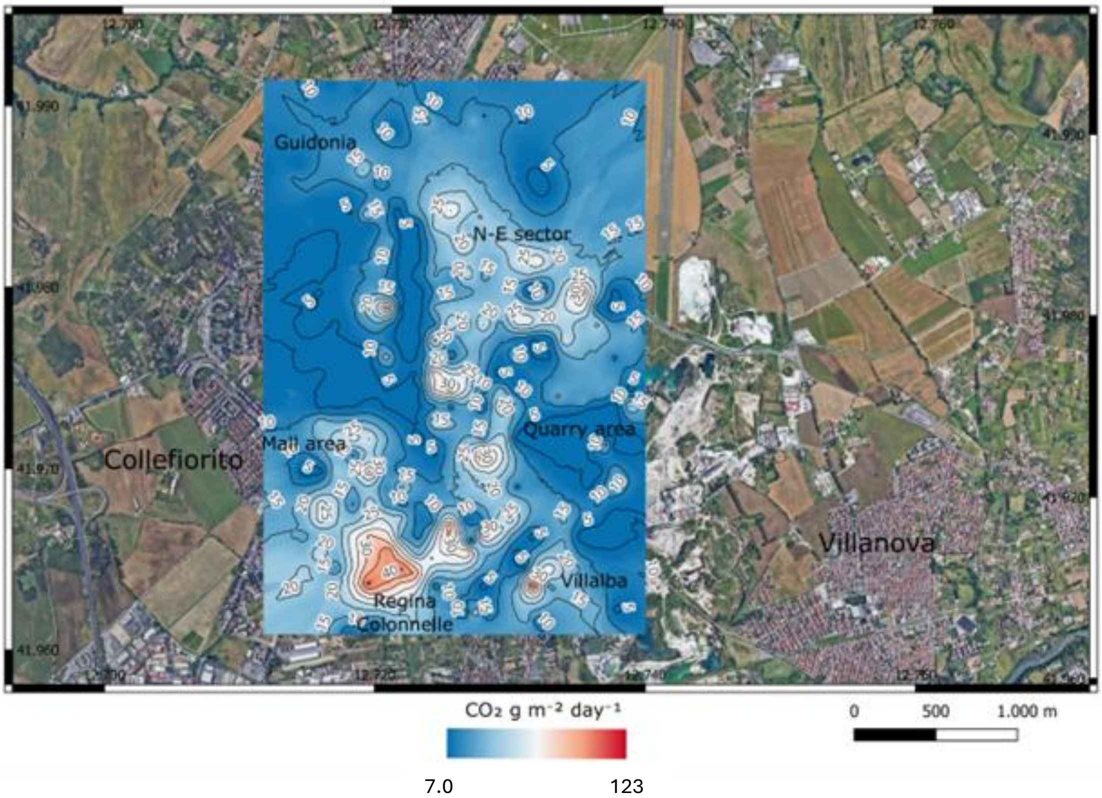

Figure 3.7- Soil CO_2 interpolated map.

Soil CO_2 flux data measured in the AAB field are represented in Tab. 3.1 (Chapter 7, Appendix A). We measured 403 points. Soil CO_2 flux samples are evenly spatially distributed across the study area. High-degassing zones (in red) are characterized by fluxes between 30 and 45 g/m²·day, with the maximum anomaly (~120 g/m²·day) recorded near the Regina and Colonnelle thermal lakes. These anomalies are bordered by areas of lower degassing. In particular, four high degassing spots are present in the western part of the area, and eight high degassing area are present in the eastern part. Degassing spots are mostly spreaded on the mall area (W); Regina and Colonnelle lakes and in proximity of Villalba, in the southern side. Low-flux zones are mainly concentrated within the quarry sector where the travertine outcrops; to the east and along a N–S-trending belt, comprehending the central portion of the area. This low degassing area comprehend the new railway of Guidonia and part of the southern farmlands; showing values of low degassing even if a biogenic background is present. The average value of degassing in the Guidonia area is 14.538 gm-

$^{2}day^{-1}$. The average degassing in the Guidonia study area, express in tons for days is 94.55 t/d.

A Normal Probability Plot (NPP; Chiodini et al., 2008) has been done to identify the population of data, to look for any different origin of the CO_2 degassing. Plot is presenting in Fig.3.8. The graph demonstrates the probability of cumulative frequency and the log of measured soil CO_2 fluxes. The inflection points show several populations composing the dataset. We recognized three populations based on the two thresholds. The first inflection point is calculated at y= 0.4 that correspond to 2.8 $gm^{-2}d^{-1}$ and the second point is y= 1.5, estimated at 32.2 g $m^{-2}d^{-1}$.

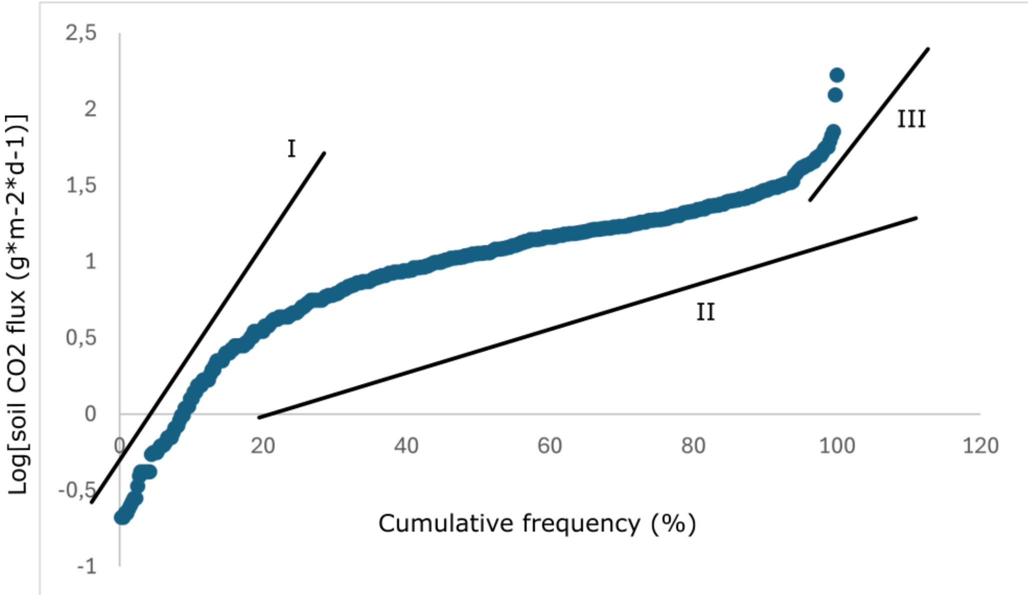

Figure 3.8- Normal Probability Plot (NPP). Black lines show the three populations.

Furthermore, the soil CO_2 flux dataset was combined with δ¹³C values reported in Fig.3.7.

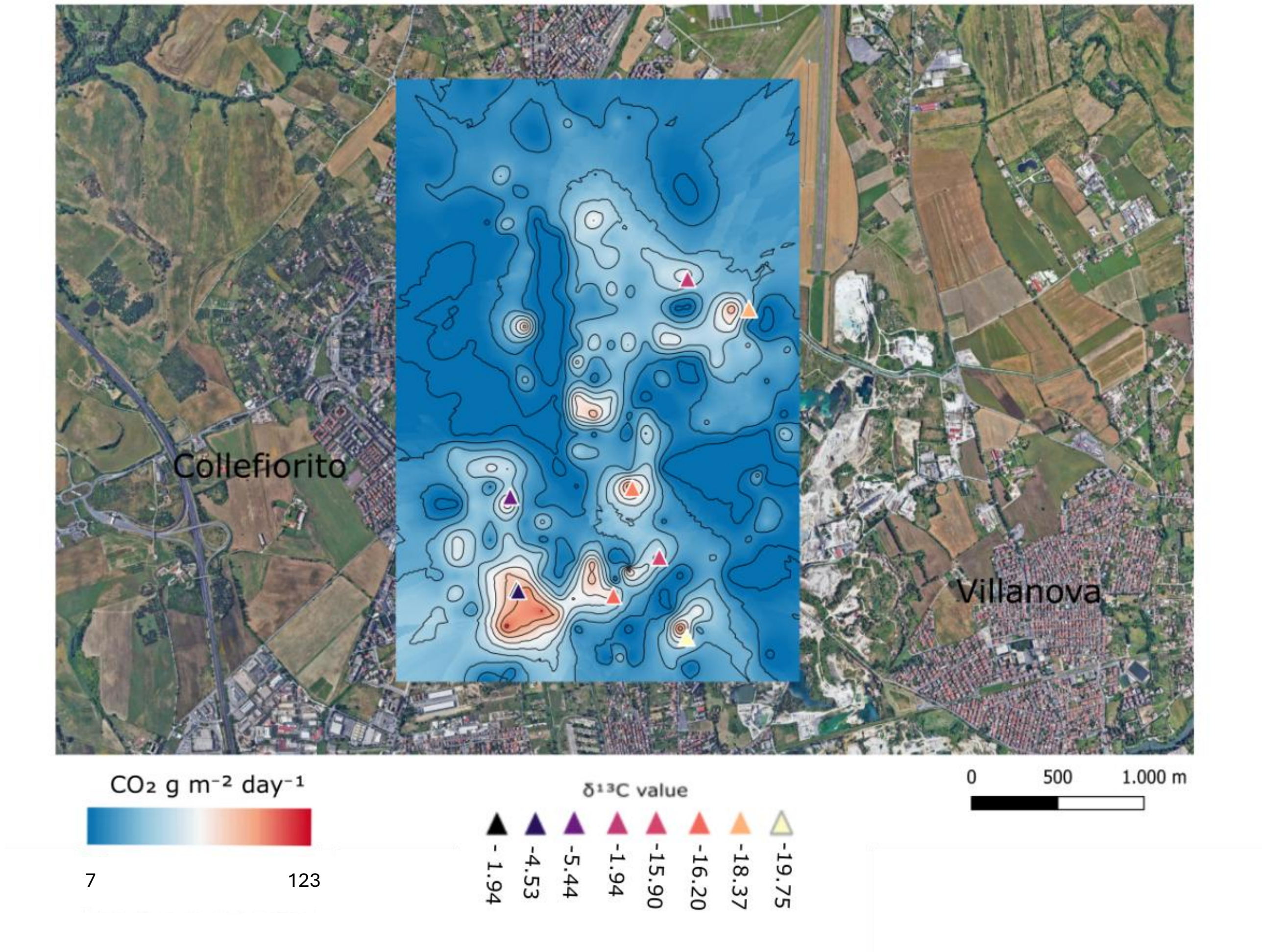

Figure 3.9- Soil CO2 interpolated map with d13C values.

Triangles indicate sampling sites located in proximity to CO_2 anomalies. At least two samples were taken from nine sites where degassing levels were higher (L1, 3 vials, L2 4 vials, L3, 2 vials, L4, 4 vials, L5, 2 vials, L6, 2 vials, L8, 2 vials) except for L7 and L9 (1 vial each). Degassing sites are reported in Figure 3.9 with triangles. Due to the same geographic coordinates, we have chosen to show only the most representative value on the map. Darker triangles correspond to higher δ¹³C values, reflecting a hydrothermal contribution, whereas lighter triangles denote lower δ¹³C values, indicative of a predominantly biogenic source. The complete set of δ¹³C measurements is reported in Table 3.2 (Chapter 7, Appendix A). Purple triangles (hydrothermal component) are distributed in the two anomalies of the western sector as shown by the Fig.3.9. Two points comprehending mixing degassing component are spreaded on the northern part of the study area and on the south/eastern part of the area. Finally, biogenic contributions are spreaded on three degassing anomalies located in the eastern part of the measured area.

The $\delta^{13}C$ values, plotted against CO_2 fluxes, define two distinct patterns (Fig. 3.10). A cluster around -1‰ and -5%, mostly spread in the western sector and a cluster from -15% to -19‰ prevalently distributed in the eastern part of the study area.

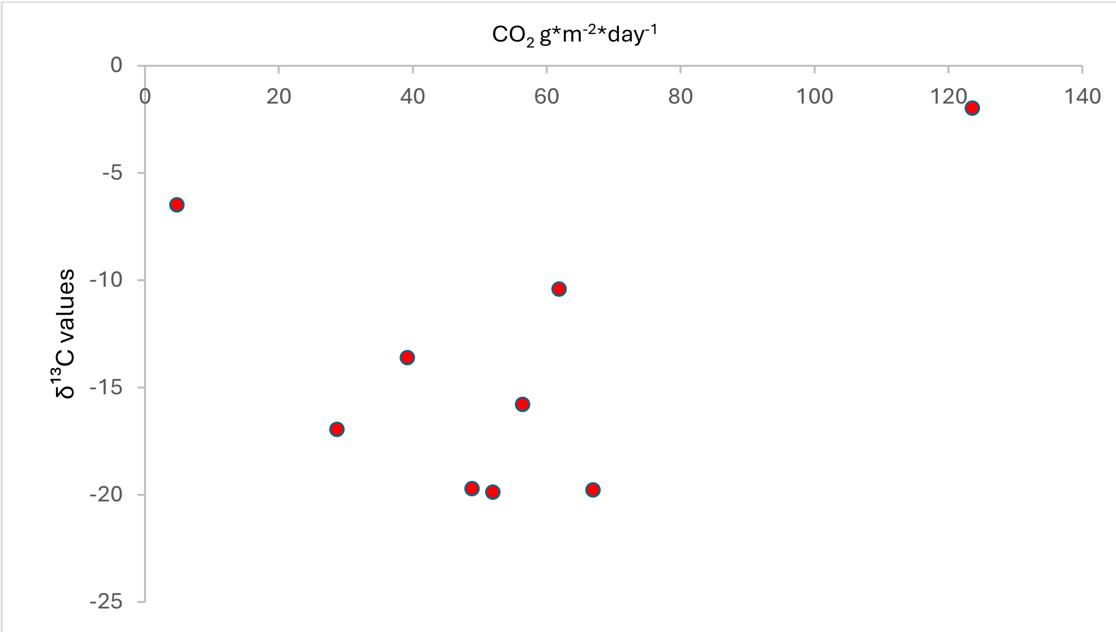

Figure 3.9- Potted values of $\delta^{13}C$ values respect to the higher CO_2 flux.

3.5 Discussion

The CO_2 interpolation map reveals high and low anomalies that align with N–S and NE–SW degassing trends, suggesting a structural control on fluid migration. These degassing patterns are consistent with the structural features reported by De Filippis et al. (2013) and Billi et al. (2007) and appear to follow the normal to strike-slip fault systems described in previous studies (Fig.3.11). The Normal Probability Plot (NPP, Fig. 3.8) shows three types of population.

The first population may correspond to high-compact travertine degassing with an end-member value of 2.5 g m^{-2} d^{-1}.The second population reflects a biogenic background, characterized by an end-member of 32.2 g m^{-2} d^{-1}. Finally, fluxes greater than 32.2 g m^{-2} d^{-1} represent a third population, which can be attributed to predominantly hydrothermal degassing or a mixture between biogenic and hydrothermal.

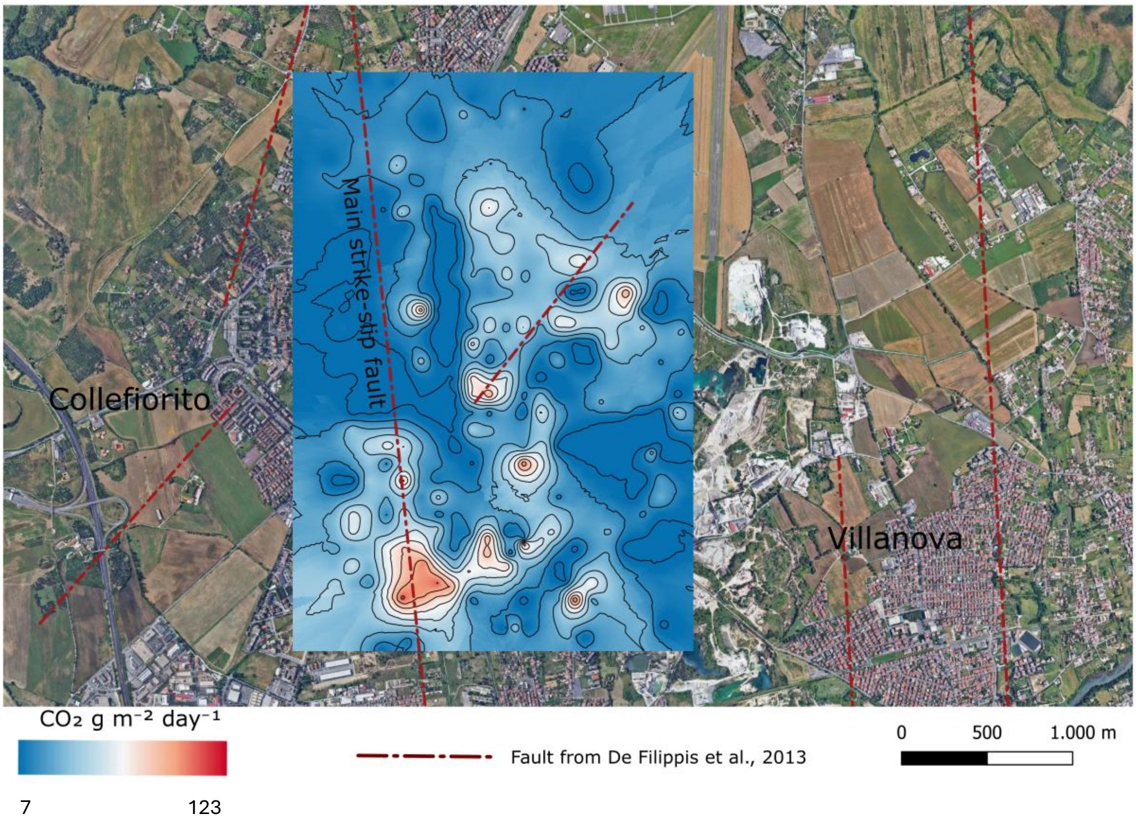

Figure 3.11- Soil CO_2 interpolated map compared with tectonic settings described by De Filippis et al., 2013.

The spatial overlap between anomalously high soil CO_2 fluxes and hydrothermal spring discharge indicates that diffuse degassing represents the near-surface expression of deep hydrothermal circulation. The low-degassing zone (5–10 g m^{-2} d^{-1}) aligned with the N–S Guidonia fault may reflect a barrier effect on vertical permeability along fault planes, while potentially maintaining lateral hydrothermal connectivity at depth. Conversely, the highest fluxes (>80 g m^{-2} d^{-1}) measured in proximity to the Regina and Colonnelle lakes highlight zones where structural discontinuities promote both thermal water upwelling and enhanced CO_2 release, emphasizing the role of fault-controlled permeability in governing fluid migration.

Interpreted in the context of soil CO_2 fluxes and the geological framework of the AAB described by De Filippis et al., (2013), these findings suggest that hydrothermal circulation is most pronounced in the western sector of the study area. Our data further indicate that hydrothermal CO_2 degassing is spatially associated with the major flux anomalies near the Regina and Colonnelle springs. Elevated $\delta^{13}C$ values (approximately -1/-5‰) are predominantly distributed along the N–S fault zone, with only a single mixed-biogenic-hydrothermal signature detected further east. In contrast, mixed and predominantly biogenic contributions (around -19‰) are chiefly concentrated within the high-flux anomalies in the eastern to southeastern portion of the basin (Figure 3.12 a,b). Plotting our main values (Table 3.2, Chapter 7, Appendix A) on the Chiodini et al. (2008) diagram, it is shown that our data span a range from hydrothermal to purely biogenic sources, highlighting a mixed hydrothermal-biogenic component in the plain (Figure 3.13). $\delta^{13}C$ values further indicate a progressive reduction of the hydrothermal contribution from west to east, consistent with a lateral decrease in deep fluid input.

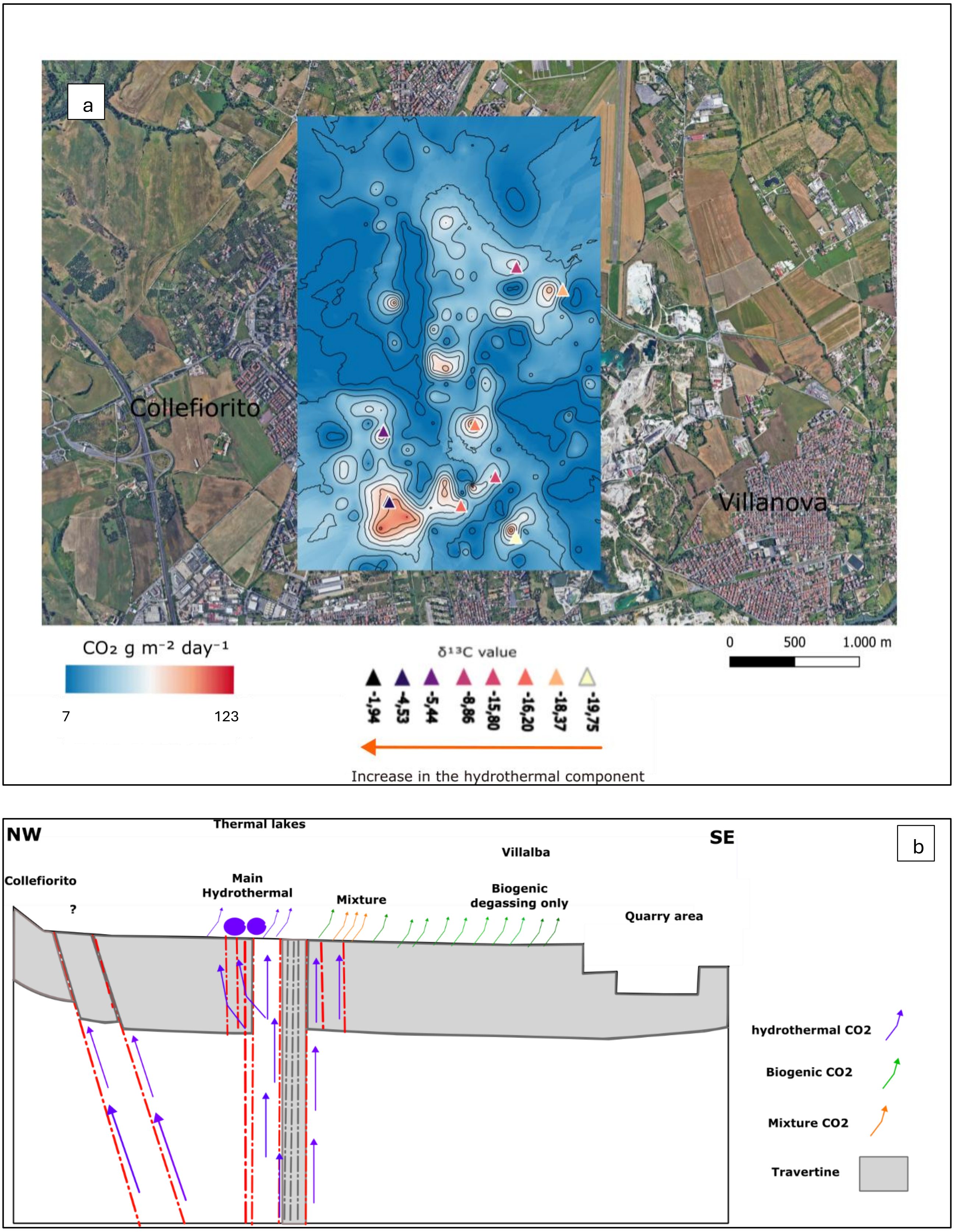

Figure 3.12- Interpolation map with the $\delta^{13}C$ values and the respective profile. As mentioned, hydrothermalism becoming higher in the western sector, as the higher values (represented by darkest triangle) becoming darker toward east.

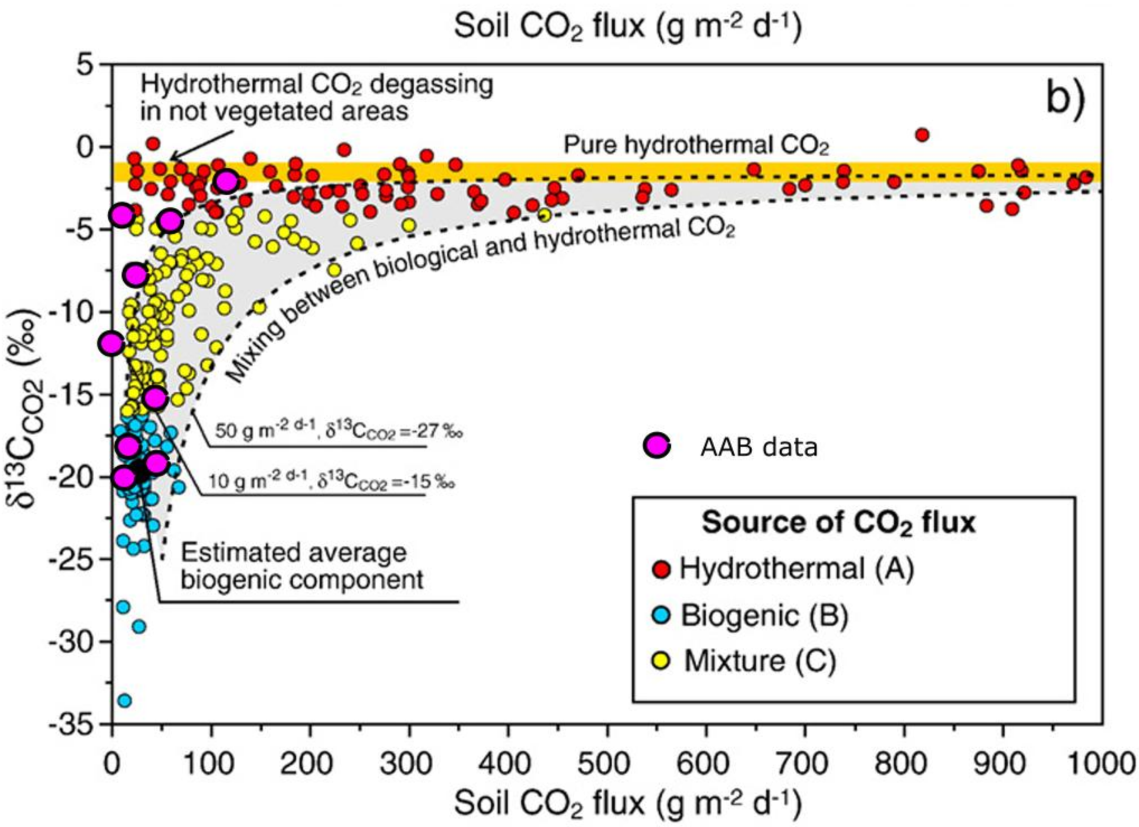

Figure 3.13- Diagram plotting the CO_2 flux vs. carbon isotopic composition of soil CO2 efflux of Phlegrean Field. Purple points representing plotted values from the AAB degassing (modified after Chiodini et al., 2008)

These patterns support the interpretation that the AAB is a pull-apart basin, where the south-western part of the major N–S strike-slip fault zone (Billi et al., 2007) acts as the primary conduit for hydrothermal fluids, while minor transtensive structures in the western sector (Collefiorito ridge) continue to accommodate active degassing and fluid circulation. The upwelling of thermal waters at the Regina and Colonnelle lakes demonstrates that fluid circulation is facilitated not only along the principal tectonic structure, but it can also coincide within the transtensive NE–SW fault system related to the Colle Fiorito Ridge. This interpretation is consistent with De Filippis et al. (2013), who also documented evidence of recent travertine deposition and ongoing degassing in the Colle Fiorito ridge. The sector characterized by low degassing may be interpreted as a former fluid conduit that has progressively evolved into a structural trap, likely due to the continuous deposition of travertine along the fault zone, which reduces permeability over time as shown by Figure 3.14.

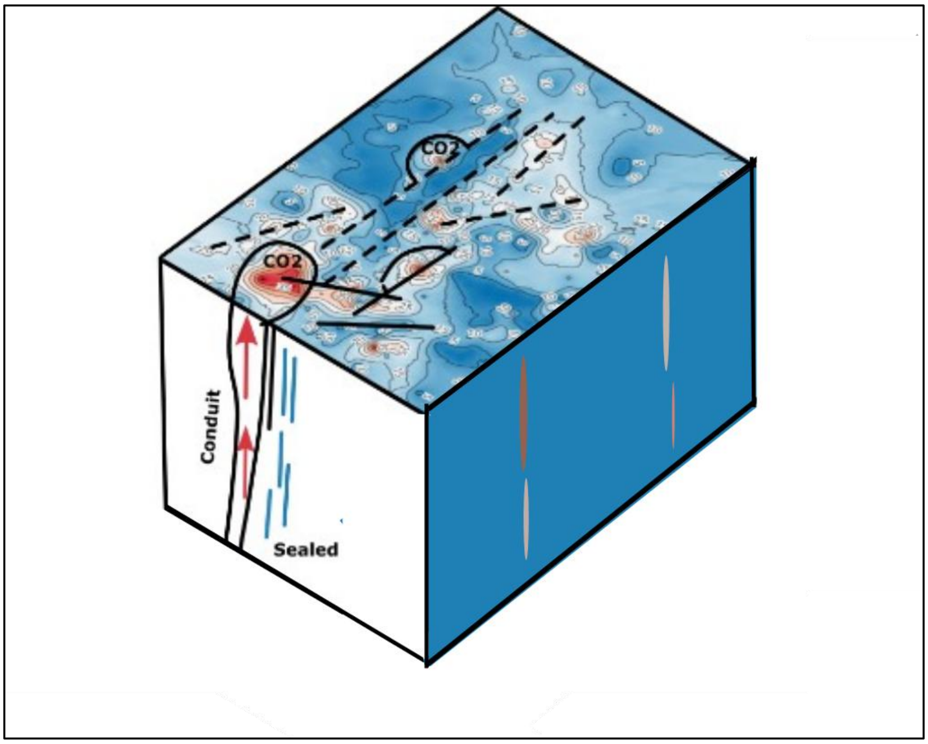

Figure 3.14- A preliminary 3D model showing the role of the N-S strike slip fault in the geothermal fluid circulation in the AAB.

This progressive sealing process could limit the efficiency of vertical fluid migration in certain segments of the fault, redistributing the hydrothermal flow toward more permeable pathways. As a result, fluid ascent is now concentrated in localized zones and along fault segments that still act as effective conduits, highlighting the dynamic interaction between tectonic structures and mineral deposition in controlling present-day fluid circulation.

A preliminary NW-SE cross-section of fluid circulation is outlined in Figure 3.15.

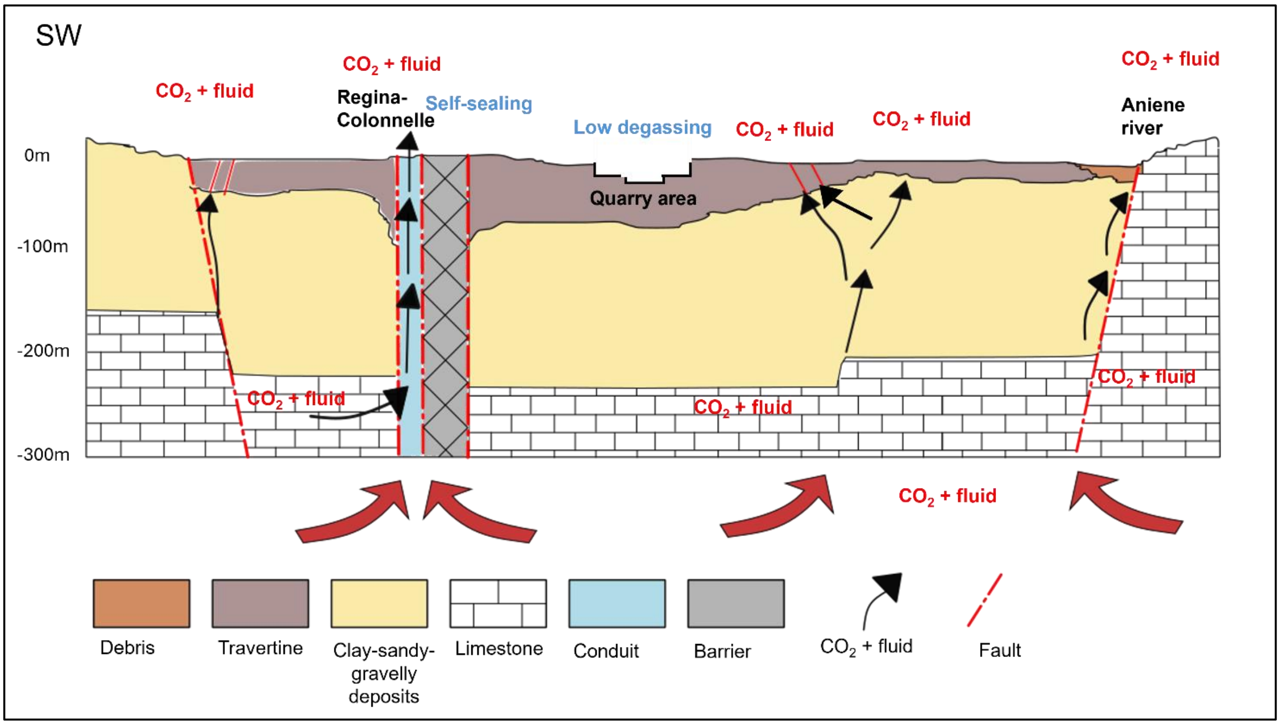

Figure 3.15- Cross-section of the fluid circulation in the study area (AAB).

The N–S fault zone displays a dual hydraulic behavior, with certain segments acting as preferential conduits for upward fluid migration, while others function as barriers due to progressive sealing processes. This heterogeneity may be attributed to the superposition of present-day hydrothermal circulation and paleo-fluid pathways. Conversely, the quarry area is characterized by markedly low CO_2 degassing, which can be explained by the high compaction and reduced porosity of the travertine deposits. The travertine body likely acts as an impermeable barrier to both CO_2 escape and fluid rise, redirecting fluid flow toward more fractured and structurally weakened sectors of the basin where permeability is enhanced.

3.6 Limitation of the study

The present study is subject to several limitations. The survey did not cover the entire Acque Albule Basin, and therefore the spatial extent of the results is restricted to the investigated areas. Soil CO_2 flux surveys were conducted across different seasons and under variable atmospheric pressure and temperature conditions. These factors may represent potential limitations of the study. During the rainy season, infiltrating water can saturate soil pore spaces and partially obstruct gas pathways. This factor can reduce the measured CO_2 flux. Atmospheric pressure fluctuations may also influence soil gas emissions. Pressure should remain stable, as variations can lead to under- or over-estimation of fluxes due to barometric pumping effects. Temperature is another critical parameter: low temperatures may cause instrumental malfunctions, including rapid battery discharge or condensation within the equipment; resulting an underestimation of CO_2 flux. Although such environmental variations may affect the magnitude of degassing anomalies, they are unlikely to compromise the overall reliability of the dataset. In this study, all measurements were performed under high atmospheric pressure, on sunny days, and during late-morning hours to avoid the influence of morning dew. Consequently, the resulting dataset can be considered robust and suitable for interpretation.

Another important limitation concerns the $\delta^{13}C$ measurements, which do not cover all sampling points due to the limited number of available vials for isotopic analyses. We chose to prioritize multiple replicates from selected areas in order to obtain more reliable and representative values at a minimum of nine sites. The selected sites correspond to the main degassing anomalies, and therefore provide strong constraints for our data interpretation. Nevertheless, additional $\delta^{13}C$ laboratory measurements should be collected in future surveys to further improve the robustness of the model.

In addition, the role of anthropogenic dewatering related to quarrying activities remains elusive. It is possible that quarry-induced dewatering has modified the natural fluid circulation, potentially facilitating upflow of deep hydrothermal aquifer in some areas. However, the extent of this effect is not yet fully constrained.

3.7 Conclusion

The results obtained from soil CO_2 flux surveys and isotopic analyses in the Acque Albule Basin highlight how the structural setting controls fluid circulation and surface degassing. The spatial distribution of CO_2 fluxes and $\delta^{13}C$ values shows that the main fault systems play a key role in directing hydrothermal fluids toward the surface. Higher degassing zones, (particularly near the Regina and Colonnelle thermal lakes) correspond to the intersection of major fault segments, confirming that these areas act as the main upflow zones. In contrast, sectors characterized by lower CO_2 fluxes are associated with former conduits that have gradually evolved into structural traps by travertine precipitation. This transition can be explained by the continuous deposition of travertine along fault planes, progressively reducing permeability and redirecting fluid ascent toward more permeable pathways. The N-S and NE-SW alignment of degassing anomalies, together with a clear west-to-east decrease in the hydrothermal contribution indicated by $\delta^{13}C$ values, suggests a lateral reduction in deep fluid input. Finally, the findings point to a dynamic system where tectonic structures, permeability changes, and mineral precipitation continuously interact. The progressive sealing of fault-related conduits may influence the spatial distribution of CO_2 fluxes and reflects the ongoing evolution of the hydrothermal system. These results provide new insight into how fault geometry and mineral deposition jointly control present-day fluid circulation in a geothermal environment.

3.8 References

Baubron, J. C., Allard, P., Sabroux, J. C., Tedesco, D., & Toutaln, J. P. (1991). Soil gas emanations as precursory indicators of volcanic eruptions. *Journal of the Geological Society*, *148*(3), 571-576.

Billi, A., Valle, A., Brilli, M., Faccenna, C., & Funiciello, R. (2007). Fracture-controlled fluid circulation and dissolutional weathering in sinkhole-prone carbonate rocks from central Italy. *Journal of Structural Geology*, *29*(3), 385-395.

Camarda, M., De Gregorio, S., Di Martino, R. M., Favara, R., & Prano, V. (2020). Relationship between soil CO2 flux and tectonic structures in SW Sicily. *Ann. Geophys*, *63*(1).

Cappelli, L., Wallace, P. A., Randazzo, A., Kamau, P. M., Njoroge, R. W., Otieno, V., ... & Fontijn, K. (2023). Diffuse soil CO2 emissions at rift volcanoes: Structural controls and total budget of the Olkaria Volcanic Complex (Kenya) case study. *Journal of Volcanology and Geothermal Research*, *443*, 107929.

Carapezza, M. L., Badalamenti, B., Cavarra, L., & Scalzo, A. (2003). Gas hazard assessment in a densely inhabited area of Colli Albani Volcano (Cava dei Selci, Roma). *Journal of Volcanology and Geothermal Research*, *123*(1-2), 81-94.

Carapezza, M. L., & Granieri, D. (2004). CO2 soil flux at Vulcano (Italy): comparison between active and passive methods. *Applied Geochemistry*, *19*(1), 73-88.

Carapezza, M. L., Ricci, T., Ranaldi, M., & Tarchini, L. (2009). Active degassing structures of Stromboli and variations in diffuse CO2 output related to the volcanic activity. *Journal of Volcanology and Geothermal Research*, *182*(3-4), 231-245.

Carapezza, M. L., Ranaldi, M., Gattuso, A., Pagliuca, N. M., & Tarchini, L. (2015). The sealing capacity of the cap rock above the Torre Alfina geothermal reservoir (Central Italy) revealed by soil CO2 flux investigations. *Journal of Volcanology and Geothermal Research*, *291*, 25-34.

Castorina, F., Masi, U., Billi, A., De Filippis, L., & Nisi, S. (2023). Elemental and Sr–Nd isotopic evidence for unravelling the origin of the low-temperature geothermal fluids of Tivoli Terme (Latium, central Italy) between erosional S4 and S3 phases (upper Pleistocene) and neotectonics implications. *Applied Geochemistry*, *158*, 105794.

Chiodini, G., Cioni, R., Guidi, M., Raco, B., & Marini, L. (1998). Soil CO2 flux measurements in volcanic and geothermal areas. *Applied geochemistry*, *13*(5), 543-552.

Chiodini, G., Baldini, A., Barberi, F., Carapezza, M. L., Cardellini, C., Frondini, F., ... & Ranaldi, M. (2007). Carbon dioxide degassing at Latera caldera (Italy): evidence of geothermal reservoir and evaluation of its potential energy. *Journal of Geophysical Research: Solid Earth*, *112*(B12).

Chiodini, G., Caliro, S., Cardellini, C., Avino, R., Granieri, D., & Schmidt, A. (2008). Carbon isotopic composition of soil CO2 efflux, a powerful method to discriminate different sources feeding soil CO2 degassing in volcanic-hydrothermal areas. *Earth and Planetary Science Letters*, *274*(3-4), 372-379.

Chiodini, G., Cardellini, C., Di Luccio, F., Selva, J., Frondini, F., Caliro, S., ... & Ventura, G. (2020). Correlation between tectonic CO2 Earth degassing and seismicity is revealed by a 10-year record in the Apennines, Italy. *Science Advances*, *6*(35), eabc2938.

David, M. (2012). *Geostatistical ore reserve estimation*. Elsevier.

De Filippis, L., Anzalone, E., Billi, A., Faccenna, C., Poncia, P. P., & Sella, P. (2013). The origin and growth of a recently-active fissure ridge travertine over a seismic fault, Tivoli, Italy. *Geomorphology*, *195*, 13-26.

Del Bon, A., Sbarbati, C., Brunetti, E., Carucci, V., Lacchini, A., Marinelli, V., & Petitta, M. (2015). Groundwater flow and geochemical modeling of the Acque Albule thermal basin (Central Italy): A conceptual model for evaluating influences of human exploitation on flowpath and thermal resource availability. *Central European Geology*, *58*(1-2), 152-170.

Faccenna, C. (1994). Structural and hydrogeological features of Pleistocene shear zones in the area of Rome (Central Italy). *Annals of Geophysics*, *37*(1).

Faccenna, C., Soligo, M., Billi, A., De Filippis, L., Funiciello, R., Rossetti, C., & Tuccimei, P. (2008). Late Pleistocene depositional cycles of the Lapis Tiburtinus travertine (Tivoli, Central Italy): possible influence of climate and fault activity. *Global and Planetary Change*, *63*(4), 299-308.

Fridriksson, T., Kristjánsson, B. R., Armannsson, H., Margrétardóttir, E., Ólafsdóttir, S., & Chiodini, G. (2006). CO2 emissions and heat flow through soil, fumaroles, and steam heated mud pools at the Reykjanes geothermal area, SW Iceland. *Applied geochemistry*, *21*(9), 1551-1569.

Frondini, F., Cardellini, C., Caliro, S., Beddini, G., Rosiello, A., & Chiodini, G. (2019). Measuring and interpreting CO2 fluxes at regional scale: the case of the Apennines, Italy. *Journal of the Geological Society*, *176*(2), 408-416.

Frondini, F., Caliro, S., Cardellini, C., Chiodini, G., & Morgantini, N. (2009). Carbon dioxide degassing and thermal energy release in the Monte Amiata volcanic-geothermal area (Italy). *Applied Geochemistry*, *24*(5), 860-875.

Gasparini, C., Di Maro, R., Pagliuca, N. M., Pirro, M., & Marchetti, A. (2002). Recent seismicity of the «Acque Albule» travertine basin. *Annals of Geophysics*, *45*(3-4).

Hanson, M. C., Oze, C., & Horton, T. W. (2014). Identifying blind geothermal systems with soil CO2 surveys. *Applied Geochemistry*, *50*, 106-114.

Hong, J., Kim, H., Lee, W., Yu, J., Fischer, T. P., Takahata, N., ... & Lee, H. (2023). Fault-related basins as carbon reservoirs: Soil CO2 emissions in the SE Korean Peninsula. *Catena*, *231*, 107300.

Italiano, F., Martinelli, G., & Plescia, P. (2008). CO2 degassing over seismic areas: the role of mechanochemical production at the study case of Central Apennines. *Pure and Applied Geophysics*, *165*(1), 75-94.

Jentsch, A., Duesing, W., Jolie, E., & Zimmer, M. (2021). Monitoring the response of volcanic CO2 emissions to changes in the Los Humeros hydrothermal system. *Scientific Reports*, *11*(1), 17972.

La Vigna, F., Carucci, V., Mariani, I., Minelli, L., Pascale, F., Mattei, M., ... & Tallini, M. (2012). Intermediate-field hydrogeological response induced by L'Aquila earthquake: the Acque Albule hydrothermal system (Central Italy). *Italian Journal of Geosciences*, *131*(3), 475-485.

La Vigna, F., Mazza, R., & Capelli, G. (2013). Detecting the flow relationships between deep and shallow aquifers in an exploited groundwater system, using long-term monitoring data and quantitative hydrogeology: the Acque Albule basin case (Rome, Italy). *Hydrological Processes*, *27*(22), 3159-3173.

Li Vigni, L., Cardellini, C., Temovski, M., Ionescu, A., Molnár, K., Palcsu, L., ... & D'Alessandro, W. (2022). Duvalo "volcano"(North Macedonia): A purely tectonic-related CO2 degassing system. *Geochemistry, Geophysics, Geosystems*, *23*(4), e2021GC010198.

Liu, F., Zhou, X., Dong, J., Yan, Y., Tian, J., Li, J., ... & Zhang, Y. (2023). Soil gas CO2 emissions from active faults: a case study from the Anninghe—Zemuhe fault, Southeastern Tibetan Plateau, China. *Frontiers in Earth Science*, *11*, 1117862.

Mancini, A., Cornacchia, I., Lamal, J., Capezzuoli, E., Swennen, R., & Brandano, M. (2024). Using stable isotopes in deciphering climate changes from travertine deposits: the case of the Lapis Tiburtinus succession (Acque Albule Basin, Tivoli, Central Italy). *Frontiers in Earth Science*, *12*, 1355693.

Minissale, A., Kerrick, D. M., Magro, G., Murrell, M. T., Paladini, M., Rihs, S., ... & Vaselli, O. (2002). Geochemistry of Quaternary travertines in the region north of Rome (Italy): structural, hydrologic and paleoclimatic implications. *Earth and Planetary Science Letters*, *203*(2), 709-728.

Parkinson, K. J. (1981). An improved method for measuring soil respiration in the field. *Journal of applied ecology*, 221-228.

Petitta, M., Primavera, P., Tuccimei, P., & Aravena, R. (2011). Interaction between deep and shallow groundwater systems in areas affected by Quaternary tectonics (Central Italy): a geochemical and isotope approach. *Environmental Earth Sciences*, *63*(1), 11-30.

Rissmann, C., Christenson, B., Werner, C., Leybourne, M., Cole, J., & Gravley, D. (2012). Surface heat flow and CO2 emissions within the Ohaaki hydrothermal field, Taupo Volcanic Zone, New Zealand. *Applied Geochemistry*, *27*(1), 223-239.

Werner, T., Köllmer, I., Bartrina, I., Holst, K., & Schmülling, T. (2006). New insights into the biology of cytokinin degradation. *Plant biology*, *8*(03), 371-381.

4- Integrating Soil CO_2 Flux measurements in the structural interpretation of the Acque Albule Basin.

Abstract

Buried faults within tectonic basins can be particularly challenging to identify, especially in heavily anthropized areas where intensive industrial and agricultural activities have significantly altered the natural landscape. Identifying the presence of tectonic structures in this type of basin is essential for assessing the potential presence of geothermal resources and for their exploitation. The Acque Albule Basin is characterized by extensive hydrothermal activity across a tectonic plain. The intense fluid circulation within this system offers valuable insights into the fluid flow in fractured carbonate environments. In this work, several CO_2 surveys have been conducted in the AAB area. A map of CO_2 flux has been made and several minors transects have been carried out using the accumulation chamber method to detect the N-S fault zone responsible for the development of the pull-apart basin and the respective fluid circulation system. Transects were carried out in the Cretone area, the Sant'Angelo Romano area; Bagni di Tivoli area and Corcolle area. The results show high CO_2 degassing values in the Acque Albule basin, with values reaching 120 $gm^{-2}day^{-1}$ near the hydrothermal springs, as well as several high degassing spots in the plain corresponding to minor NE–SW lineaments. Degassing appears to reflect a trend of decreasing hydrothermalism from west to east. This is confirmed by the $\delta^{13}C$ isotope analysis of soil gas samples. Cretone, Sant'Angelo and Corcolle seem to have low degassing in comparison to the AAB, but some areas could reach 14 gm^{-2} day^{-1} as major degassing, especially where the fault zone is exposed and in the thermal area of Cretone. Hydrothermal activity in the Cretone area indicates faulting and fluid migration in the northern sector of the main strike-slip zone. No additional degassing anomalies were detected. The Sant'Angelo and Corcolle areas also show no significant anomalies. These observations suggest that fluid circulation is mostly limited to the Acque Albule Basin.

4.1 Introduction

Buried faults in tectonic basins can be especially difficult to detect, particularly in densely anthropized areas where extensive industrial and agricultural activities have profoundly modified the natural landscape. The identification of such tectonic faults is crucial for evaluating the potential presence of geothermal resources and for their effective exploitation. In an area with intense thermal activity, such as the Acque Albule basin, it is important to detect faults and understand their role in terms of fluid circulation to the use of geothermal energy. Several studies have been conducted to determine the role of faults in fluid circulation and fluid-triggered earthquake mechanisms. These include studies by Stibson (1996), Cappa et al. (2011), Brodsky & Lajoie (2013), Ciotoli et al. (2016), Frondini et al. (2018), Vitigliano et al. (2024) and Pontikou et al. (2025). Fluids seem to play an important role, particularly in the Central Apennines, where a CO_2 gas trap is present and fluid rise through the main tectonic discontinuities (Chiodini et al., 2008), suggesting the presence of a geothermal reservoir whose formation and dynamics are controlled by fault structures. The results of deep fluid circulation in the Apennines chain are several outcropping hydrothermal springs (e.g. Triponzo, Acque Albule, Terme di Viterbo, Fiuggi and Suio). These springs are mostly bicarbonate-sulfate-calcareous and are characterized by relatively low temperatures (20-70 °C) and high conductivity (200-3570 micro-siemens/cm). These springs are linked to thermal waters arising due to the upward migration of deep fluids enriched in CO_2 along active tectonic faults, which facilitate the mixing of meteoric waters with deeper geothermal fluids. Both buried and active faults are crucial in governing fluid circulation in these basins; hence, identifying degassing along faults is essential to understanding their role in large-scale fluid dynamics. The Acque Albule Basin was chosen as the case study for this project because it is characterized by extensive hydrothermal activity across the tectonic plain (Faccenna et al., 2008). Hydrothermal activity has led to the formation of one of the most productive travertine plateaus in the world. The intense fluid circulation within this system offers valuable insights into the mechanisms that facilitate or hinder fluid flow in carbonate environments. In this work, several CO_2 surveys have been conducted in the AAB area. A map of CO_2 flux has been made and several minors transects have been carried out using the accumulation chamber method to detect the N-S fault zone responsible for the development of the pull-apart basin. Transects were carried out in the Cretone area, the Sant’Angelo Romano area; Bagni di Tivoli and Corcolle area. This study aims to compare CO_2 flux data with the structural framework of the AAB, as outlined in previous literature, to reconstruct the fault architecture and assess its role in controlling fluid circulation and the geothermal system.

4.2 Structural background

Acque albule basin is a transtensive basin located 10 km east of Rome (Fig. 4.1). It is bounded by the Appennine chain (the Cornicolani and Lucretili mountains) to the north-east and the Alban Hills to the south. The area has been widely known since Roman times due to its significant hydrothermal activity and the associated travertine deposits, which have been quarried since Roman times. The AAB is located at the boundary between the Apennine fold-and-thrust belt and the western Tyrrhenian margin and is linked to a strike-slip zone merging different stress regimes (Faccenna & Funiciello, 1993; Faccenna, 1994; Faccenna et al., 2008).

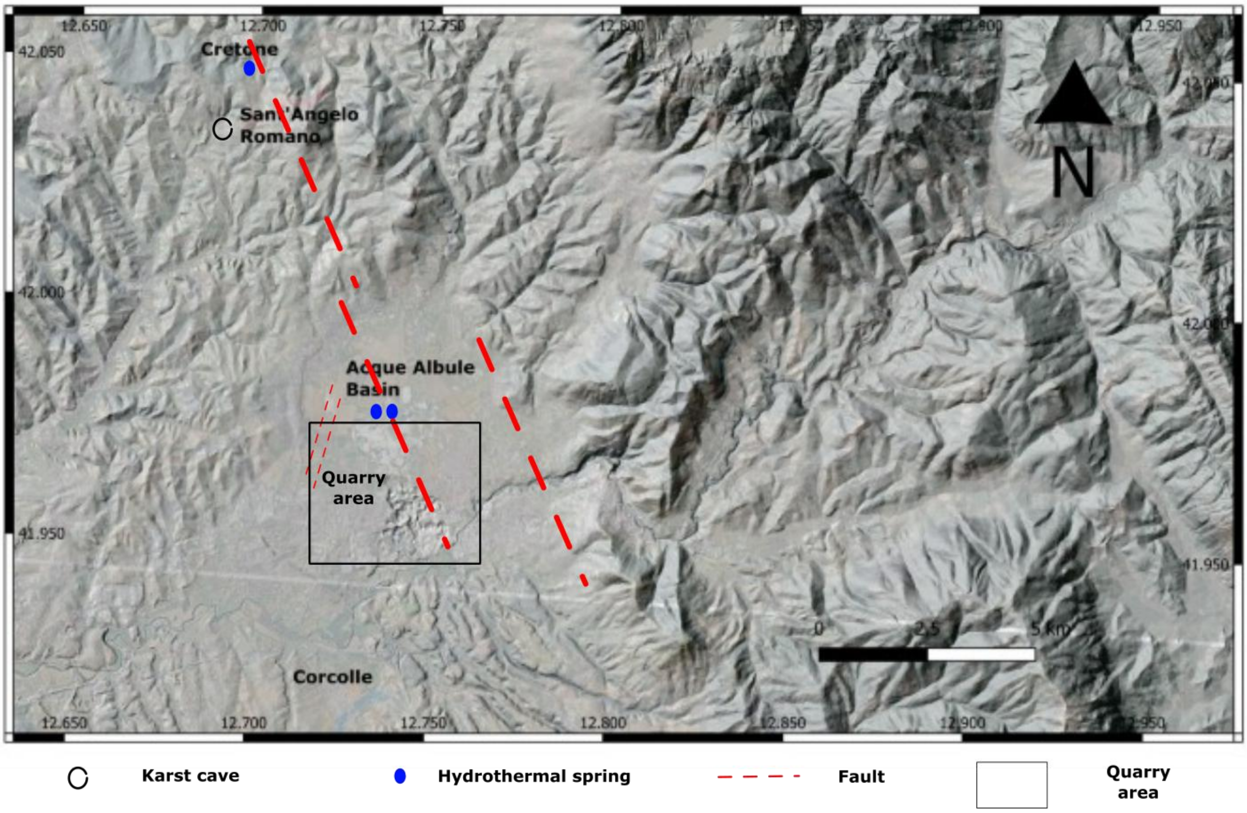

Figure 4.1 - Geographic framework of the Acque Albule Basin.

The Tiburtini–Lucretili Mountains exhibit both brittle and ductile deformation associated with compressional orogenic processes. Ductile deformation is evident by folding, with axes oriented approximately N 20-25°, and in some cases characterized by sub-horizontal axial planes (Faccenna, 1994; Cosentino et al., 2010). Brittle deformation is marked by the presence of reverse faults dipping 20-30° westward, which are interpreted as part of the main thrust system. Additionally, the area records a strike-slip tectonic phase, with fault systems striking N 40° (N-S) and N 130° (NW-SE), likely occurring during or shortly after the main compressional phases (Faccenna, 1994). The area was subsequently overprinted by extensional tectonics, evidenced by E–W and NW–SE striking normal faults and extensional joints (Faccenna, 1994; Faccenna et al., 2008). Right-lateral strike-slip faults are particularly evident in the Cornicolani mounts (Sant'Angelo Romano), where several quarries are present (Billi et al., 2007). Evidence of strike-slip and extensional tectonics is also present in the Cava Buzzi Unicem (Guidonia, Rome, Italy), where a system of N 40 and N 200 joints is present in the clay and pyroclastic deposits related to the Colli Albani activity. Faccenna,1994 investigated all the pyroclastic deposits and revealed some N 30 oblique lineaments linked to the shear zone of the AAB. In the north-eastern part of the AAB, Villa Adriana (Tivoli) exhibits right lateral strike-slip and associated N 40 joints. These lineaments could be attributed to the second set of strike-slip faults related to the AAB. Previous studies have never fully constrained this second strike-slip fault as sinkholes and hydrothermal springs in the plain do not exhibit a clear north-south pattern in the eastern part of the plain. However, the pattern of N 40 striking normal faults associated with N 30-N 60 extensional joints is widespread across the entire area: Villa Adriana, Colle Cesarano and the western part of Colle Fiorito. These faults cut the most recent pyroclastic and alluvial deposits. Lineaments in these deposits follow the σ_3 (minimum compressional axis) (Faccenna, 1994; Billi et al., 2007). The most recent deformation is in the southern and western parts of Guidonia, where the N 40 and N 120 faults have affected the unconsolidated travertine deposits. U-Th dating of the travertine deposits in this area yielded a date of 28+-16 ka (Faccenna, 1994). Within the AAB, there is a trend of fractures in the travertine, followed by several karstic sinkholes and thermal springs, which reflect the regional N-S tectonics. These fractures are also located in the southernmost quarry area in the Bagni di Tivoli province. The same trend seems to be present in the Corcolle area, where several other structural surveys have been conducted. In the northern part (the Cretone area), a straight north-south-trending valley is marked by the presence of hydrothermal springs that are chemically consistent with AAB hydrothermalism (Petitta et al., 2011). However, there are apparently no clear lineaments in this area. Structural data are represented in Figure 4.2. To summarize, the geometry of the travertine deposits (isopach) and associated joints reflect the presence of two N-S strike-slip right-lateral faults. The western faults appear to be the most significant and can be traced from Cretone to Corcolle, possibly extending as far as Colli Albani (27 km, Faccenna, 1994).

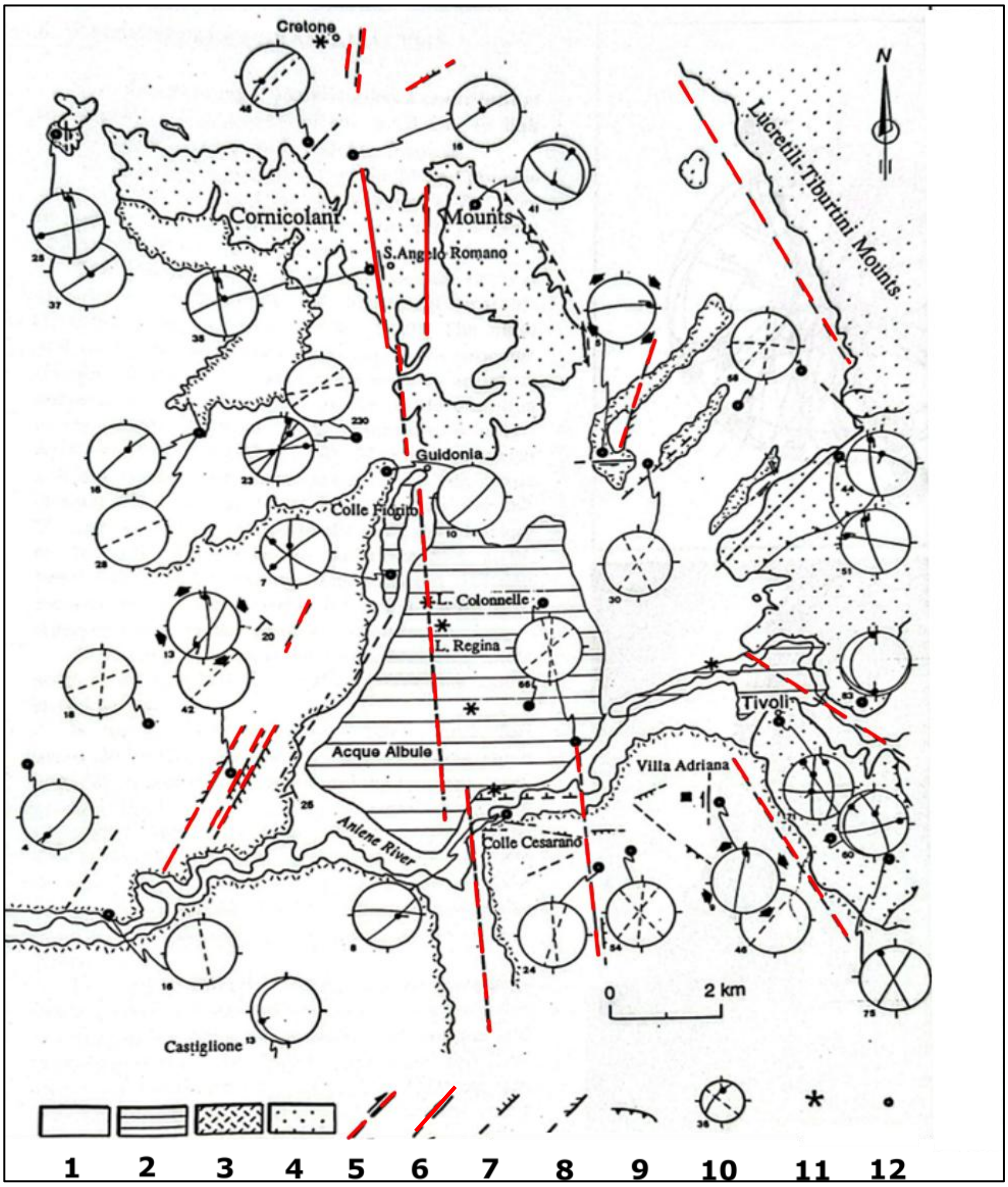

Figure 4.2- Structural data reported by Faccenna et al., 1994. 1) Plio-pleistocene sedimentary unit.2) Travertine plateau. 3) Alban Hills volcanic deposits. 4) Meso-Cenozoic carbonate units.5) Master faults (continue line when inferred). 6) strike slip lineaments. 7-8-9) normal-oblique and reverse faults. 10) stereoplots. 11) hydrothermal springs. 12) measurement points. (Modified after Faccenna, 1994).

4.2.1 Traverine and calcite veins chronological data

U/Th dating was performed in several part of the Acque Albule basin and in the nearest sectors from Faccenna, 1994; Faccenna et al., 2008 and Billi et al., 2007. The results show an age of deposition between 148 and 40 ka in the AAB. Recent studies (Faccenna et al., 2008; De Filippis et al., 2012; Castorina et al., 2023) dated the travertine in this area to 115 ka. The sedimentation rate is around 0.43 mm per year, which is comparable with other several Quaternary Italian travertine plateau (e.g. Fiano, Rocchetta a Volturno, Adrano, Gallicano, Fiora river; Faccenna et al., 1994). Instead, the Colle Fiorito area appears to be the most recent travertine deposit, ranging from 28 ka to historic times. Degassing on the Colle Fiorito ridge has been active in recent times, which can explain the presence of small pipes at the top of the ridge (De Filippis et al., 2013). Furthermore, recent seismic activity (the 2001 seismic swarm, Gasparini et al., 2002) appears to be related to the Collefiorito NE-SW and the N-S main strike-slip fault of the AAB. This means that these faults are still active and can still promote fluid circulation. Finally, Billi et al. (2007) attempted to determine the origin of the calcite veins based on the tectonic context through stable isotope analysis. They found a correlation between some meteoric processes of vein formation and other calcite veins related to interaction with hydrothermal fluids, particularly in the vicinity of fault zones. This process is evident in the AAB, where several karst phenomena, including sinkholes, cavities, and hydrothermal springs, have formed. This highlights the presence of the buried faults promoting the fluid circulation especially in the N-S shear zone. The fluids produce some dissolution and precipitation processes in several selected areas of the basin, reflecting an area characterized by intense tectonic.

The pyroclastic deposits have also been investigated, with the U/Th methodology applied to the veins within the Pliocene-Pleistocene deposits to understand the fault's age of activity. Deposits outcrops in Cava Buzzi Uncem (along the Tiburtina road), Colle Cesarano, Villa Adriana and the western part of the Colle Fiorito area. Faults affect all the Pliocene Quaternary deposits, including post-volcanic and Aniene River deposits. Therefore, the results show that the master fault was active from the emplacement of the pyroclastic flow (5000–300 ka) until 49 ka, with a climax around 178 ka (the age of the calcite filling the tectonic features). At that time, Colle dello Stonio and Colle Fiorito ridges were forming (Faccenna, 1994). The main deposition of the travertine in the AAB occurred around 115–80 ka (Faccenna et al., 2008; De Filippis et al., 2013). The onset of deposition occurred around 115 ka, while the end occurring around 29 ka in non-consolidated tuff, including in the pyroclastic deposits at Colle Fiorito ridge (Faccenna et al., 2008).

4.3 Methodology

4.3.1 Soil CO2 diffuse degassing measurements

Soil CO_2 flux surveys have proven to be an efficient tool for identifying zones of high permeability at depth that produce degassing anomalies that are recognizable at the surface (Chiodini et al., 2007). Nevertheless, soil CO_2 flux surveys seem to be a very important tool for investigating fault locations and the role of faults at depth, and for reconstructing the permeability context. The accumulation chamber method was chosen for this survey as it does not require corrections or assumptions regarding the soil's characteristics. After the measurements have been taken, a spatial distribution analysis should be performed to detect fault and fracture distribution. Finally, the characterization of the CO_2 degassing by isotopes should detect deep contributions related to hydrothermal fluids from the biogenic CO_2 background (see Chapter 3 for more details).

In order to investigate the role of the fault in the Acque Albule pull-apart basin, we conducted some soil CO_2 surveys on the main north-south fault zone, as described by Faccenna et al. (2008, 1994) and Billi et al. (2007). Starting from the north, we conducted one east-west (E-W) transect (T1; 5.5 km) to the Cretone area, where a thermal spring with the same signature as Acque Albule is present. The elongation of the transect was E-W to detect anomalies related to strike-slip faults. The measurement distance was 100 m (depending on the characteristics of the territory). Another 2.0 km transect was conducted in Sant'Angelo Romano (T2) for the same purpose. A third transect (T4; 2.1 km in length) was carried out in the Corcolle area, oriented along the same north-south axis as the previous surveys, but located to the south of the AAB. Furthermore, the same data from Chapter 3 were used to investigate the interior of the AAB (the Guidonia and quarries area), including a CO_2 degassing profile in the southern part of the Bagni di Tivoli area (T3; 4.2 km). We acquired the data between January 2024 and May 2025. We used geostatistical methods to interpolate the spatial data. The transect and areal measurement points are shown in Figure 4.3.

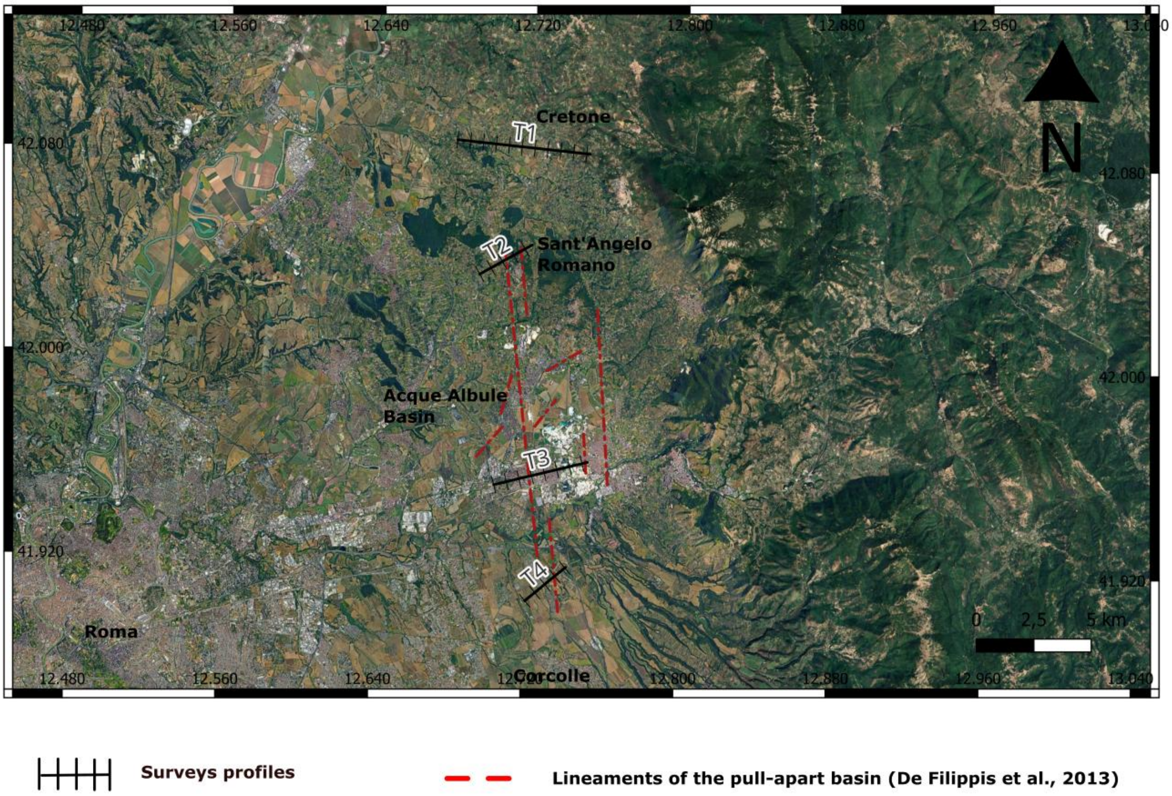

Figure 4.3- Map showing the location of the soil CO_2 flux surveys profile.

We used the areal dataset presented in Chapter 3 of this thesis. Dataset was processed using the QGIS Smart Map plug-in to perform geostatistical interpolation through ordinary kriging. An exponential variogram model was selected to describe the spatial autocorrelation structure of the soil CO_2 flux data (see Chapter 3).

4.4 Results

We investigated the CO_2 soil flux in the Acque Albule area and its surroundings, searching for any anomalies in the location and role of the faults that characterize the pull-apart basin. Starting from the northern part of the study area in the Cretone region (T1), the fluxes are characterized by values ranging from 1.7 to 26.4 g m^{-2} day^{-1}, corresponding to the Cretone thermal pool and the surrounding agricultural landscape (400 meters from the thermal rise). The higher values are found in the western part of the profile. Values of the Soil CO_2 flux about the Cretone profile are represented in the Table 4.1 (see Chapter 7, Appendix B).

T2 is located in the northern part of Sant'Angelo Romano, where the strike-slip fault zone is exposed. The results of the CO_2 soil degassing show relatively low fluxes, characterized by values ranging from 1.4 to 21.8 g m^{-2} day^{-1}, with no apparent evidence of a major degassing zone. Data about T2 are shown in Table 4.2 (see Chapter 7, Appendix B).

T4 was conducted near the Corcolle area, where faults are just supposed by previous studies. The results show very low fluxes of between 1 and 15.4 g m^{-2} day^{-1}, with no evidence of high degassing. Data about T4 are shown in Table 4.3 (see Chapter 7, Appendix B). T3, in an area close to Bagni di Tivoli shows the highest degassing values compared to T1, T2 and T4. Values range from 1.4 to 76.4 g m^{-2} day^{-1}. The highest values are in the western part of the profile where some points are characterized by values of 75 and 20 g m^{-2} day^{-1}. Data about T3 are shown in Table 4.4 (see Chapter 7, Appendix B).

Finally, we combine data about the AAB (presented in the chapter 3) with the transepts. Figure 4.4 shows four transepts regarding degassing. Transept points dimension is proportional to the degassing values.

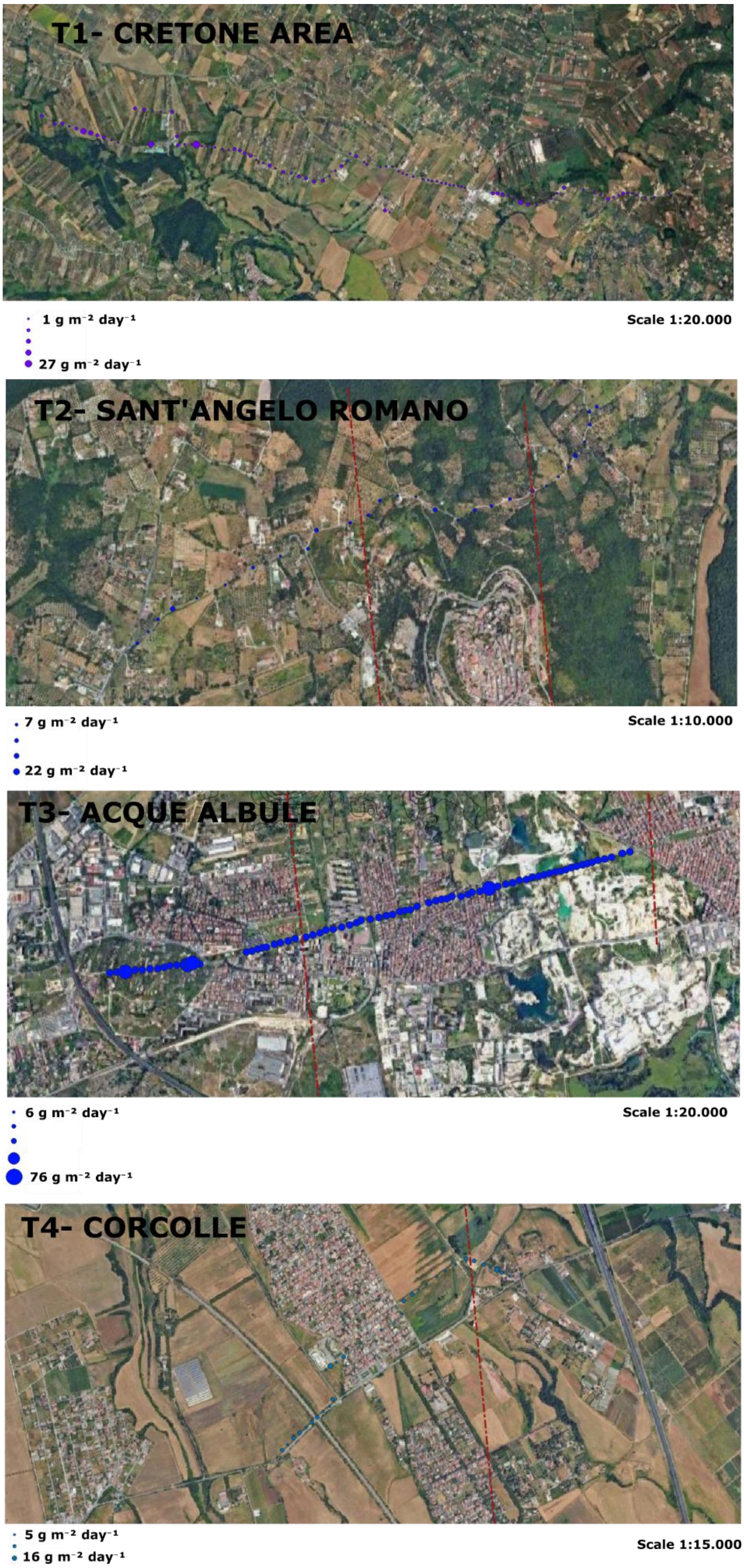

Figure 4.4 - Soil CO_2 flux surveys profiles along Cretone (T1); Sant'Angelo Romano (T2); Bagni di Tivoli (T3); Corcolle (T4).

Moving to the interpolation maps of the northern AAB (Chapter 3; Fig.3.7), the CO_2 soil flux background values are around 20 g m^{-2} day^{-1}, respect to the 5 g m^{-2} day^{-1} of the Cretone. Corcolle and Sant'Angelo Romano. Anomalies in this area are mostly found in correspondence with active thermal lakes (Regina and Colonnelle) and along some active N-S and NE-SW lineaments (Chapter 3, Fig.3.10) where CO_2 values can reach 120 g m^{-2} day^{-1}. $\delta^{13}C$ analyses from Chapter 3 show a progressive increase in the $\delta^{13}C$ component from east to west with some pure hydrothermal values concentrated in the western part of the area (Fig.3.12).

Figure 4.5 presents the comparison between soil CO_2 flux values and longitude along all transects aimed at detecting any preferential degassing direction. The background soil CO_2 flux is approximately 5 g m^{-2} day^{-1}. A clear increase in CO_2 flux is observed between UTM X = 308454 and 309651 (western sector of the profiles), where several transects show elevated degassing values. Toward the eastern portion of the study area. CO_2 flux values generally remain close to the background level.

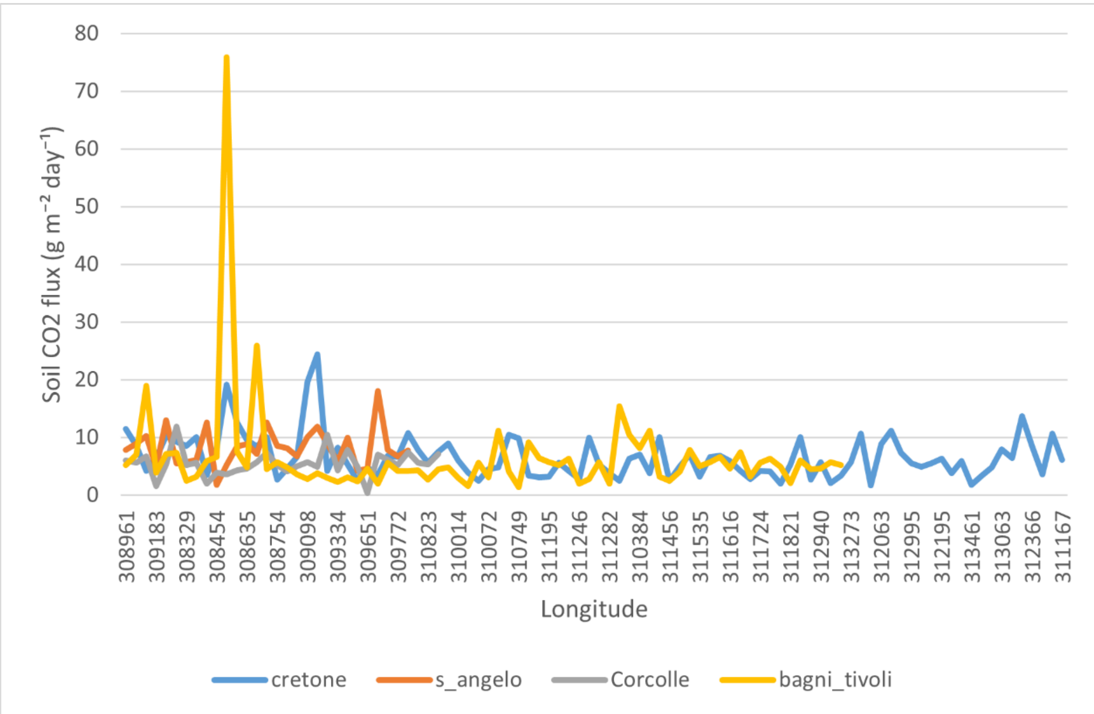

Figure 4.5- Comparison between the Soil CO2 flux and the longitude in all the localities.

4.5 Discussion

Degassing measurements are spread along the north-south direction in the shear zone described by Faccenna et al., (1994. 2008), De Filippis et al., 2012 and Billi et al., 2007. As previous literature describes, the area is characterized by the presence of an N-S strike-slip shear zone and several NE-SW transtensive lineaments, which are associated by 2001 seismicity (Gasparini et al., 2002). This tectonic framework can also be detected by CO_2 flux surveys. We investigated the northern part of the supposed N-S shear zone in the T1 area of Cretone. T1 shows relatively low values except for significant degassing where hydrothermal springs are present. Apart from the 400 m little anomaly near the hydrothermal spring, no other degassing anomalies were recorded. T2 in Sant'Angelo Romano shows a higher degassing background, which may be due to a difference in biogenic CO_2 flux than hydrothermal anomaly. There is just one point of higher degassing to the north-south direction of the T1 anomaly (18.06 g m^{-2} day^{-1}).

The major CO_2 degassing points observed at Cretone (26.7 $gm^{-2}d^{-1}$) may suggest the presence of an underlying fault zone considering that the background CO_2 flux in the T1 and T2 areas is comparatively low. The Corcolle and Sant’Angelo areas (T3) did not show any anomalies and is not affected by hydrothermalism related to the fault zone, although some micro-seismic events can be attributed to this area. Major fluxes are concentrated in the Bagni di Tivoli and Guidonia area, as shown by T4 and the flux map distribution. This area is characterized by intense hydrothermal activity because of the presence of several hydrothermal and paleo-springs, and some active sinkholes aligned in the north-south direction. Furthermore, quarry activity is present in this area due to the significant thickness of the travertine. The travertine horst contains hydrothermal water with temperatures of up to 23 °C and a conductivity of 2700 mS/cm (La Vigna et al. 2013).

Thermal water is the mixing of several end member (Facies A, Ca-HCO_3; Facies B, Ca-HCO_3-SO_4; Facies C Ca-Mg-HCO_3-SO_4); the major contribution is related to the deep carbonate aquifer, which horst a 90°C medium enthalpy fluid circulation (Del Bon et al. 2015; Petitta et al 2011; Castorina et al. 2023; Mancini et al. 2024). Degassing background is higher in the Guidonia- Bagni di Tivoli area, around 20-30 g m^{-2} day^{-1}. High anomalies are present, especially in correspondence of the hydrothermal springs (Regina and Colonnelle). Other minor anomalies reach 40-50 g m^{-2} day^{-1} are spreaded along the plain. As Chapter 3 shown, higher anomalies seem to follow a tectonic trends N-S and NE-SW, while lower values of CO_2 fluxes are recording in the area characterized by important thickness of the travertine (Figure 4.6).

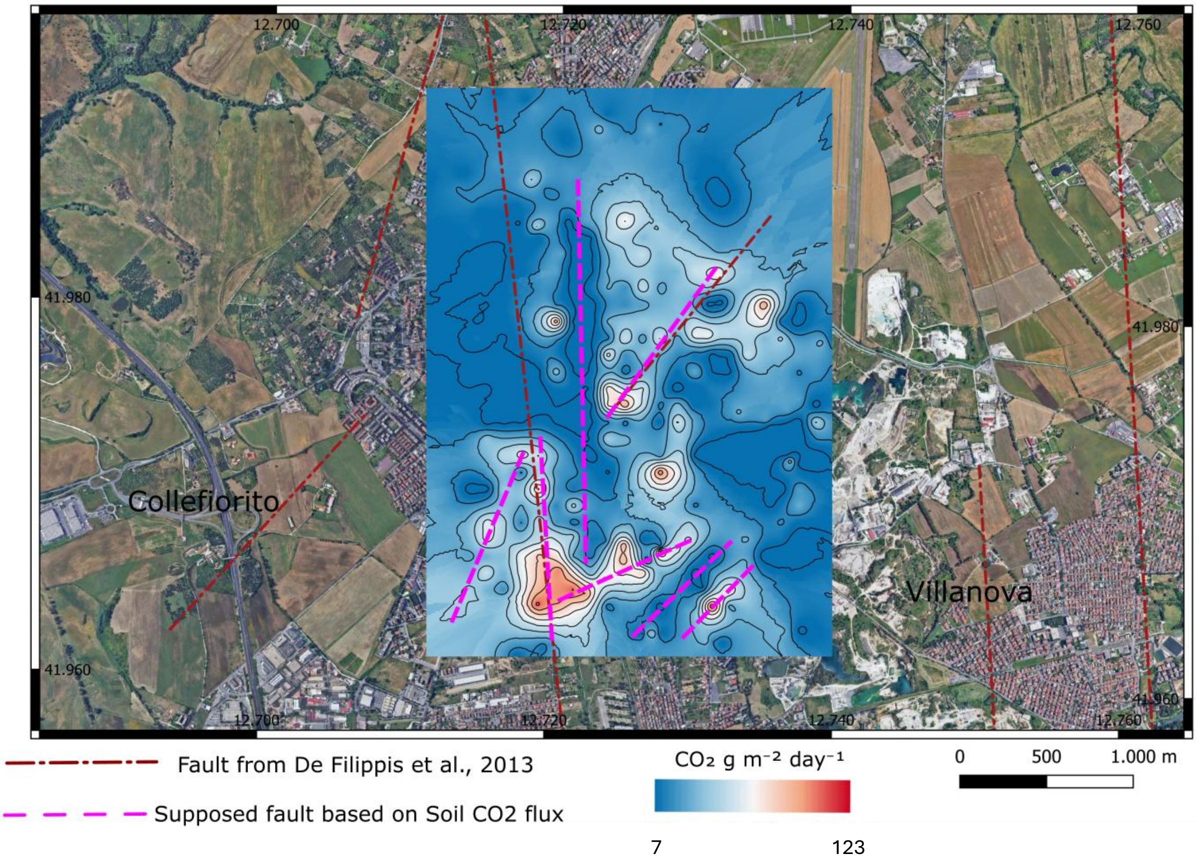

Figure 4.6 - structural setting based on the CO_2 soil flux compared with the structural setting proposed by De Filippis et al., 2013.

Travertine could act as an impermeable layer and can testify old conduits for fluid circulation and degassing, now sealed. This can also be occurred in Sant'Angelo Romano, where the strike-slip faults are outcropping, and the calcite veins can inhibit the CO_2 flux degassing in surface because of the sealing of fractures and faults (Billi et al., 2007). According to Faccenna et al. (1994b) and de Filippis et al., 2012. calcite veins and old travertine are ascribed to old preferential conduits, and the most active areas regarding fluid circulation correspond to the western part of the AAB (Colle Fiorito area). Recent seismicity and chronological dating of the travertine indicate that the western part of the basin, especially the Colle Fiorito area, has the youngest travertine deposits characterized by gas pipes structures. Therefore, fluid circulation appears to be active in the western part of the basin and inside the basin itself. This is also supported by the $\delta^{13}C$ data from Chapter 3, which indicates a stronger hydrothermal component in the western part of the basin and positive

CO_2 diffuse degassing concentrated along the NE-SW transtensive lineaments. Studies included in De Filippis et al., 2013 confirmed a link between fissure ridge growth and active normal tectonics. This implies that fault-related extensional fracturing promotes geothermal fluid circulation. Positive CO_2 anomalies in this study suggest that degassing and the rising of geothermal fluids is linked to active normal faults, which are sometimes associated with strike-slip tectonics, as in the Colle Fiorito Ridge case study (De Filippis et al. 2013; Gediz and Menderes grabens. Western Turkey. Çakır. Z. 1999).

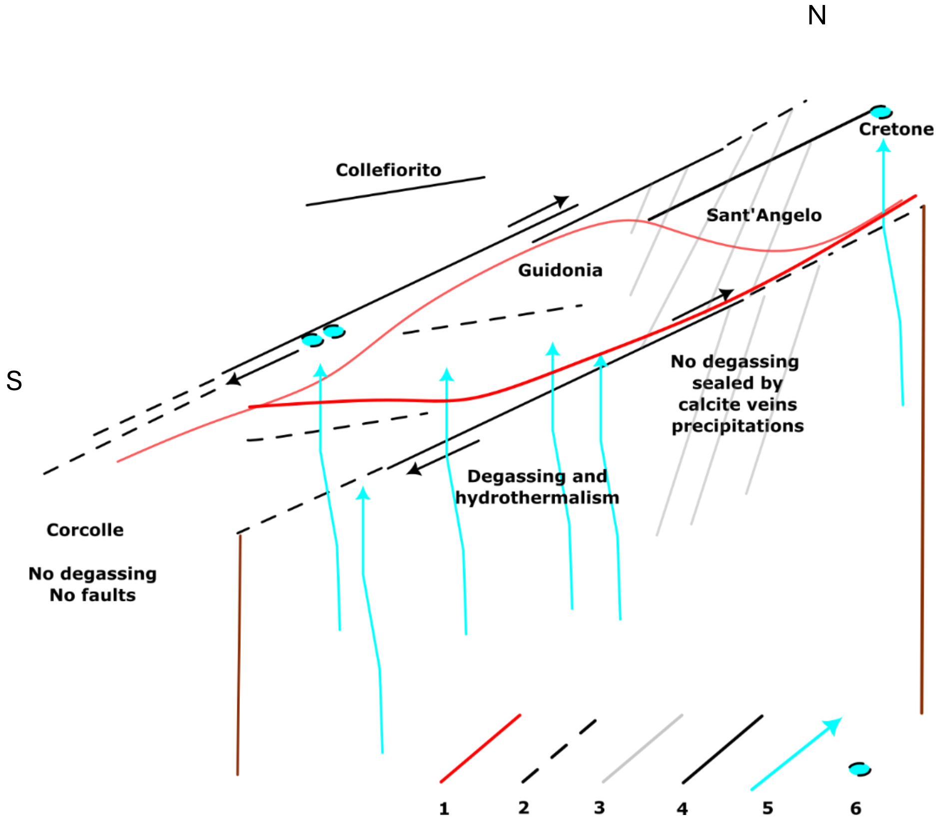

Figure 4.7- Schematic representation about the distribution of hydrothermalism and fluid circulation along the N-S strike slip faults and the respective pull-apart basin. 1) Pull-apart basin limit. 2) Supposed fault. 3) Sealing. 4) Fault trace. 5) Fluids and CO_2. 6) Hydrothermal spring.4

4.6 Comparative insights from other tectonic settings and implication for the AAB fluid circulation

Several studies have investigated CO_2 degassing along fault zones, for identifying the structural controls governing fluid circulation. Research focusing on fluid flow and permeability architecture has mainly been conducted in geothermal or high-temperature volcanic regions (e.g., Taussi et al., 2023; Sbrana et al., 2020; Chiodini et al., 2001; Harvey et al., 2017; Bini et al., 2023; Peiffer et al., 2015; Fridriksson et al., 2006). These studies generally highlight the role of fault intersections, damage zones, and lithological contrasts in enhancing vertical permeability and promoting deep CO_2 ascent.

Other investigations have instead focused on active degassing associated with fault activity, examining how variations in fault-zone porosity and permeability may occur immediately after earthquakes or during inter-seismic periods (Li Vigni et al., 2025; Liu et al., 2023; Ciotoli et al., 2016; Camarda et al., 2020; Italiano et al., 2008; Chiodini et al., 2001). These works demonstrate that seismic events can transiently modify gas pathways, leading to short-term increases or decreases in CO_2 flux depending on the mechanical response of the fault system. CO_2 and hydrothermal fluids are strongly controlled by tectonic structures, particularly in active tectonic settings where high heat flow and favorable conditions for geothermal circulation are present. Most of the examples discussed in this section refer to areas characterized by active degassing and geothermal exploitation, where fault zones and fracture networks play a key role in enhancing vertical permeability and driving fluid ascent. By comparing the results of these studies with the Acque Albule Basin (AAB), it is possible to better constrain the degassing behavior of the area and to place it within a broader framework of structurally-controlled fluid flow. This comparison also highlights the presence of several boundary conditions that make the AAB an interesting site for investigating CO_2 migration and fault-controlled hydrothermal circulation. The Acque Albule Basin (AAB) represents a low- to medium-enthalpy hydrothermal system that is strongly controlled by the activity of a N–S-trending strike-slip shear zone.

The Acque Albule Basin (AAB) can be framed within the broader context of structurally controlled CO_2-rich hydrothermal systems by comparing its thermal regime, fluid geochemistry, and tectonic architecture with several well-studied Mediterranean and global analogues. Although the AAB is classified as a low- to medium-enthalpy system, with a thermal travertine aquifer with temperature around 23 °C and a deeper carbonate reservoir estimated at ~90 °C (Minissale et al., 2002; Petitta et al., 2011). These degassing dynamics are consistent with those observed in more active geothermal provinces. High-temperature fields such as Larderello and Mt. Amiata exhibit reservoir temperatures exceeding 300-360 °C and CO_2 emissions of several thousand tons per day (Chiodini et al., 2001; Sbrana et al., 2020), driven by metamorphic decarbonation and magmatic heat sources. In contrast, the AAB displays more moderate CO_2 output (~95 t/d), as Vulcano Island (~75 t/d;2 km^2 Chiodini et al., 1998) and the Duvalo mofette system in North Macedonia (~66 t/d) Li Vigni et al., 2025), both characterized by diffuse degassing controlled by active fault networks

(Table 4.5, chapter 7, Appendix B). The higher isotopic composition of CO_2 in the AAB ($\delta^{13}C$ = −5 to −1‰) indicates a deep crustal contribution related to the decarbonation of Mesozoic limestones (Castorina et al., 2023), similar to the signatures observed in Larderello (Taussi et al., 2023), Mt. Amiata (Chiodini et al., 2004, Sbrana et al., 2020), and the Tiber Delta at Fiumicino, where deep CO_2 mixes with thermogenic methane along active faults (Ciotoli et al., 2016). Structurally, the AAB is governed by a N–S strike-slip shear zone with secondary NE-SW lineaments, a configuration that mirrors the structural control documented in Larderello (Harvey et al., 2017), Duvalo (Li Vigni et al., 2025), and Fiumicino (Ciotoli et al., 2020), where fault intersections and transfer zones act as preferential conduits for deep fluid ascent. A distinctive feature of the AAB is the exceptional thickness of its travertine deposits (30-90 m), which act as a low-permeability cap, redirecting fluids toward fractured sectors. This behavior is analogous to the “hidden geothermal system” of Acoculco, Mexico, where low-permeability lithologies impede vertical fluid migration and promote lateral flow (Peiffer et al., 2015). The spatial distribution of the hydrothermalism in the AAB is diffuse across the basin plain and locally focused at Cretone resembles patterns observed in Micciano and Palazzo al Piano (Taussi et al., 2023), where hydrothermal activity is concentrated in structurally weakened zones. Unlike seismically active systems such as Monte Vettore (Ciotoli et al., 2016), the AAB has not experienced major recent earthquakes, although historical events (e.g., 2001) produced transient changes in degassing and aquifer behavior, likely due to porosity variations within the travertine (Gasparini et al., 2002; La Vigna et al., 2012). Overall, the AAB emerges as a structurally complex, low-enthalpy hydrothermal system where deep CO_2 ascends through a combination of fault-controlled pathways and groundwater-driven advection, mixing with cold karstic recharge from the Apennines. Its unique travertine-dominated permeability architecture, long-lasting hydrothermal history, and moderate but persistent CO_2 emissions make it a distinctive natural laboratory for both geothermal and tectonically controlled degassing systems (Castorina et al., 2023; Mancini et al., 2024).

4.7 Limitation of the study

There are several limitations regarding the study area. which is characterized by private properties. active quarrying. industrial activity and an army airport. Consequently. the area is not uniformly covered by soil CO_2 flux surveys. Soil CO_2 flux surveys were conducted between January 2024 and May 2025; therefore, the measurements were not performed under uniform atmospheric pressure and temperature conditions. These findings suggest that. despite potential variability in individual values, the observed anomalies are unlikely to exert a significant influence on the final interpolation outcomes. For this reason, all measurements were performed under high atmospheric pressure, on sunny days, and during late-morning hours to avoid the influence of morning dew. Consequently, the resulting dataset can be considered robust and suitable for interpretation.

4.8 Conclusion

In summary, our measurements revealed that the main hydrothermalism is distributed inside the AAB, along the most important NS shear zone and along the NW-SE lineaments. We collected all published and unpublished studies relating to the structural geology of the AAB. Furthermore, we conducted four transects to measure soil CO_2 fluxes in Cretone. Sant'Angelo Romano, Bagni di Tivoli and Corcolle. We combined these data with the soil CO_2 flux data from Chapter 3. The results show that the soil carbon dioxide flux appears to follow the N-S and NW-SE lineaments. $\delta^{13}C$ analysis indicates decrease of thermalism from west to east, consistent with chronological data on travertine from Faccenna et al. (1994. 2008) and De Filippis et al., 2013. This implies that the westernmost part of the basin, where Collefiorito Ridge is present, represents the youngest hydrothermal manifestation in the plain according to De Filippis et al.,2013. This also means that fluid circulation is mostly concentrated in the NW-SE and N-S spots, which are flanked by areas characterized by high sealing with thick travertine where paleo-fluid circulation was present. Hydrothermal activity in the Cretone area indicates faulting and fluid migration in the northern sector of the main strike-slip zone. No additional degassing anomalies were detected. The Sant'Angelo and Corcolle areas also show no significant anomalies. These observations suggest that fluid circulation is mostly limited to the basin itself.

4.9 References

Acocella. V.. & Funiciello. R. (2006). Transverse systems along the extensional Tyrrhenian margin of central Italy and their influence on volcanism. *Tectonics*. *25*(2).

Billi. A.. Valle. A.. Brilli. M.. Faccenna. C.. & Funiciello. R. (2007). Fracture-controlled fluid circulation and dissolutional weathering in sinkhole-prone carbonate rocks from central Italy. *Journal of Structural Geology*. *29*(3). 385-395.

Bini, G., Chiodini, G., Ricci, T., Sciarra, A., Caliro, S., Mortensen, A. K., ... & Costa, A. (2023). Soil CO2 emission and stable isotopes (13C/12C, 18O/16O) of CO2 and calcites reveal the fluid origin and thermal energy in the supercritical geothermal system of Krafla, Iceland.

Brown. D.. DuTeaux. R.. Kruger. P.. Swenson. D.. & Yamaguchi. T. (1999). Fluid circulation and heat extraction from engineered geothermal reservoirs. *Geothermics*. *28*(4-5). 553-572.

Camarda, M., De Gregorio, S., Di Martino, R., Favara, R., & Prano, V. (2020). Relationship between soil CO2 flux and tectonic structures in SW Sicily. *Annals of Geophysics*, *63*(1).

Castorina, F., Masi, U., Billi, A., De Filippis, L., & Nisi, S. (2023). Elemental and Sr–Nd isotopic evidence for unravelling the origin of the low-temperature geothermal fluids of Tivoli Terme (Latium, central Italy) between erosional S4 and S3 phases (upper Pleistocene) and neotectonics implications. *Applied Geochemistry*, *158*, 105794.

Chiodini, G., Frondini, F., Cardellini, C., Granieri, D., Marini, L., & Ventura, G. (2001). CO2 degassing and energy release at Solfatara volcano, Campi Flegrei, Italy. *Journal of Geophysical Research: Solid Earth*, *106*(B8), 16213-16221.

Chiodini. G.. Cardellini. C.. Amato. A.. Boschi. E.. Caliro. S.. Frondini. F.. & Ventura. G. (2004). Carbon dioxide Earth degassing and seismogenesis in central and southern Italy. *Geophysical Research Letters*. *31*(7).

Ciotoli, G., Etiope, G., Marra, F., Florindo, F., Giraudi, C., & Ruggiero, L. (2016). Tiber delta CO2-CH4 degassing: a possible hybrid, tectonically active sediment-hosted geothermal system near Rome. *Journal of Geophysical Research: Solid Earth*, *121*(1), 48-69.

Ciotoli, G., Sciarra, A., Ruggiero, L., Annunziatellis, A., & Bigi, S. (2016). Soil gas geochemical behaviour across buried and exposed faults during the 24 August 2016 central Italy earthquake. *Annals of geophysics*, *59*.

Cipollari. P.. Cosentino. D.. & Parotto. M. (1995). Modello cinematicostrutturale dell'Italia centrale. *Studi Geologici Camerti*. *2*(135143). 1997.

Cosentino. D.. Cipollari. P.. Marsili. P.. & Scrocca. D. (2010). Geology of the central Apennines: a regional review. *Journal of the virtual explorer*. *36*(11). 1-37.

Cosentino. D.. Asti. R.. Nocentini. M.. Gliozzi. E.. Kotsakis. T.. Mattei. M.. ... & Di Fiore. V. (2017). New insights into the onset and evolution of the central Apennine extensional intermontane basins based on the tectonically active L'Aquila Basin (central Italy). *Bulletin*. *129*(9-10). 1314-1336.

De Filippis. L.. Anzalone. E.. Billi. A.. Faccenna. C.. Poncia. P. P.. & Sella. P. (2013). The origin and growth of a recently-active fissure ridge travertine over a seismic fault. Tivoli. Italy. *Geomorphology*. *195*. 13-26.

De Filippis. L.. Faccenna. C.. Billi. A.. Anzalone. E.. Brilli. M.. Soligo. M.. & Tuccimei. P. (2013). Plateau versus fissure ridge travertines from Quaternary geothermal springs of Italy and Turkey: Interactions and feedbacks between fluid discharge. paleoclimate. and tectonics. *Earth-Science Reviews*. *123*. 35-52.

DELLA VEDOVA. B.. Mongelli. F.. Pellis. G.. Squarci. P.. Taffi. L.. & Zito. G. (1991). Heat flow map of Italy. *Geothermics*. *24*. 115-129.

Faccenna. C. (1994). Structural and hydrogeological features of Pleistocene shear zones in the area of Rome (Central Italy). *Annals of Geophysics*. *37*(1).

Faccenna. C.. Soligo. M.. Billi. A.. De Filippis. L.. Funiciello. R.. Rossetti. C.. & Tuccimei. P. (2008). Late Pleistocene depositional cycles of the Lapis Tiburtinus travertine (Tivoli. Central Italy): possible influence of climate and fault activity. *Global and Planetary Change*. *63*(4). 299-308.

Faccenna. C.. De Filippis. L.. Soligo. M.. Billi. A.. Funiciello. R.. Rossetti. C.. & Tuccimei. P. (2009). Cicli deposizionali del travertino Lapis Tiburtinus durante il tardo Pleistocene (Tivoli. Italia Centrale): influenze climatiche e tettoniche. *Rend. Online Soc. Geol. It*. *5*. 86-88.

Fridriksson, T., Kristjánsson, B. R., Armannsson, H., Margrétardóttir, E., Olafsdottir, S., & Chiodini, G. (2006). CO2 emissions and heat flow through soil, fumaroles, and steam heated mud pools at the Reykjanes geothermal area, SW Iceland. *Applied geochemistry*, *21*(9), 1551-1569.

Gasparini. C.. Di Maro. R.. Pagliuca. N. M.. Pirro. M.. & Marchetti. A. (2002). Recent seismicity of the «Acque Albule» travertine basin. *Annals of Geophysics*. *45*(3-4).

Giordano. G. (2013). La geotermia e gli acquiferi dell'Italia centrale. *Acque Sotterranee-Italian Journal of Groundwater*. *2*(4).

Giordano. G.. De Benedetti. A. A.. Bonamico. A.. Ramazzotti. P.. & Mattei. M. (2014). Incorporating surface indicators of reservoir permeability into reservoir volume calculations: Application to the Colli Albani caldera and the Central Italy Geothermal Province. *Earth-Science Reviews*. *128*. 75-92.

Harvey, M. C., Rowland, J. V., Chiodini, G., Rissmann, C. F., Bloomberg, S., Fridriksson, T., & Oladottir, A. A. (2017). CO2 flux geothermometer for geothermal exploration. *Geochimica et Cosmochimica Acta*, *213*, 1-16.

Invernizzi. C.. Pierantoni. P. P.. Chiodi. A.. Maffucci. R.. Corrado. S.. Baez. W.. ... & Viramonte. J. (2014). Preliminary assessment of the geothermal potential of Rosario de la Frontera area (Salta. NW Argentina): Insight from hydro-geological. hydro-geochemical and structural investigations. *Journal of South American Earth Sciences*. *54*. 20-36.

Italiano, F., Martinelli, G., & Plescia, P. (2008). CO2 degassing over seismic areas: the role of mechanochemical production at the study case of Central Apennines. *Pure and Applied Geophysics*, *165*(1), 75-94.

Jolivet. L.. Faccenna. C.. Goffé. B.. Mattei. M.. Rossetti. F.. Brunet. C.. ... & Parra. T. (1998). Midcrustal shear zones in postorogenic extension: example from the northern Tyrrhenian Sea. *Journal of Geophysical Research: Solid Earth*. *103*(B6). 12123-12160.

Li Vigni, L., Temovski, M., Cardellini, C., Molnár, K., Ionescu, A., Mirčovski, V., ... & D’Alessandro, W. (2025). Toward solving the mystery of elevated tectonic degassing in South Eastern Europe: Insights from gas discharges along the Vardar suture (North Macedonia). *Geochemistry, Geophysics, Geosystems*, *26*(7), e2025GC012177.

Liu, L., Chen, Z., Li, Y., Liu, Z., Hu, L., Wang, X., ... & Zhou, X. (2023). Emission of Rn and CO2 from soil at fault zones caused by seismic waves. *Earth and Space Science*, *10*(6), e2023EA003012.

Liotta. D.. Ruggieri. G.. Brogi. A.. Fulignati. P.. Dini. A.. & Nardini. I. (2010). Migration of geothermal fluids in extensional terrains: the ore deposits of the Boccheggiano-Montieri area (southern Tuscany. Italy). *International Journal of Earth Sciences*. *99*(3). 623-644.

Lund. J. W.. Freeston. D. H.. & Boyd. T. L. (2011). Direct utilization of geothermal energy 2010 worldwide review. *Geothermics*. *40*(3). 159-180.

Lund. J. W.. & Toth. A. N. (2021). Direct utilization of geothermal energy 2020 worldwide review. *Geothermics*. *90*. 101915.

Mancini, A., Cornacchia, I., Lamal, J., Capezzuoli, E., Swennen, R., & Brandano, M. (2024). Using stable isotopes in deciphering climate changes from travertine deposits: the case of the Lapis Tiburtinus succession (Acque Albule Basin, Tivoli, Central Italy). *Frontiers in Earth Science*, *12*, 1355693.

Maffucci. R.. Bigi. S.. Corrado. S.. Di Paolo. L.. & Chiodi. A. (2012). Fracture modeling applied to the geothermal system potential reservoir of Rosario de La Frontera (La Candelaria Ridge. NW Argentina). *Rend. Online Soc. Geol. Ital*. *21*. 829-831.

Minissale, A., Kerrick, D. M., Magro, G., Murrell, M. T., Paladini, M., Rihs, S., ... & Vaselli, O. (2002). Geochemistry of Quaternary travertines in the region north of Rome (Italy): structural, hydrologic and paleoclimatic implications. *Earth and Planetary Science Letters*, *203*(2), 709-728.

Minissale. A.. Donato. A.. Procesi. M.. Pizzino. L.. & Giammanco. S. (2019). Systematic review of geochemical data from thermal springs. gas vents and fumaroles of Southern Italy for geothermal favourability mapping. *Earth-Science Reviews*. *188*. 514-535.

Mongelli. F.. Zito. G.. Della Vedova. B. R. U. N. O.. Pellis. G.. Squarci. P.. & Taffi. L. (1991). Geothermal regime of Italy and surrounding seas. In *Terrestrial heat flow and the lithosphere structure* (pp. 381-394). Berlin. Heidelberg: Springer Berlin Heidelberg.

Peiffer, L., Wanner, C., & Pan, L. (2015). Numerical modeling of cold magmatic CO2 flux measurements for the exploration of hidden geothermal systems. *Journal of Geophysical Research: Solid Earth*, *120*(10), 6856-6877.

Petitta, M., Primavera, P., Tuccimei, P., & Aravena, R. (2011). Interaction between deep and shallow groundwater systems in areas affected by Quaternary tectonics (Central Italy): a geochemical and isotope approach. *Environmental Earth Sciences*, *63*(1), 11-30.

Rossetti. F.. Aldega. L.. Tecce. F.. Balsamo. F.. Billi. A.. & Brilli. M. (2011). Fluid flow within the damage zone of the Boccheggiano extensional fault (Larderello–Travale geothermal field. central Italy): structures. alteration and implications for hydrothermal mineralization in extensional settings. *Geological Magazine*. *148*(4). 558-579.

Rubio-Maya. C.. Díaz. V. A.. Martínez. E. P.. & Belman-Flores. J. M. (2015). Cascade utilization of low and medium enthalpy geothermal resources− A review. *Renewable and Sustainable Energy Reviews*. *52*. 689-716.

Sbrana, A., Marianelli, P., Belgiorno, M., Sbrana, M., & Ciani, V. (2020). Natural CO2 degassing in the Mount Amiata volcanic–geothermal area. *Journal of Volcanology and Geothermal Research*, *397*, 106852.

Tamburello. G.. Chiodini. G.. Ciotoli. G.. Procesi. M.. Rouwet. D.. Sandri. L.. ... & Masciantonio. C. (2022). Global thermal spring distribution and relationship to endogenous and exogenous factors. *Nature Communications*. *13*(1). 6378

Taussi, M., Nisi, B., Brogi, A., Liotta, D., Zucchi, M., Venturi, S., ... & Vaselli, O. (2023). Deep regional fluid pathways in an extensional setting: The role of transfer zones in the hot and cold degassing areas of the Larderello geothermal system (Northern Apennines, Italy). *Geochemistry, Geophysics, Geosystems*, *24*(6), e2022GC010838.

5- Numerical modeling of the Acque Albule Basin

Abstract

The Acque Albule Basin is a transtensional depression in the eastern Rome area characterized by active hydrothermal circulation, fault-controlled CO_2 degassing, and periodic seismic swarms. CO_2 fluxes reach 120 g m^{-2} day^{-1} near the Regina and Colonnelle thermal lakes, where anomalies align with N–S and NE–SW fault systems. Carbon-isotope compositions show a west-east decrease in the deep hydrothermal component. Structural and geochemical evidence indicates that the southwestern segment of the main N–S strike-slip fault and associated transtensive structures currently act as the main conduits for CO_2 and hydrothermal fluids. At the same time, low degassing zones are associated with sealed paleo-conduits and massive travertine bodies that locally reduce vertical permeability. Numerical simulations performed with the TOUGH2 code. Geology, hydrogeology, thermal, and gas-flux data, were used to investigate the controls on diffuse degassing. The model includes a ~2 km-thick Mesozoic–Cenozoic carbonate reservoir overlain by Pliocene clays and a thick travertine unit hosting the shallow aquifer. The deep carbonate basement exhibits a thermal gradient of ~90 °C, which is strongly reduced in the overlying travertine aquifer (~20 °C). Simulation results show that shallow meteoric recharge dominate the cold thermal structure of the system, despite the presence of warm temperatures at depth. CO_2 continues to ascend in the fault zone, even if the cold water dominates the conduit. Gas-lift controls CO_2 exsolution and upward migration, reproducing the observed coexistence of low temperatures and vigorous degassing at Regina and Colonnelle lakes. Persistent CO_2-rich flow can promote carbonate precipitation and progressive fault sealing. The model suggests a cyclic alternation between chemical sealing and tectonic reactivation.

5.1- Introduction

The Acque Albule Basin is a transtensional Basin located northeast of Rome and it is characterized by active hydrothermal circulation, periodic seismic swarms, and diffuse CO_2 degassing (Faccenna, 1994; Minissale et al., 2002; Faccenna et al., 2008; De Filippis et al., 2013; Carucci et al., 2012; Mancini et al.,2024). The highest CO_2 fluxes, reaching up to 120 $g\,m^{-2}\,day^{-1}$, occur in proximity to the Regina and Colonnelle thermal lakes, which represent the main upflow zones of the system. Based on previous chapters, the average value of CO_2 diffuse degassing measured across the study area (6 km^2) is 14,538 $g{\cdot}m^{-2}{\cdot}day^{-1}$ while the total daily emission for the Guidonia study area is estimated at 94.55 tons per day (t/d). Carbon-isotope analyses ($\delta^{13}C$) reveal a marked west-east decrease in the deep hydrothermal contribution: values between −1‰ and −5‰ characterize the central and western sector near the Colle Fiorito Ridge, whereas the eastern area exhibits predominantly biogenic signatures (−15‰ to −19‰). A conceptual model developed for the area. CO_2 flux anomalies are spatially correlated with N-S and NE-SW fault systems, which function as preferential conduits for fluid circulation. We identified the southwestern segment of the main N-S strike-slip fault and transtensive structures parallel to the Collefiorito Ridge as the currently active conduits for CO_2-rich fluids. Conversely, low-degassing zones are interpreted as paleo-conduits progressively sealed by travertine precipitation along fault planes, which reduces vertical permeability (fault sealing). The thick, compact travertine body exposed in quarry areas further acts as an impermeable barrier, forcing gas migration toward more fractured sectors of the basin. Diffuse gas emissions are closely linked to the dynamics of fluid circulation, as the main anomalies coincide with the hydrothermal springs. The basin is also affected by seismic activity correlated with the shallow travertine aquifer and associated degassing patterns (Gasparini et al., 2002; La Vigna et al., 2012). This fluid-seismicity coupling indicate that deep fluids are strongly controlled by fault geometry and activity.

This chapter presents numerical simulations of heat and fluid circulation aimed at constraining the mechanisms governing diffuse degassing in the Acque Albule Basin. Multi-phase and multi-component simulations were performed using the TOUGH2 simulator (Pruess et al., 1999). Simulation based on a simple geological framework integrates stratigraphic and structural information from the northern sector of the basin (Guidonia–Collefiorito to Bagni di Tivoli). Furthermore, simulation included data on gas fluxes, local hydrogeology, and rock thermal properties. The deep reservoir corresponds to a

~2000 m-thick Mesozoic–Cenozoic carbonate succession overlain by Pliocene clays aquiclude. A thick travertine plateau was also incorporated on the top of the layers to represent the shallow hydrogeological system. The thermal regime is strongly influenced by karst processes within the carbonate basement, which reduce the geothermal gradient from ~90 °C (Castorina et al., 2023) to ~23 °C (Petitta et al., 2011; Carucci et al., 2012; La Vigna et al., 2013) within the overlying travertine aquifer. The simulations evaluate the effects of carbonate-basement aquifer, cap-rock properties, deep CO_2 supply rate, and the presence of permeable pathways through the layers. Results indicate that the fault acts as a preferential pathway for cold meteoric recharge, reducing the temperature of the geothermal system. At the same time, CO_2 degassing persists along the damage zone. Gas-lift, is identified as the main driver of CO_2 exsolution, allowing gas ascent even in a cooled hydraulic regime. This behaviour is consistent with the Acque Albule springs, where low temperatures coexist with vigorous CO_2 release.

5.2- Methodology

The fluid circulation within the Acque Albule Basin was simulated using the TOUGH2 geothermal reservoir simulator (Pruess et al., 1999). This multi-phase and multi-component numerical framework describe the coupled transport of heat and fluids through heterogeneous porous media. In the present application, the modeled fluid components are water and carbon dioxide.

The simulator based on the Henry's law (Equation 5.1). Henry's law describes the phase transitions of water and gas as a function of the main thermodynamic conditions. Henry's law represents the fundamental constitutive relation governing CO_2 solubility in our simulations.

$$P_{NCG} = K_h \, x_{aq}^{NCG}$$

Equation 1 -The partial pressure of the non-condensable gas (NCG) is proportional to its mole fraction in the aqueous phase (XNCGaq). Kh denotes the temperature-dependent Henry constant governing CO_2 solubility in water (Pruess et al., 1999).

All available geological, geophysical, geochemical, and hydrogeological data for the Acque Albule Basin were integrated to construct a simple and consistent representation of the study area. The physical and hydraulic properties assigned to each lithological unit are summarized in Table 5.1 (see Chapter 7, Appendix C). Layers modeled for the AAB context are explained as follow:

The uppermost stratigraphic unit is the travertine deposit, with 60 m thickness. This value is in agreement within the observed range of 30–90 m documented in boreholes (Faccenna et al., 2009). This unit is characterized by high secondary permeability resulting from pervasive fracturing and localized karstification, but in this model it was considered as a homogeneous porous layer. The intermediate stratigraphic unit consists of Plio-Pleistocene clay, which is represented in the model as an aquitard. These Plio–Pleistocene marine and continental deposits, modeled with a thickness of 280 m, should act as an impermeable barrier that ideally restricts vertical fluid migration and promotes pressure within the reservoir. Finally, the Meso-Cenozoic carbonate bedrock constitutes the deep reservoir. This unit forms a regional aquifer and hosts the hydrothermal circulation system. Fluids can reach temperatures of up to 90 °C at depth, as indicated by recent studies on travertine deposits (Castorina et al., 2023; Mancini et al., 2024). The model also incorporates a damage zone representing the fault and fracture systems, including the N-S trending structure. This zone is characterized by high permeability and functions as a preferential conduit for the ascent of CO_2-rich thermal waters toward the surface. Schematic stratigraphic sequences were defined to represent the typical geological conditions of the basin. For modeling purposes, the domain was simplified into three main units: (i) the travertine deposits (Lapidus Tiburtinus travertine; Faccenna et al., 2009), (ii) the Plio–Pleistocene clay sequence, and (iii) the underlying carbonate rocks (Figure 5.1).

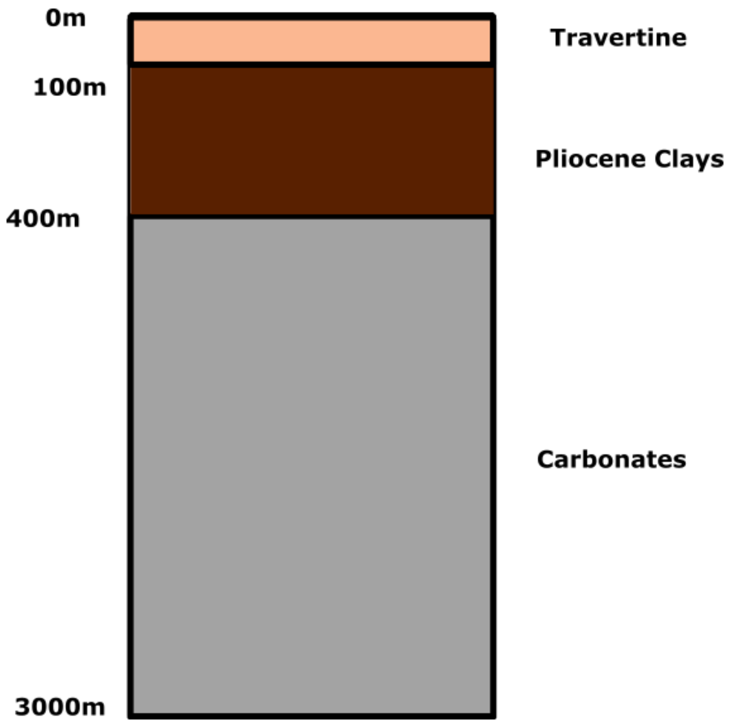

Figure 5.1- Schematic stratigraphic sequence of the numerical domain.

The numerical model in this study is a simplified configuration designed to simulate a 2-D cross-section of the degassing system. Boundary conditions include a fixed surface temperature of 20 °C, and a pressure of 1013,25 millibar (atmospheric conditions). At the bottom CO_2 source is distributed with mass flux of 10^{-5} kg m^{-2} s^{-1}. The carbonate reservoir basement has an initial temperature of 90°C. The computational domain extends to a depth of -3000 m, corresponding to the level at which anhydrite-bearing formations are present and where sulfur species dissolve into the hydrothermal fluids (Minissale et al., 2002; Castorina et al., 2023; Mancini et al., 2022). The model geometry and boundary conditions are illustrated in Fig. 3.

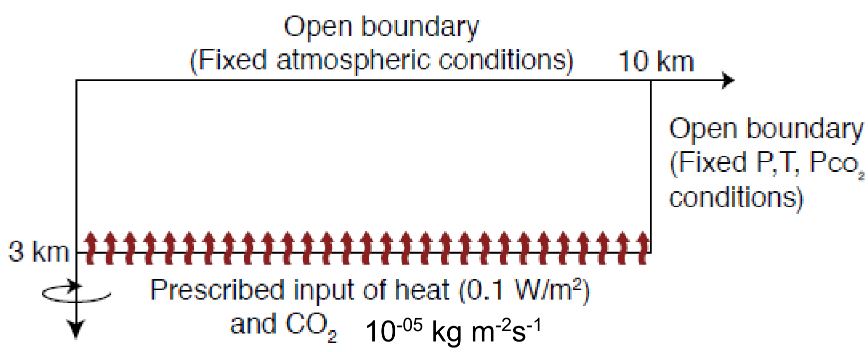

Figure 5.3- Boundary condition of the numerical simulation (Modified after Todesco et al., 2010).

The model domain is initially cold and fully water-saturated. Heat (0.1 W m^{-2}), warm fluids at 90 °C, and CO_2 at a mass flux of 10^{-5} kg m^{-2} s^{-1} are injected along the base of the domain until steady-state conditions are reached (after approximately 100 years for each simulation). The estimated average regional surface emission rate (10^{-7} kg m^{-2} s^{-1}) does not represent the mass flux at the base of the deep hydrothermal system. In structurally controlled hydrothermal settings such as Guidonia, deep degassing is not homogeneous, but it is focused within a network of fractures and partially sealed conduits that channel ascending fluids. For this reason, a basal flux of 10^{-5} kg m^{-2} s^{-1} was imposed to reproduce a “feeding-zone” configuration. Fault-sealing processes were not included due to lack of time, but it will be incorporated in future models.

5.3- Simulation and results

The simulation results are presented in Fig. 5.4. We report the spatial distribution of temperature, pressure, CO_2 partial pressure, and gas saturation. The objective was to reproduce the evolution of the system toward steady-state conditions under the imposed thermal and fluid-flow constraints. The domain is initially cold and fully water-saturated.

The choice to allow exchange with the atmospheric boundary reflects the need to simulate the interaction between shallow meteoric recharge (represented by cold surface waters) and the underlying hydrothermal system. This configuration enables us to evaluate how near-surface hydrological processes influence the ascent and dispersion of deep CO_2-rich fluids.

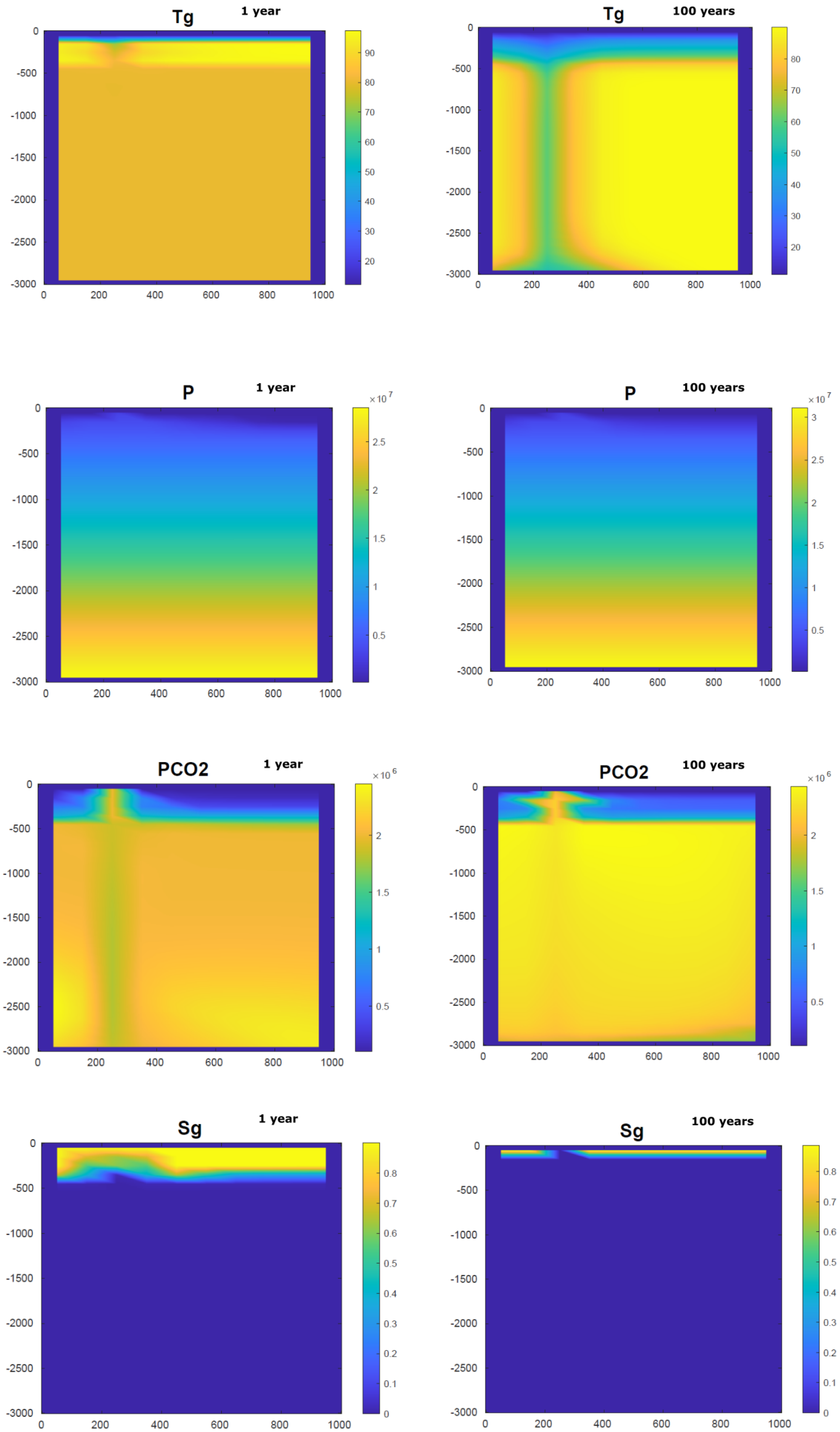

Tg
1 year
Tg
100 years
P
1 year
×10^7
P
100 years
×10^7
PCO2
1 year
×10^6
PCO2
100 years
×10^6
Sg
1 year
Sg
100 years

Figure 5.4- Numerical simulation results obtained with TOUGH2. The images illustrate the evolution at t=1 year and t=100 years of the temperature, pressure, CO_2 partial pressure, and gas saturation.

The modeled domain consists of three horizontally stratified layers and includes a high-permeability vertical discontinuity (damage zone or fault) with a width of 100 m that extends through the entire depth of the system. The upper boundary is defined as an open boundary with constant pressure and temperature, whereas the base of the model is subjected to a uniform conductive heat and CO_2 flux.

The temperature field changes over time. After 1 year, the domain is 90 °C in all the column, except for the travertine, affected by the cooler atmospheric boundary. After 100 years, the whole system becomes significantly cooler. A clear cold anomaly develops on the vertical structure at x=300 m.

The pressure field shows no change between 1 year and 100 years of simulation. Pressure increases with depth, starting from values close to atmospheric pressure at the top and reaching about 3×10^7 Pa at the bottom, with only a small anomaly near the fault. This behavior indicates that the system remains in a stable hydrostatic regime. The overall permeability of the domain and the open upper boundary prevent the development of localized overpressures or large-scale, non-stationary hydraulic gradients.

At the beginning, the CO_2 partial pressure is high in the deep part of the domain. The system initially contains a large amount of dissolved CO_2. After 100 years, PCO_2 remain stable in the deeper part and the lateral- upper sectors of the faults has higher values.

Finally, a thick zone with high gas saturation (Sg= 0.8) is present in the upper 400 m of the domain, showing that CO_2 is mostly in a free-gas phase during the early stage. After 100 years, the free-gas phase almost completely disappears from the upper part of the system. Gas remains only as a very thin layer just below the atmospheric boundary and as a small, trapped anomaly near the fault.

5.4- Discussion

At t=1 year, the system is still homogeneous, with temperatures around 90 °C in the carbonate layer, while the clay and travertine layers remain at atmospheric temperature condition. After 100 years, the situation changes: the system becomes significantly colder, especially within the fault zone, where a strong temperature decrease occurs due to the downwelling of cold meteoric water. The fault acts as a conduit for the downward cold flow, and the resulting cooling spreads laterally into the reservoir through thermal conduction. Pressure remains hydrostatic for the entire duration of the simulation, except for a small decrease near the fault. This indicates that the system is hydraulically well connected despite the clay low permeability.

The partial pressure of CO_2 is initially high in the deeper part of the domain, consistent with CO_2 being dissolved at depth. After 100 years, PCO_2 increase along the fault zone, where the downward-moving meteoric water dilutes the deep CO_2-rich fluid. In contrast, the deeper lateral sectors maintain high PCO_2 values.

Gas saturation is initially high in the upper 400 m due to the open-air boundary, which allows the presence of a free-gas phase. After 100 years, gas saturation decreases, except for the upper part of the travertine layer. This reduction is controlled by the cooling of the system: as temperature decreases, CO_2 solubility increases, and more CO_2 dissolves into the liquid phase, reducing the amount of free gas. Within this framework, the model indicates that the system becomes progressively controlled by cold karstic recharge, which cools the hydrothermal reservoir. As temperature decreases, CO_2 solubility increases, and CO_2 is more easily dissolved in the colder water. This leads to a reduction of the separate CO_2 gas phase. Under warmer environmental conditions, these CO_2-rich fluids can contribute to travertine precipitation (Della Porta et al., 2021). After 100 years, the system is therefore dominated by cold recharge, which dissolves CO_2 and produces CO_2-rich water throughout the travertine aquifer and the Acque Albule Basin plain. In the early stage, a strong deep CO_2 input can reach the surface, producing degassing and travertine deposition. However, when the fault remains an open conduit for a long time, cold karstic water can penetrate deeply, cool the system, and promote CO_2 dissolution. Hydrothermal water in the AAB lakes (Regina and Colonnelle) rise due to a gas-lift mechanism (e.g. Hutchison et al., 2023). High CO_2 partial pressure within the fault reduces fluid density, allowing upward flow even without a strong thermal gradient. Thus, although the system is cooled by meteoric recharge, CO_2 at the base of the model can still generate gas-lift. At hydrostatic pressure, CO_2 remains dissolved. When CO_2-rich water rises through a cold conduit (gas-lifting process), it can reach the surface thorough hydrothermal springs such as the Regina and Colonnelle lakes, where mineralized water with bubbling is observed. This is consistent with the gas saturation results, which show gas accumulation near the open-air boundary and within the travertine layer.

When CO_2-rich water rises through the fault, mineral precipitation may progressively seal the conduit and forming an impermeable barrier. The process may repeat along another discontinuity, producing similar effects. Based on the numerical modeling, we interpret the geological setting of Regina and Colonnelle as like the early stage of the simulation, where the hydrothermal system is still relatively warm, and degassing is vigorous along the fault. Areas with lower degassing correspond instead to the later stage of the simulation, where the system is colder and partially sealed.

5.5- Conclusions

The main results of this study can be summarized as follows:

The long-term simulation (100 years) highlights a clear recharge-controlled regime. The damage zone acts as a preferential hydraulic pathway for cold meteoric fluids entering from the atmospheric upper boundary and producing a marked thermal decrease in temperature within the conduit. However, the downward penetration of cold meteoric water does not inhibit CO_2 degassing: the basal CO_2 input maintains a modest partial pressures (PCO_2) along the fault axis. The analysis of gas saturation at 100 years shows the persistence of a free-gas at travertine. The numerical results indicate that the main driver of degassing is not a positive thermal anomaly, but the gas-lift process experienced by the fluid during ascent. Based on Henry's law and on the model, gas can ascend even in a cold hydraulic regime. This behavior reproduces the field evidence from the hydrothermal spring in the Acque Albule system, which display low surface temperatures but vigorous and continuous CO_2 release. In the Guidonia Basin, persistent degassing in cold environment induces systematic pH reduction in the fluids, triggering calcium carbonate precipitation (travertine plateau). This process leads to progressive mineral cementation and hydraulic sealing of the fault. Finally, the long-term persistence of the Acque Albule hydrothermal system suggests that the basin is governed by a cyclic behavior phases of chemical interrupted by transient seismo-tectonic reactivations, restoring the initial flow conditions observed in the early stages of the simulation.

5.6- Limitation and future work

The numerical modelling presented here is preliminary due to time constraints. At this stage, only a limited set of 2D simulations has been performed, and further numerical development is required to obtain a fully constrained representation of the Acque Albule Basin (AAB). Future improvements should include longer simulation times, 3D modelling, a more complex mesh, and additional simulation steps and runs. These developments could not be completed before the thesis deadline, but they will be addressed in future work.

5.7- References

Carucci, V., Petitta, M., & Aravena, R. (2012). Interaction between shallow and deep aquifers in the Tivoli Plain (Central Italy) enhanced by groundwater extraction: a multi-isotope approach and geochemical modeling. *Applied Geochemistry*, *27*(1), 266-280.

De Filippis, L., Anzalone, E., Billi, A., Faccenna, C., Poncia, P. P., & Sella, P. (2013). The origin and growth of a recently-active fissure ridge travertine over a seismic fault, Tivoli, Italy. *Geomorphology*, *195*, 13-26.

Della Porta, G., Hoppert, M., Hallmann, C., Schneider, D., & Reitner, J. (2022). The influence of microbial mats on travertine precipitation in active hydrothermal systems (Central Italy). *The Depositional Record*, *8*(1), 165-209.

Faccenna, C. (1994). Structural and hydrogeological features of Pleistocene shear zones in the area of Rome (Central Italy). *Annals of Geophysics*, *37*(1).

Faccenna, C., Soligo, M., Billi, A., De Filippis, L., Funiciello, R., Rossetti, C., & Tuccimei, P. (2008). Late Pleistocene depositional cycles of the Lapis Tiburtinus travertine (Tivoli, Central Italy): possible influence of climate and fault activity. *Global and Planetary Change*, *63*(4), 299-308.

Gasparini, C., Di Maro, R., Pagliuca, N. M., Pirro, M., & Marchetti, A. (2002). Recent seismicity of the «Acque Albule» travertine basin. *Annals of Geophysics*, *45*(3-4).

Hutchison, W., Ogilvie, E. R., Birhane, Y. G., Barry, P. H., Fischer, T. P., Ballentine, C. J., ... & Guðbrandsson, S. (2023). Gas emissions and subsurface architecture of fault-controlled geothermal systems: A case study of the north Abaya geothermal area. *Geochemistry, Geophysics, Geosystems*, *24*(4), e2022GC010822.

La Vigna, F., Carucci, V., Mariani, I., Minelli, L., Pascale, F., Mattei, M., ... & Tallini, M. (2012). Intermediate-field hydrogeological response induced by L'Aquila earthquake: the Acque Albule hydrothermal system (Central Italy). *Italian Journal of Geosciences*, *131*(3), 475-485.

La Vigna, F., Mazza, R., & Capelli, G. (2013). Detecting the flow relationships between deep and shallow aquifers in an exploited groundwater system, using long-term monitoring data and quantitative hydrogeology: the Acque Albule basin case (Rome, Italy). *Hydrological Processes*, *27*(22), 3159-3173.

Mancini, A., Cornacchia, I., Lamal, J., Capezzuoli, E., Swennen, R., & Brandano, M. (2024). Using stable isotopes in deciphering climate changes from travertine deposits: the case of the Lapis Tiburtinus succession (Acque Albule Basin, Tivoli, Central Italy). *Frontiers in Earth Science*, *12*, 1355693.

Minissale, A., Kerrick, D. M., Magro, G., Murrell, M. T., Paladini, M., Rihs, S., ... & Vaselli, O. (2002). Geochemistry of Quaternary travertines in the region north of Rome (Italy): structural, hydrologic and paleoclimatic implications. *Earth and Planetary Science Letters*, *203*(2), 709-728.

Nespoli, M., Todesco, M., Serpelloni, E., Belardinelli, M. E., Bonafede, M., Marcaccio, M., ... & Gualandi, A. (2016). Modeling earthquake effects on groundwater levels: evidences from the 2012 Emilia earthquake (Italy). *Geofluids*, *16*(3), 452-463.

Petitta, M., Primavera, P., Tuccimei, P., & Aravena, R. (2011). Interaction between deep and shallow groundwater systems in areas affected by Quaternary tectonics (Central Italy): a geochemical and isotope approach. *Environmental Earth Sciences*, *63*(1), 11-30.

Pruess, K., Oldenburg, C. M., & Moridis, G. J. (1999). TOUGH2 user's guide version 2.

Tescione, I., Todesco, M., & Giordano, G. (2021). Geothermal fluid circulation in a caldera setting: The Torre Alfina medium enthalpy system (Italy). *Geothermics*, *89*, 101947.

Todesco, M., & Giordano, G. (2010). Modelling of CO2 circulation in the Colli Albani area.

6- Conclusion

6.1- Summary of degassing evidence and hydrothermal activity in the Acque Albule Basin

The integrated analysis of soil CO_2 flux measurements and isotopic data presented in Chapters 3 and 4 provides a framework for understanding the structural controls governing hydrothermal fluid circulation within the Acque Albule Basin (AAB). Accumulation-chamber surveys reveal pronounced degassing anomalies (locally up to 120 g m^{-2} day^{-1}) concentrated around the Regina and Colonnelle thermal lakes, in correspondence with the major N–S strike-slip and NE–SW transtensional fault systems. Results show also area characterized by very low degassing (5 g m^{-2} day^{-1}). The spatial pattern of $\delta^{13}C$ values, marked by a progressive eastward attenuation of the deep hydrothermal signature, further indicates a lateral decrease in deep fluid contribution. The study identified the western sector, and the faults associate with Colle Fiorito Ridge as the most recent and structurally active up flow zones for hydrothermal fluids. Moreover, regional transects across Cretone, Sant'Angelo Romano, and Corcolle demonstrate that active fluid migration is largely restricted to the AAB, whereas adjacent segments of the shear zone appear hydraulically inactive or sealed by pervasive mineral precipitation. Overall, these results depict a dynamic hydrothermal system in which tectonic structures act as conduit-barrier elements. In this system, permeability is continuously affected by the ongoing fault opening and self-sealing processes associated with travertine deposition.

6.2- Implications of Numerical Modelling for Fluid Circulation in the Acque Albule Basin

The numerical simulations were performed using the TOUGH2 code to investigate hydrothermal circulation within the Acque Albule Basin (AAB). Models were based on a simplified 2-D cross-sectional domain that integrates regional stratigraphic, structural, and geothermal data. The model architecture was representing a 3000 m deep section where the Travertine plateau, the Plio-Pleistocene clay aquitard, and a deep Meso-Cenozoic carbonate reservoir formed a three-layer system. The model included a 100 m-wide high-permeability vertical damage zone to represent the main fault system. For modeling purposes, these units were simplified as homogeneous porous media, and time-dependent fault-sealing processes were excluded from this preliminary stage.

The results demonstrate a progressive cooling of the system over the 100-year simulation period. The fault zone acts as a preferential conduit for cold meteoric recharge, which progressively reduce the reservoir temperature in proximity to the fault (from 90 °C to approximately 60 °C and ultimately reaching surface conditions of around 20 °C). The models also reveal that this thermal cooling does not inhibit CO_2 ascent. Upward migration is interpreted as being driven by a gas-lift mechanism, whereby high CO_2 partial pressures reduce fluid density within the fault zone. This mechanism reproduces field evidence from the Regina and Colonnelle lakes, which exhibit vigorous degassing despite their relatively low temperatures. Overall, the discussion of these results suggests that the simulated behaviour of the fault zone may represent the base mechanism governing fluid circulation in the Acque Albule Basin. Nevertheless, further investigation is required to fully validate this interpretation.

6.3- Methodological Validation and International Field Campaigns

Diffuse soil CO_2 degassing represents a powerful diagnostic tool for assessing near-surface permeability and identifying zones of active fluid circulation. Measuring soil CO_2 flux is an effective, non-invasive method for detecting natural degassing phenomena that reflect the geological and structural characteristics of an area, while also supporting the evaluation of gas-related hazards across diverse geological settings. Soil-flux surveys allow the quantification of both the intensity and spatial distribution of emissions, enabling the recognition of anomalous degassing zones that commonly correspond to fault systems, upflow areas, or hydrothermal discharge zones.

This final section summarizes the soil CO_2 flux measurements carried out during this Ph.D. across a range of geological environments. The aim was to show the robustness of the method and its potential as a comparative and diagnostic tool beyond the Acque Albule Basin. In addition to the Acque Albule Basin, several other sites were investigated:

1. **Urban green areas of Rome**, including Parco del Pineto, Circo Massimo, Terme di Caracalla, Villa Celimontana, Porta Metronia, San Giovanni, and Garbatella, as well as selected sectors of the Acque Albule Basin (part of the AMUSED project). These sites were used to characterize the interplay between biogenic background, anthropogenic contributions, and natural degassing in densely populated environments.

2. **The Marano Equo site**, located in the Simbruini Mountains (central Apennines), which was surveyed as a structural and hydrogeological analogue to the Acque Albule system, allowing a direct comparison between carbonate-hosted degassing in different tectonic contexts.
3. **Vulcano Island (Italy)**, where soil CO_2 flux was monitored during an active phase of volcanic unrest, providing insights into the sensitivity of the method under rapidly evolving magmatic–hydrothermal conditions.
4. **Poás Volcano** (Costa Rica, AVERT project), also investigated during a period of unrest, offering an opportunity to apply the methodology in a high-temperature volcanic environment characterized by strong fumarolic activity and dynamic degassing processes.

All the investigated sites collectively span a wide spectrum of degassing mechanisms, ranging from deep crustal CO_2 leakage to high-temperature volcanic emissions. This diversity provides a powerful framework for testing the versatility and diagnostic tool of soil CO_2 flux measurements. The inclusion of case studies from both Italy and Costa Rica further highlights the international relevance of the methodological approach demonstrating its applicability to natural, hydrothermal, and volcanic degassing environments under markedly different geological and tectonic conditions.

6.3.1- AMUSED Project

The AMUSED project (A MUltidisciplinary Study of past global climatE changes from continental and marine archives in the Mediterranean region) is a European multidisciplinary research program coordinated by the Istituto Nazionale di Geofisica e Vulcanologia (INGV) in collaboration with several partner institutions. The project aims to reconstruct past environmental and climatic changes in the central Mediterranean through integrated geological, geophysical, and geochemical investigations. A key component of the program focuses on the analysis of natural soil CO_2 emissions from biogenic, anthropogenic, and geological sources. Within this framework, soil CO_2 flux measurements are employed to quantify the contribution of endogenous carbon to the local atmospheric budget and to identify structural or tectonic controls on gas release. Field activities were conducted at multiple sites across the Lazio region, including the Acque Albule thermal basin (Tivoli). Additional surveys were carried out in urban and green areas of Rome, providing comparative datasets useful for distinguishing natural degassing from anthropogenic CO_2 contributions.

Between April and October 2024, several field campaigns were conducted in urban green areas of Rome to investigate soil CO_2 degassing (Fig. X). My contribution focused on the identification, measurement, and spatial mapping of CO_2 emission sites in Parco del Pineto, Circo Massimo, Terme di Caracalla, Villa Celimontana, Porta Metronia, San Giovanni, and Garbatella, as well as in selected sectors of the Acque Albule Basin (AAB) near Tivoli.

Figure 6.1 - Soil CO2 flux measurements in roman city center.

6.3.2- Marano Equo

In April 2024, a four-day field campaign was carried out to measure soil CO_2 emissions in the area surrounding Marano Equo (Rome province). The site lies within the Aniene Valley, between the Simbruini and Ruffi Mountains, and was selected to investigate potential analogies and contrasts with the Acque Albule Basin. Marano Equo belongs to the Latium-Abruzzi sector of the central Apennines and is characterized by a thick Mesozoic carbonate platform succession, deformed within the fold-and-thrust belt typical of the Apennine chain. The area displays widespread karst features, including caves, sinkholes, and spring systems. Karst features exert strong control on groundwater circulation (Di Salvo et al., 2013; Cangemi et al., 2021).

The Aniene Valley hosts extensive Quaternary calcareous tufa and travertine deposits formed through the degassing of CO_2-rich groundwater and subsequent carbonate precipitation. One of the most distinctive characteristics of the valley is the abundance of thermo-mineral springs, sustained by deep-circulating fluids interacting with the carbonate reservoir. The upward migration and degassing of CO_2-enriched waters often promote travertine deposition and mineralization (Cangemi et al., 2021), indicating a strong coupling between deep-seated CO_2 fluxes and surface hydrothermal activity. This conceptual framework suggests that Marano Equo lies within a hydrogeochemical and tectonic setting favorable to soil CO_2 release.

The thermo-mineral springs of Marano Equo (e.g., the Oriella spring; Fig. 6.2) exhibit temperatures of 18–20 °C, likely reflecting the mixing of deep, warm fluids with cold recharge waters circulating through the karstic carbonate system (Cangemi et al., 2021). Field measurements revealed soil CO_2 fluxes ranging from 9.8 to 168 g m^{-2} day^{-1}, with an average value of approximately 42 g m^{-2} day^{-1}. Degassing is at least twice higher respect to the mean degassing rate observed at the Acque Albule site (see Chapters 3 and 4). Considering the stratigraphic contrast between the two areas (where the Acque Albule Basin is sealed by a thick travertine cap, whereas Marano Equo is dominated by limestones and calcarenites), we hypothesize that the travertine cover at Guidonia may partially mask the true magnitude of gas release and fluid ascent in the Acque Albule system. Further analyses and integration of the Marano Equo dataset will be required to fully constrain the mechanisms governing CO_2 migration and surface degassing in this sector of the Aniene Valley.

Figure 6.2 - Oriella thermal springs and survey with the accumulation chamber (Marano Equo).

6.3.3- Monitoring Campaign at Vulcano Island

From 27 to 30 May 2024, I participated in a monitoring campaign on Vulcano Island (Aeolian Archipelago, Italy) to investigate active soil CO_2 degassing during an ongoing phase of volcanic unrest (Fig. 6.3). The work was carried out in collaboration with the INGV geochemistry team, which routinely collects geochemical data on behalf of the Italian Civil Protection to assess the current state of volcanic activity. Measurement sites were primarily located near residential areas where degassing poses a significant hazard, along the popular Levante beach, and in the northwestern sector of La Fossa crater. Additional surveys were conducted in the Palizzi and Vallonazzo areas, which host the most intense CO_2 emission zones, with fluxes exceeding 1000 g m^{-2} day^{-1}. These high-degassing areas are aligned along distinct volcano-tectonic lineaments, which likely represent key structures controlling gas ascent. Identifying and monitoring these alignments is essential for understanding the degassing dynamics and structural evolution of the volcano during periods of unrest.

Figure 6.3 - CO_2 soil flux surveys in Vulcano island.

6.3.4- The AVERT PROJECT (Poàs, Costa Rica)

This field activity was conducted within the framework of the AVERT Project (Anticipating Volcanic Eruptions in Real Time), which aims to improve real-time monitoring and the understanding of volcanic unrest and degassing processes. The Poás Volcano campaign provided an opportunity to apply the soil CO_2 flux methodologies developed during this Ph.D. to an international context characterized by active volcanic degassing. A field campaign was carried out between 9 and 15 March 2025 to measure soil CO_2 flux at Poás Volcano (Costa Rica) during a phase of volcanic unrest. Poás is part of the northwest-trending Central American Volcanic Arc and is one of the world's most active volcanoes. It is renowned for its intense phreatic and phreatomagmatic activity, which is difficult to forecast and constitute a significant hazard to the thousands of tourists who visit the volcano daily. Monitoring soil CO_2 degassing and soil temperature is essential for investigating the hydrothermal processes occurring within the volcanic edifice and for assessing the role of tectonic structures in controlling fluid circulation.

At the time of the survey, access to the crater rim was restricted due to heightened volcanic activity. Measurements of CO_2 flux and soil temperature were therefore conducted both by walking along accessible portions of the crater rim and using a drone-based sampling system. Additional measurements were collected on the upper terrace inside the crater to assess whether diffuse degassing extended beyond the main fumarolic areas (Fig. 6.4). A total of 251 soil CO_2 flux and soil temperature measurements were acquired. The results show low CO_2 fluxes along the crater rim, with an average value of 1.89 ± 0.05 g m^{-2} day^{-1}, whereas significantly higher emissions were recorded within the main fumarolic field, averaging 624 g m^{-2} day^{-1}. These findings indicate a near-absence of diffuse degassing around the crater rim, with most gas release concentrated within the central conduit zone, where fumarolic activity is most intense.

A scientific paper "García-Martínez, N., Girona, T., Drymoni, K., Emili, S., Picciallo, M., Lev, E., ... & Benavente, D. (2026). Soil CO2 Degassing and Temperature at Poás Volcano: Evidence From the 2025 Eruptive Phase. *Geofluids*, *2026*(1), 9516969" has been published.

Figure 6.4 - CO_2 measurements along the crater rim at Poàs Volcano (Costa Rica).

6.4 Opportunities for Territorial Regeneration within the NRRP Framework

The following section outlines the practical implications of this Ph.D. project, without aiming to provide a formal urban planning proposal. This research is funded by the Rome Technopole within the NRRP (PNRR) framework, specifically under the project *"Geothermal energy resources for the energy transition in urban regeneration and construction.* The tectonic and geochemical analyses developed in this thesis offer a critical dataset for formulating integrated regeneration strategies. These strategies are intended to support environmental restoration, social revitalization, and energy innovation within the municipalities of Guidonia and Tivoli. It is widely recognized that the redevelopment of urban and peri-urban areas affected by long-term exploitation represents one of the major challenges of contemporary territorial planning. Areas characterized by degraded suburbs and interrupted economic activities, such as the Acque Albule Basin, require an integrated approach that combines environmental rehabilitation, social inclusion, and renewable-energy innovation. In this context, the energy transition provides a strategic opportunity to transform marginal city areas into green hubs capable of promoting sustainable energy production, rehabilitating abandoned infrastructures, and enhancing local natural resources. Sustainable redevelopment implies not only the functional recovery of compromised spaces, but also the reintegration of ecological, social, and economic functions within the territory. Within this framework, local natural resources can play a central role as drivers of integrated regeneration. The Acque Albule Basin, located between Tivoli and Guidonia Montecelio, lies in a peri-urban area with significant environmental potential but also evident signs of degradation. The districts of Villalba, Villanova, and Tivoli Terme display clear indicators of territorial vulnerability, including building decay, abandoned quarries, and fragmented public spaces. These material conditions are accompanied by social challenges and forms of marginality, creating a complex landscape where past quarrying activity has left a heavily altered environment that nonetheless retains valuable resources for future regeneration.

Among these resources, particular attention is given to the thermal-mineral waters and the historical travertine quarry system, which have shaped the geological and cultural identity of the area for centuries. The mineralized waters of the Acque Albule represent an important natural asset with both environmental and potential energy applications. The presence of abandoned quarries and water-filled basins offers opportunities for installing geothermal and solar energy systems, combining heat pumps or thermal exchangers with floating photovoltaic (PV) panels. Such systems would enable the simultaneous production of thermal and electrical energy by exploiting groundwater with stable temperatures (12–23 °C) and the surface of quarry lakes, transforming abandoned extraction sites into hubs of sustainable energy production.

Furthermore, mineralized water resulting from quarrying activities could be recovered and treated using solar-still technologies to produce freshwater suitable for irrigation or industrial processes, such as travertine processing. Treated quarry wastewater could also be re-used by the nearby Tivoli thermal baths, which are widely exploited for therapeutic and wellness purposes. After appropriate chemical and bacteriological treatment, the water could be reinjected into the subsurface, promoting a circular water-management model for the area.

The site also offers the potential for establishing a *Geological Park of the Acque Albule*. A network of thematic trails could be developed to highlight the geological significance of travertine, the history of the stone-working industry, the morphological evolution of the landscape, and the cultural memory of ancient quarrying. Several existing quarries preserve a direct link to the Roman Empire; for example, the Cava del Barco, whose travertine was used to construct major imperial monuments. Decommissioned quarry areas could be converted into cultural and recreational spaces, such as amphitheaters or open-air cinemas, contributing to the urban and social regeneration of Guidonia. The trail network could be enriched with educational and interactive installations dedicated to geology, history, and renewable-energy technologies. Overall, Guidonia has the potential to become a *green cultural hub*, where renewable energy, geo-tourism, and historical heritage converge into a replicable model for ecological transition and the enhancement of natural assets (Fig. 6.5).

Figure 6.5 – Example of a rendering illustrating the Acque Albule Basin (AAB) Geo-Park, integrating geological and environmental heritage with renewable energy production (image generated with AI).

6.5- References

Cangemi, M., Ranaldi, M., Carapezza, M. L., Vinci, M., & Madonia, P. (2021). Preliminary geochemical characterization of the Mts. Simbruini karst aquifer (Central Italy). Annals of Geophysics, 64(6), HS659-HS659.

Di Salvo, C., Mazza, R., & Capelli, G. (2013). Gli acquiferi in travertino del Lazio: schemi idrogeologici e caratteristiche chimico-fisiche. Rend. Online Soc. Geol. Ital, 27, 54-76.

García-Martínez, N., Girona, T., Drymoni, K., Emili, S., Picciallo, M., Lev, E., ... & Benavente, D. (2025). Dataset of soil CO2 degassing, ground temperature, meteorological parameters, and soil CO_2 concentrations at Poás Volcano (Costa Rica), March 9-15, 2025. Dataset of soil CO_2 degassing, ground temperature, meteorological parameters, and soil CO_2 concentrations at Poás Volcano (Costa Rica), March 9-15, 2025.

García-Martínez, N., Girona, T., Drymoni, K., Emili, S., Picciallo, M., Lev, E., ... & Benavente, D. (2026). Soil CO_2 Degassing and Temperature at Poás Volcano: Evidence From the 2025 Eruptive Phase. Geofluids, 2026(1), 9516969.

6.6- Sites

Amused Web

Home - Real-Time Volcano Monitoring System | AVERT - LDEO Columbia University

7- Appendices

Appendix A- Chapter 3

OBJECTS	X UTM33 WGS 84	Y UTM33 WGS 84	CO2 ppm/s	CO2g_m^{2}day
4203	310368	4650842	0.41	5.74
4202	310450	4650819	0.59	8.26
4201	310550	4650799	0.77	10.78
4206	310585	4650884	0.37	5.18
2323	310616	4648404	1.53	21.42
2917	310616	4648504	1.12	15.68
2896	310616	4648604	0.93	13.02
2875	310616	4648704	1.13	15.82
2854	310616	4648804	1.16	16.24
2812	310616	4649004	0.05	0.7
4200	310635	4650720	0.76	10.64
4199	310635	4650996	0.67	9.38
4224	310653	4650506	0,62	8.68
2610	310654	4649999	0.29	4.06
4212	310657	4651397	0.81	11.34
2630	310662	4649899	0.63	8.82
4223	310677	4650396	0.11	1.54
4189	310677	4650660	0.433	6.062
4197	310677	4650978	0.61	8.54
4204	310686	4650785	0.81	11.34
2672	310690	4649702	0.12	1.68
2324	310716	4648404	1.06	14.84
2918	310716	4648504	1.98	27.72
2897	310716	4648604	0.98	13.72
2876	310716	4648704	2.11	29.54
2855	310716	4648804	2.1	29.4
2834	310716	4648904	1	14
2813	310716	4649004	0.06	0.84
2752	310716	4649304	1.44	20.16
2732	310716	4649404	0.1	1.4
2693	310716	4649604	0.48	6.72
2651	310716	4649804	0.27	3.78
2591	310716	4650104	0.33	4.62
2573	310716	4650204	0.3	4.2
2558	310716	4650304	0.16	2.24
2546	310716	4650404	0.11	1.54
4188	310733	4650642	0.47	6.58
4198	310762	4650945	0.89	12.46
4211	310781	4651373	0.4	5.6
2325	310816	4648404	0.63	8.82
2919	310816	4648504	1.03	14.42
2898	310816	4648604	1.16	16.24
2877	310816	4648704	1.42	19.88
2856	310816	4648804	1.57	21.98

2814	310816	4649004	1.52	21.28
2793	310816	4649104	1.35	18.9
2773	310816	4649204	1.7	23.8
2733	310816	4649404	0.2	2.8
2713	310816	4649504	0.31	4.34
2694	310816	4649604	0.12	1.68
2673	310816	4649704	0.25	3.5
2631	310816	4649904	0.27	3.78
4187	310831	4650613	0.5	7
2835	310854	4648903	1.3	18.2
4213	310860	4651354	0.68	9.52
4205	310885	4650696	0.44	6.16
4181	310886	4648006	0.19	2.66
2920	310899	4648500	1.85	25.9
4186	310904	4650590	0.22	3.08
4196	310909	4650882	0.8	11.2
2326	310916	4648404	1.84	25.76
2899	310916	4648604	2.16	30.24
2878	310916	4648704	1.18	16.52
2857	310916	4648804	0.49	6.86
2836	310916	4648904	0.97	13.58
2815	310916	4649004	1.22	17.08
2794	310916	4649104	0.4	5.6
2774	310916	4649204	2.17	30.38
2734	310916	4649404	0.25	3.5
2714	310916	4649504	0.11	1.54
2695	310916	4649604	0.18	2.52
4214	310948	4651325	0.36	5.04
4191	310950	4650676	0.62	8.68
4190	310964	4650663	0.51	7.14
4194	310974	4650849	1.63	22.82
4215	310989	4651281	1	14
2532	311002	4650572	1.7	23.8
2343	311006	4648316	3.55	49.7
2879	311014	4648688	1.65	23.1
2900	311016	4648604	2.71	37.94
2858	311016	4648804	1.86	26.04
2837	311016	4648904	1.37	19.18
2816	311016	4649004	2.97	41.58
2795	311016	4649104	4.42	61.88
2775	311016	4649204	1.92	26.88
2735	311016	4649404	0.53	7.42
2715	311016	4649504	0.19	2.66
2696	311016	4649604	0.16	2.24
2675	311016	4649704	0.23	3.22
2539	311016	4650504	0.21	2.94
4166	311039	4648060	0.4	5.6
4195	311054	4650792	0.62	8.68
2327	311055	4648385	3.91	54.74
2921	311066	4648527	8.84	123.76
4165	311068	4648062	0.86	12.04

4167	311086	4648076	0.6	8.4
2880	311093	4648727	1.79	25.06
4168	311109	4648085	1.32	18.48
2859	311116	4648804	0.75	10.5
2838	311116	4648904	0.57	7.98
2817	311116	4649004	0.78	10.92
2796	311116	4649104	0.86	12.04
2776	311116	4649204	1.15	16.1
2736	311116	4649404	0.27	3.78
2716	311116	4649504	0.38	5.32
2697	311116	4649604	0.54	7.56
2676	311116	4649704	1.5	21
2655	311116	4649804	0.61	8.54
2634	311116	4649904	0.74	10.36
2614	311116	4650004	3.25	45.5
2595	311116	4650104	0.56	7.84
2577	311116	4650204	0.76	10.64
2562	311116	4650304	1.09	15.26
2540	311116	4650504	0.85	11.9
2533	311116	4650604	0.94	13.16
4193	311119	4650761	0.65	9.1
2901	311126	4648623	2.25	31.5
4169	311130	4648090	1.1	15.4
2344	311130	4648328	2.96	41.44
4210	311132	4651139	0.53	7.42
2922	311134	4648520	3.22	45.08
2550	311151	4650409	1.14	15.96
4209	311179	4651094	0.33	4.62
2534	311185	4650596	0.03	0.42
4192	311186	4650732	0.88	12.32
2596	311190	4650102	0.43	6.02
2923	311202	4648500	5.11	71.54
4239	311203	4650901	0.92	12.88
2881	311210	4648724	1.67	23.38
2329	311212	4648406	3.42	47.88
2345	311216	4648304	2.2	30.8
2902	311216	4648604	0.86	12.04
2860	311216	4648804	0.39	5.46
2839	311216	4648904	1.82	25.48
2818	311216	4649004	0.47	6.58
2797	311216	4649104	0.82	11.48
2777	311216	4649204	0.71	9.94
2737	311216	4649404	0.14	1.96
2717	311216	4649504	0.3	4.2
2698	311216	4649604	0.5	7
2677	311216	4649704	0.3	4.2
2656	311216	4649804	0.015	0.21
2635	311216	4649904	0.045	0.63
2615	311216	4650004	0.17	2.38
2578	311216	4650204	0.16	2.24
2563	311216	4650304	0.019	0.266

2551	311216	4650404	0.078	1.092
2541	311216	4650504	0.044	0.616
4208	311217	4651042	0.58	8.12
4207	311265	4651005	0.73	10.22
2535	311267	4650594	1.01	14.14
2346	311288	4648309	2.25	31.5
2330	311292	4648379	3.03	42.42
2924	311316	4648504	0.95	13.3
2903	311316	4648604	0.44	6.16
2882	311316	4648704	0.53	7.42
2861	311316	4648804	0.66	9.24
2840	311316	4648904	0.86	12.04
2819	311316	4649004	0.66	9.24
2798	311316	4649104	0.62	8.68
2778	311316	4649204	0.024	0.336
2758	311316	4649304	0.32	4.48
2738	311316	4649404	0.25	3.5
2718	311316	4649504	0.12	1.68
2699	311316	4649604	0.25	3.5
2678	311316	4649704	0.35	4.9
2657	311316	4649804	0.059	0.826
2636	311316	4649904	0.31	4.34
2616	311316	4650004	0.09	1.26
2597	311316	4650104	0.065	0.91
2579	311316	4650204	0.58	8.12
2564	311316	4650304	0.18	2.52
2552	311316	4650404	0.23	3.22
2542	311316	4650504	0.21	2.94
4240	311364	4651155	1.33	18.62
2841	311390	4648904	0.75	10.5
2925	311394	4648471	2.35	32.9
2883	311398	4648695	0.46	6.44
2862	311398	4648799	0.8	11.2
4241	311411	4651238	0.4	5.6
2347	311416	4648304	0.31	4.34
2331	311416	4648404	1.46	20.44
2820	311416	4649004	0.57	7.98
2799	311416	4649104	0.25	3.5
2779	311416	4649204	0.65	9.1
2759	311416	4649304	1.67	23.38
2739	311416	4649404	0.55	7.7
2719	311416	4649504	2.41	33.74
2700	311416	4649604	2.63	36.82
2679	311416	4649704	0.97	13.58
2658	311416	4649804	2.3	32.2
2637	311416	4649904	0.49	6.86
2617	311416	4650004	1.26	17.64
2598	311416	4650104	0.76	10.64
2580	311416	4650204	1.21	16.94
2565	311416	4650304	1.17	16.38
2553	311416	4650404	1.08	15.12

2543	311416	4650504	1.68	23.52
2536	311416	4650604	4.03	56.42
2905	311505	4648578	2.89	40.46
2884	311506	4648669	3.1	43.4
2780	311516	4649204	0.82	11.48
2760	311516	4649304	1.22	17.08
2740	311516	4649404	0.36	5.04
2720	311516	4649504	3.07	42.98
2701	311516	4649604	1.63	22.82
2680	311516	4649704	0.31	4.34
2659	311516	4649804	0.66	9.24
2638	311516	4649904	1.96	27.44
2618	311516	4650004	1.33	18.62
2599	311516	4650104	0.7	9.8
2581	311516	4650204	0.71	9.94
2566	311516	4650304	1.34	18.76
2554	311516	4650404	1.43	20.02
2544	311516	4650504	1.48	20.72
2537	311516	4650604	2.36	33.04
4238	311560	4651155	0.61	8.54
4174	311580	4648140	0.4	5.6
4173	311613	4648141	0.31	4.34
2927	311616	4648504	2.8	39.2
2885	311616	4648704	0.18	2.52
2781	311616	4649204	1.11	15.54
2761	311616	4649304	0.95	13.3
2741	311616	4649404	1.02	14.28
2721	311616	4649504	1.78	24.92
2702	311616	4649604	1.96	27.44
2681	311616	4649704	1.09	15.26
2660	311616	4649804	1.36	19.04
2639	311616	4649904	0.72	10.08
2619	311616	4650004	1.42	19.88
2600	311616	4650104	0.89	12.46
2582	311616	4650204	1.85	25.9
2567	311616	4650304	1.35	18.9
2555	311616	4650404	1.8	25.2
2545	311616	4650504	1.09	15.26
2906	311639	4648581	0.047	0.658
4172	311643	4648143	1.26	17.64
4237	311654	4651149	1.16	16.24
4171	311679	4648143	1.52	21.28
4236	311714	4651176	0.65	9.1
2350	311716	4648304	0.079	1.106
2928	311716	4648504	1.03	14.42
2802	311716	4649104	3.49	48.86
2782	311716	4649204	0.69	9.66
2762	311716	4649304	0.87	12.18
2742	311716	4649404	0.2	2.8
2722	311716	4649504	0.52	7.28
2703	311716	4649604	0.78	10.92

2682	311716	4649704	1.05	14.7
2661	311716	4649804	1.06	14.84
2640	311716	4649904	2.03	28.42
2620	311716	4650004	1.3	18.2
2601	311716	4650104	1.08	15.12
2583	311716	4650204	0.91	12.74
2568	311716	4650304	1.1	15.4
2556	311716	4650404	1.17	16.38
4170	311718	4648145	0.2	2.8
2907	311718	4648631	3.55	49.7
2886	311718	4648662	0.03	0.42
4235	311762	4651201	0.79	11.06
2704	311809	4649602	0.04	0.56
2824	311816	4649004	1.59	22.26
2803	311816	4649104	2.09	29.26
2743	311816	4649404	2.08	29.12
2723	311816	4649504	1.37	19.18
2683	311816	4649704	0.43	6.02
2662	311816	4649804	0.71	9.94
2641	311816	4649904	0.82	11.48
2621	311816	4650004	1.25	17.5
2602	311816	4650104	1.25	17.5
2584	311816	4650204	1.28	17.92
2569	311816	4650304	1.11	15.54
2557	311816	4650404	1.58	22.12
2908	311819	4648632	1.92	26.88
2887	311819	4648659	1.87	26.18
2783	311837	4649202	1.76	24.64
2763	311838	4649302	1.43	20.02
4234	311850	4651151	0.79	11.06
2351	311867	4648288	1.03	14.42
2867	311883	4648799	1.54	21.56
4233	311885	4651098	0.65	9.1
2888	311886	4648700	2.05	28.7
2909	311891	4648617	1.01	14.14
2603	311893	4650104	1.12	15.68
2352	311916	4648304	0.8	11.2
2930	311916	4648504	0.05	0.7
2846	311916	4648904	0.53	7.42
2784	311916	4649204	0.15	2.1
2724	311916	4649504	0.32	4.48
2705	311916	4649604	0.33	4.62
2684	311916	4649704	1.21	16.94
2663	311916	4649804	0.45	6.3
2622	311916	4650004	1.66	23.24
2570	311916	4650304	1.82	25.48
2642	311918	4649921	2.19	30.66
2585	311921	4650209	1.35	18.9
4232	311923	4651045	0.56	7.84
2337	311947	4648360	1.16	16.24
2336	311959	4648416	0.08	1.12

2785	311963	4649227	0.017	0.238
2571	311985	4650290	12	168
4225	311985	4650963	0.43	6.02
4175	311987	4648097	1.36	19.04
2586	311989	4650203	1.5	21
2643	311994	4649920	2.2	30.8
2604	311995	4650106	0.058	0.812
2623	311996	4650003	1.3	18.2
4226	312000	4650885	0.42	5.88
4176	312011	4648098	0.6	8.4
2353	312016	4648304	3.71	51.94
2931	312016	4648504	0.91	12.74
2910	312016	4648604	0.042	0.588
2725	312016	4649504	0.52	7.28
2706	312016	4649604	0.67	9.38
2685	312016	4649704	0.31	4.34
2664	312016	4649804	0.14	1.96
2868	312025	4648813	1	14
4227	312033	4650804	0.1	1.4
2572	312050	4650287	2.32	32.48
4177	312051	4648098	0.71	9.94
4231	312053	4650434	0.87	12.18
2605	312069	4650117	0.07	0.98
4178	312072	4648088	0.28	3.92
2786	312072	4649193	0.03	0.42
4228	312073	4650728	0.09	1.26
2587	312082	4650199	1.08	15.12
2624	312085	4650006	1.4	19.6
4230	312091	4650532	0.77	10.78
4229	312101	4650641	0.53	7.42
2644	312102	4649924	1.7	23.8
4179	312105	4648089	0.52	7.28
2354	312116	4648304	0.73	10.22
2338	312116	4648404	2.34	32.76
2318	312116	4648504	1.21	16.94
2911	312116	4648604	0.82	11.48
2686	312116	4649704	0.2	2.8
2665	312116	4649804	0.25	3.5
4180	312139	4648089	0.81	11.34
2937	312168	4649462	1.27	17.78
2339	312181	4648402	1.57	21.98
2319	312183	4648505	1.23	17.22
2767	312183	4649293	0.039	0.546
2355	312195	4648332	1.4	19.6
2787	312197	4649223	0.018	0.252
2912	312208	4648568	1.19	16.66
2891	312216	4648704	1.23	17.22
2666	312216	4649804	1.91	26.74
2645	312216	4649904	1.53	21.42
2625	312216	4650004	1.8	25.2
2606	312216	4650104	4.78	66.92

2588	312216	4650204	1.15	16.1
2768	312286	4649305	0.05	0.7
2913	312316	4648604	0.016	0.224
2829	312316	4649004	0.4	5.6
2788	312316	4649204	0.04	0.56
2667	312316	4649804	1.22	17.08
2646	312316	4649904	1.09	15.26
2626	312316	4650004	2.23	31.22
2607	312316	4650104	3.16	44.24
2589	312316	4650204	1.19	16.66
2936	312327	4649417	1.05	14.7
2356	312333	4648164	1.06	14.84
3499	312355	4648913	0.2	2.8
2748	312356	4649368	0.03	0.42
2769	312396	4649297	0.07	0.98
2914	312416	4648604	0.04	0.56
2893	312416	4648704	0.61	8.54
2872	312416	4648804	0.81	11.34
2851	312416	4648904	0.58	8.12
2830	312416	4649004	0.03	0.42
2668	312416	4649804	1.18	16.52
2647	312416	4649904	1.66	23.24
2627	312416	4650004	0.34	4.76
2608	312416	4650104	1.33	18.62
2590	312416	4650204	4.03	56.42
2357	312426	4648159	1.22	17.08
2789	312443	4649215	0.028	0.392
2749	312450	4649474	1.03	14.42
2790	312466	4649168	1.59	22.26
2648	312486	4649955	0.42	5.88
2669	312510	4649779	1.03	14.42
2915	312516	4648604	0.02	0.28
2894	312516	4648704	0.015	0.21
2873	312516	4648804	0.4	5.6
2852	312516	4648904	1.2	16.8
2831	312516	4649004	1	14
2770	312516	4649331	0.02	0.28
2750	312516	4649404	0.03	0.42
2711	312516	4649604	0.83	11.62
2690	312516	4649704	0.61	8.54
2628	312516	4650004	0.12	1.68
2609	312516	4650104	0.16	2.24
2730	312517	4649539	1.03	14.42
2810	312521	4649153	0.054	0.756
2358	312527	4648160	0.13	1.82
2771	312616	4649304	0.75	10.5
2751	312616	4649404	1.75	24.5
2731	312616	4649504	0.016	0.224
2691	312616	4649704	0.9	12.6
2670	312616	4649804	1	14
2791	312630	4649179	0.044	0.616

2649	312647	4649881	1.3	18.2
2692	312716	4649704	0.6	8.4
2671	312716	4649804	0.72	10.08
2650	312716	4649904	0.2	2.8

Table 3.1- Soil CO_2 flux data measured in the AAB for the interpolation CO2 flux map.

Sample sites	**Higher CO_2 flux measured with the accumulation chamber ($g/m^2 \cdot day$)**	**Lower CO^2 flux measured with the accumulation chamber ($g/m^2 \cdot day$)**	**Mean CO_2 flux (higher flux+ lower flux /2)**	**CO_2 %**	**$\delta^{13}C$**
L1	123.76	34.3	79.03	3.50%	-1.957
L1	123.76	34.3	79.03	3.50%	-1.940
L1	123.76	34.3	79.03	3.50%	-2.021
L2	4.76	4.34	4.55	2.10%	-4.268
L2	4.76	4.34	4.55	2.10%	-4.282
L2	4.76	4.34	4.55	2.10%	-4.253
L2	4.76	4.34	4.55	2.10%	-13.169
L3	66.92	14	40.46	0.52%	-19.748
L3	66.92	14	40.46	0.52%	-19.824
L4	48.86	28.56	38.71	1.34%	-19.704
L4	48.86	28.56	38.71	1.34%	-19.597
L4	48.86	28.56	38.71	1.34%	-19.867
L5	28.7	---	28.7	0.76%	-16.195
L5	28.7	---	28.7	0.76%	-17.733
L6	39.2	---	39.2	1.12%	-8.857
L6	39.2	---	39.2	1.12%	-18.369
L7	51.94	---	51.94	0.67%	-19.888
L8	61.88	---	61.88	0.72%	-5.442
L8	61.88	---	61.88	0.72%	-15.395
L9	56.42	---	56.42	0.53%	-15.80

Table 3.2- d13C values measured across the higher degassing point in the AAB At least two samples were taken from nine sites where degassing levels were higher (L1, 3 vials, L2 4 vials, L3, 2 vials, L4, 4 vials, L5, 2 vials, L6, 2 vials, L8, 2 vials) except for L7 and L9 (1 vial each).

Appendix B- Chapter 4

OBJECTS	X UTM33 WGS 84	Y UTM33 WGS 84	CO2 ppm/s	CO2g_m2day
4012	308961	4662076	0.82	11.48
4011	309042	4662066	0.61	8.54
4010	309110	4662055	0.3	4.2
4009	309183	4662050	0.46	6.44
4008	309283	4662045	0.73	10.22
4023	308150	4662011	0.66	9.24
4021	308329	4661945	0.61	8.54
4022	308261	4661942	0.72	10.08
4020	308392	4661922	0.25	3.5
4019	308454	4661903	0.58	8.12
4018	308513	4661880	1.37	19.18
4017	308573	4661862	0.9	12.6
4016	308635	4661841	0.68	9.52
4026	309323	4661836	0.6	8.4
4015	308688	4661824	0.72	10.08
4014	308754	4661804	0.19	2.66
4013	308815	4661782	0.33	4.62
4007	309448	4661768	0.47	6.58
4027	309098	4661765	1.4	19.6
4006	309491	4661764	1.74	24.36
4024	309390	4661763	0.3	4.2
4025	309334	4661759	0.59	8.26
4005	309537	4661753	0.38	5.32
4004	309588	4661748	0.18	2.52
4003	309651	4661739	0.34	4.76
4002	309717	4661726	0.25	3.5
4000	309825	4661725	0.49	6.86
4001	309772	4661719	0.47	6.58
3999	309870	4661710	0.77	10.78
3998	309912	4661688	0.56	7.84
3982	310823	4661683	0.4	5.6
3997	309965	4661664	0.54	7.56
3981	310879	4661659	0.64	8.96
3996	310014	4661630	0.43	6.02
3983	310802	4661624	0.28	3.92
3980	310946	4661610	0.18	2.52
3995	310072	4661605	0.32	4.48
3979	310968	4661589	0.34	4.76
3994	310128	4661579	0.75	10.5
3984	310749	4661576	0.7	9.8
3977	311137	4661572	0.24	3.36
3978	311087	4661570	0.22	3.08
3976	311195	4661570	0.23	3.22
3993	310179	4661555	0.4	5.6
3985	310700	4661536	0.3	4.2
3975	311246	4661533	0.2	2.8

3992	310246	4661526	0.71	9.94
3991	310314	4661513	0.38	5.32
3974	311282	4661513	0.27	3.78
3973	311318	4661501	0.18	2.52
3986	310648	4661490	0.45	6.3
3990	310384	4661488	0.5	7
3970	311373	4661486	0.27	3.78
3989	310442	4661468	0.72	10.08
3969	311456	4661462	0.18	2.52
3968	311501	4661457	0.36	5.04
3987	310588	4661447	0.5	7
3967	311535	4661447	0.23	3.22
3966	311577	4661447	0.47	6.58
3988	310514	4661440	0.49	6.86
3965	311616	4661430	0.42	5.88
3964	311654	4661425	0.3	4.2
3963	311689	4661412	0.2	2.8
3962	311724	4661408	0.3	4.2
3961	311763	4661403	0.29	4.06
3960	311791	4661394	0.14	1.96
3959	311821	4661389	0.38	5.32
4039	312681	4661388	0.72	10.08
4040	312848	4661369	0.19	2.66
4041	312940	4661358	0.41	5.74
4047	313230	4661347	0.15	2.1
4038	312620	4661343	0.24	3.36
4048	313273	4661343	0.41	5.74
4046	313192	4661339	0.76	10.64
4052	313589	4661339	0.12	1.68
4028	312063	4661338	0.63	8.82
4029	312107	4661337	0.8	11.2
4030	312146	4661331	0.52	7.28
4042	312995	4661328	0.39	5.46
4045	313152	4661326	0.35	4.9
4049	313315	4661325	0.39	5.46
4031	312195	4661324	0.45	6.3
4050	313381	4661308	0.27	3.78
4044	313110	4661306	0.42	5.88
4051	313461	4661305	0.13	1.82
4032	312248	4661298	0.24	3.36
4037	312569	4661293	0.34	4.76
4043	313063	4661288	0.57	7.98
4036	312506	4661262	0.46	6.44
4033	312303	4661261	0.98	13.72
4034	312366	4661241	0.61	8.54
4035	312442	4661240	0.26	3.64
3972	311129	4661191	0.76	10.64
3971	311167	4661177	0.44	6.16

Table 4.1-Soil CO_2 flux data measured in the Cretone area (T1 profile).

OBJECTS	X UTM33 WGS 84	Y UTM33 WGS 84	CO2 ppm/s	CO2g_m2day
4262	311114	4657236	0.56	7.84
4261	311085	4657216	0.64	8.96
4260	311086	4657165	0.73	10.22
4259	311067	4657098	0.34	4.76
4258	311030	4657043	0.93	13.02
4257	311002	4657000	0.39	5.46
4242	310963	4656962	0.41	5.74
4243	310915	4656926	0.44	6.16
4244	310862	4656905	0.9	12.6
4256	310332	4656887	0.13	1.82
4250	310404	4656883	0.37	5.18
4245	310773	4656873	0.6	8.4
4254	310263	4656866	0.63	8.82
4246	310702	4656846	0.51	7.14
4249	310481	4656831	0.9	12.6
4247	310635	4656829	0.61	8.54
4255	310218	4656810	0.58	8.12
4248	310569	4656792	0.48	6.72
4253	310147	4656780	0.72	10.08
4252	310014	4656751	0.85	11.9
4251	309981	4656679	0.64	8.96
4263	309872	4656649	0.41	5.74
4264	309766	4656605	0.71	9.94
4265	309656	4656538	0.3	4.2
4267	309544	4656485	0.33	4.62
4266	309450	4656443	1.29	18.06
4268	309393	4656402	0.56	7.84
4269	309354	4656353	0.48	6.72
4270	309313	4656308	0.55	7.7

Table 4.2-Soil CO_2 flux data measured in Sant’Angelo Romano area (T2 profile).

OBJECTS	X UTM33 WGS 84	Y UTM33 WGS 84	CO2 ppm/s	CO2g_m2day
4140	312236	4643226	0.43	6.02
4141	312284	4643214	0.4	5.6
4152	312338	4643193	0.48	6.72
4139	312175	4643192	0.11	1.54
4153	312374	4643178	0.38	5.32
4154	312415	4643162	0.85	11.9
4138	312114	4643159	0.37	5.18
4156	312444	4643146	0.4	5.6
4155	312555	4643138	0.14	1.96
4157	312489	4643127	0.28	3.92
4137	312069	4643125	0.26	3.64
4136	312007	4643078	0.31	4.34
4135	311962	4643047	0.33	4.62
4134	311925	4643022	0.41	5.74
4133	311876	4642984	0.52	7.28
4132	311868	4642908	0.37	5.18
4131	311748	4642816	0.29	4.06
4130	311627	4642739	0.36	5.04
4129	311529	4642661	0.41	5.74
4128	311487	4642629	0.35	4.9
4127	311454	4642608	0.75	10.5
4126	311426	4642585	0.31	4.34
4142	311468	4642416	0.56	7.84
4143	311449	4642375	0.35	4.9
4144	311413	4642344	0.026	0.364
4145	311380	4642312	0.5	7
4146	311347	4642283	0.44	6.16
4147	311312	4642252	0.37	5.18
4148	311276	4642224	0.53	7.42
4149	311241	4642191	0.4	5.6
4150	311206	4642153	0.38	5.32
4151	311176	4642121	0.51	7.14

Table 4.3-Soil CO_2 flux data measured in the Corcolle area (T4 profile).

OBJECTS	X UTM33 WGS 84	Y UTM33 WGS 84	CO2 ppm/s	CO2g_m2day
4084	309839	4647010	0.37	5.18
4083	309887	4647016	0.5	7
4082	309947	4647017	1.35	18.9
4081	310016	4647030	0.28	3.92
4080	310066	4647032	0.51	7.14
4079	310119	4647039	0.52	7.28
4078	310174	4647041	0.18	2.52
4077	310219	4647049	0.23	3.22
4076	310258	4647060	0.42	5.88
4075	310307	4647064	0.47	6.58
4072	310382	4647066	5.42	75.88
4074	310354	4647068	0.54	7.56
4085	310468	4647071	0.34	4.76
4073	310417	4647080	1.85	25.9
4053	310795	4647156	0.32	4.48
4054	310833	4647163	0.41	5.74
4055	310873	4647177	0.34	4.76
4056	310906	4647186	0.26	3.64
4057	310934	4647190	0.2	2.8
4058	310990	4647211	0.27	3.78
4059	311032	4647221	0.21	2.94
4060	311086	4647233	0.16	2.24
4061	311135	4647250	0.22	3.08
4062	311211	4647261	0.17	2.38
4063	311259	4647275	0.33	4.62
4064	311309	4647290	0.14	1.96
4065	311351	4647310	0.4	5.6
4066	311402	4647316	0.3	4.2
4067	311461	4647330	0.3	4.2
4068	311517	4647345	0.31	4.34
4069	311565	4647362	0.19	2.66
4070	311595	4647378	0.32	4.48
4086	311661	4647386	0.34	4.76
4087	311722	4647398	0.21	2.94
4088	311774	4647411	0.11	1.54
4089	311817	4647418	0.4	5.6
4090	311867	4647439	0.22	3.08
4091	311905	4647448	0.8	11.2
4092	311942	4647452	0.29	4.06
4093	311988	4647475	0.1	1.4
4104	312070	4647501	0.65	9.1
4102	312120	4647514	0.46	6.44
4103	312159	4647525	0.41	5.74
4101	312196	4647529	0.37	5.18
4094	312232	4647545	0.45	6.3
4095	312297	4647545	0.14	1.96
4096	312345	4647559	0.2	2.8
4097	312374	4647574	0.41	5.74

4098	312429	4647580	0.14	1.96
4099	312493	4647601	1.1	15.4
4100	312553	4647615	0.75	10.5
4105	312609	4647631	0.58	8.12
4106	312656	4647640	0.8	11.2
4107	312704	4647657	0.23	3.22
4108	312754	4647663	0.18	2.52
4109	312796	4647679	0.29	4.06
4110	312840	4647686	0.56	7.84
4111	312877	4647696	0.36	5.04
4112	312916	4647708	0.41	5.74
4113	312958	4647718	0.47	6.58
4114	312994	4647722	0.33	4.62
4115	313029	4647732	0.53	7.42
4116	313068	4647747	0.23	3.22
4117	313105	4647756	0.4	5.6
4118	313145	4647766	0.45	6.3
4119	313180	4647775	0.35	4.9
4120	313214	4647784	0.15	2.1
4123	313255	4647798	0.43	6.02
4121	313301	4647807	0.32	4.48
4122	313350	4647819	0.33	4.62
4124	313424	4647846	0.41	5.74
4125	313477	4647858	0.37	5.18

Table 4.4 -Soil CO_2 flux data measured in the Bagni di Tivoli area (T4 profile).

Study Area	Country	Survey Area	Total Output ($t \cdot d^{-1}$)	$CO2$ Flux Range/Mean ($g \cdot m^{-2} \cdot d^{-1}$)
Montemiccioli	Italy	14,970 m^2	19.77	Mean 1,253.7
Solfatara (Pozzuoli)	Italy	0.09 km^2	133	24 to 10,000
Libbiano	Italy	1,945 m^2	1.36	Mean 1,673.4
Micciano-NW	Italy	2,610 m^2	0.90	--
Monterotondo-N	Italy	27,117 m^2	7.29	Mean 794.9
Sasso Pisano	Italy	10,128 m^2	2.14	Mean 200.7
Monterotondo-S	Italy	20,000 m^2	3.15	Mean 156.9
Micciano-SE	Italy	2,770 m^2	0.40	Mean 25.9
Palazzo al Piano	Italy	30,920 m^2	3.66	Mean 129.7
Sasso-Monterotondo	Italy	20,237 m^2	1.51	Mean 118.0
Reykjanes	Iceland	2.4 $\times 10^5 m^2$	--	Normalized: 61.4
Santa Ninfa (Belice)	Italy	2 km profile	--	Mean 61
Mt. Amiata	Italy	225 km^2	13,275	1.07 to 296.4 *μmol*
Belice Valley (Area D)	Italy	20 km^2	--	Mean 47
Vulcano	Italy	2 km^2	75.3	36.9
Yangbajain Field	China	3.2 km^2	138	1 to 7,000
Pisa Plain	Italy	--	3,600	Mean 6.9 *μmol*
Lagoni-Sasso	Italy	8,550 *m*2	0.28	Mean 40.6
Vesuvius (cone)	Italy	--	--	Mean 22
Acque Albule Basin	Italy	~6.5 *km*2 (Study)	94.55	Mean 14.538
Changbaishan (CHV)	China	~257 km^2	160	0.9 to 3,052
Duvalo (kosel)	Macedonia	ND	66.1	---

Table 4.5 – Soil CO_2 flux values derived from the scientific literature, used as a reference for comparison with the CO_2 soil degassing of the AAB.

Appendix C- Chapter 5

Rock Unit	Density (kg/m³)	Porosity (%)	Permeability (x,y,z) (m²)	Thermal Conductivity (W/(m·K))	Specific Heat (J/(kg·K))	Thickness (m)
Travertine	2700	0.16	$1 \cdot 10^{-9}$	2.8	900	60
Clay	2000	0.05	$1 \cdot 10^{-14}$	1.8	1050	280
Carbonates	2800	0.2	$1 \cdot 10^{-9}$	3	920	3000
Damage zone	2750	0.4	$1 \cdot 10^{-10}$	1.5	1000	25

Table 5.1 –Parameters used for TOUGH2 mesh domain.

.

Acknowledgement

*I would like to express my deepest gratitude to my supervisor, **Prof. Claudio Faccenna**, for his invaluable guidance and for helping me to shape the scientific foundations of this PhD project.*

*I am sincerely grateful to **Dr. Riccardo Reitano** for his support, mentorship, and encouragement throughout these three years.*

*My sincere thanks go to **Prof. Guido Giordano** for teaching me how to manage a PhD project, and for enabling collaborations with experts who meaningfully enhanced the scientific development of this project.*

*I am profoundly grateful to **Dr. Maria Luisa Carapezza, Dr. Massimo Ranaldi, and Dr. Luca Tarchini** for their constant support over the years. I warmly thank them for providing the Accumulation Chamber, for patiently teaching me the methodology, and for involving me in their inspiring research activities.*

*I would like to express my sincere gratitude to **Prof. Andrea Billi** as external examiner and for his valuable advice and insightful suggestions.*

*My sincere thanks also go to **Prof. Sergio Calabrese** for reviewing my thesis as external examiner.*

*My warmest thanks to **Marco Vinci** for his kindness, patience, and continuous availability. Many thanks for granting access to the study area and for involving me in the geotechnical and geophysical investigations carried out in the Acque Albule Basin. His contribution has been essential to the development of this work.*

*I am grateful to **Rocco Di Capua** for his assistance in accessing the study area.*

*My thanks also go to **Filippo Lippiello** and the Società del Travertino Romano for giving me the opportunity to conduct research within the quarry areas.*

*I am grateful to **Caucci Marmi, Estraba, Morelli, and Degemar** for providing access to the study sites.*

*Special thanks to **Prof. Valerio Acocella** for his moral support and invaluable mentorship.*

*I am grateful to **Dr. Micol Todesco** for receiving me in Bologna and for teaching me how to use the TOUGH2 software.*

*My sincere thanks to **Dr. Doreen Noak** and **Dr. Kai Mangelsdorf** for their assistance with the $\delta^{13}C$ analyses of gas samples at GFZ.*

*Thanks to **Dr. Valentina Carucci** for her good support in interpreting hydrogeological and hydrogeochemical framework of the Acque Albule Basin.*

*I warmly thank the **AVERT/OVSICORI team** for allowing me to participate in the AVERT project monitoring CO_2 at Poás Volcano, and for giving me the opportunity to experience the most extraordinary international adventure of my life.*

*I want to express her deep gratitude to **Dr. Martina Picciallo**, an excellent geologist and dear friend, for her essential assistance in collecting Accumulation Chamber data in the Acque Albule Basin. Her contribution was crucial to this study.*

*I am grateful to **Federica Davani** for sharing her results on the AAB and for her constant moral support throughout this project.*

*My heartfelt thanks go to my closest colleagues **Claudia, Masoud, Manuela, Martina, Ilaria, Simone, Mauro, Anas, Beatrice and Andrea** for sharing so many special moments during this journey.*

*I am deeply grateful to my family **Mamma, Papà, Danilo, Federica, Gaia, Giulia, Mya, Livia, Lucio and to my closest friends, Chiara, Denise, Giorgia, Mattia and Andrea,** for being present at every stage of my growth.*

*Finally, thank you, **Tiziana**, for standing by my side during these three difficult years. Thank you for allowing my light to shine and for helping me discover and bring out the best part of myself.*